U N I V E R S I T Y O F G L A S G O W

C H E M I S T R Y D E P A R T M E N T

NUCLEAR AND ELECTRON RESONANCE STUDIES OF SOME SOLIDS

BEING

SUBMITTED IN PART FULFILMENT
OF THE REQUIREMENTS FOR THE DEGREE OF
DOCTOR OF PHILOSOPHY

BY

JOHN M. BARBOUR

JANUARY 1968

PREFACE

This thesis deals with some chemical applications of the three related branches of spectroscopy, nuclear magnetic resonance spectroscopy (N.M.R.), nuclear quadrupole resonance spectroscopy (N.Q.R.) and electron paramagnetic resonance spectroscopy (E.P.R.). In this thesis these three powerful techniques have been applied, singly and jointly, to several problems concerned with molecular structure and bonding in crystalline solids.

The first investigation described is a N.M.R. study of the alleged hydrates of magnesium carbonate, $MgCO_3 3H_2O$ and $MgCO_3 H_2O$. It was undertaken with the aim of finding the nature of these solids, of characterising molecular motions within the solids, of estimating the energy barriers hindering these motions and of obtaining information about the nature of the processes involved in the interconversion of the "trihydrate" to the "monohydrate".

The remainder of the thesis is concerned with effects which may be observed if a nucleus possesses a quadrupole moment. Some complexes of mercuric chloride have been studied using N.Q.R. and N.M.R. techniques, in attempts to obtain the chlorine quadrupole coupling constants for each of the solids. The intention of this investigation was to procure information about the crystal structures of three of these complexes from a knowledge of the structures of another two complexes and of mercuric chloride itself and the quadrupole coupling constants of all six compounds.

The last part of the thesis describes how the quadrupole coupling constant of a paramagnetic ion may be extracted from the hyperfine structure observed in an E.P.R. spectrum. It is concerned with quadrupole coupling of ^{63}Cu in a single crystal of fully deuterated dibarium zinc formate tetrahydrate doped with copper (II). The nature of the bonding in the dibarium cupric formate tetrahydrate complex is discussed using parameters obtained from a full analysis of the E.P.R. spectra of the copper (II) doped zinc complex.

The thesis starts with a General Introduction and is divided into three main parts, each of which consists of several chapters. No part is self-contained. Each chapter is divided into a number of sections. Tables and figures are numbered according to the chapter and section to which they refer. Finally a list of literature

references is given.

The work described in this thesis was carried out in the Department of Chemistry of the University of Glasgow, between October 1964 and December 1967, under the direction of Professor J. M. Robertson. I am grateful to the James Fleming Scholarship Committee and the Faculty of Science of the University of Glasgow for their support throughout the duration of this work.

I wish, also, to express my appreciation of the assistance and encouragement rendered by Dr. A.L. Porte throughout the preparation of this thesis. The assistance of Messrs. A. Leven, J. Hardy, J. Rae, M. Riggans and their workshop staff is gratefully acknowledged.

Finally I wish to thank my wife for performing the unenviable task of typing the manuscripts of this thesis.

CONTENTS

GENERAL INTRODUCTION

All electrons and many nuclei behave as if they are spinning. The spin quantum number for electrons, S, is $\frac{1}{2}$, whereas for nuclei the quantum number, I, can have values $\frac{1}{2}n$, where n = 0,1,2,3, etc. When n = 0 the nucleus has no spin; examples of some common nuclei which fall into this category are ^{12}C, ^{16}O and ^{32}S.

A charged particle which has an angular momentum also has a magnetic dipole moment and this can interact with a magnetic field. This magnetic interaction produces (2S+1) nonequivalent sub-levels of the electronic ground state level and (2I+1) nonequivalent sub-levels of the nuclear ground state level. E.P.R. and N.M.R. are essentially concerned with transitions between these sub-levels.

In addition to its magnetic moment, a nucleus with $I \geqslant 1$ may have an electric quadrupole moment. This moment interacts with inhomogeneous electric field gradients and gives rise to a series of energy sub-levels for the nucleus. When I is integral one obtains (I+1) groups of such sub-levels and when I is half-integral $(I+\frac{1}{2})$ groups of sub-levels result. Transitions between these sub-levels can be detected in various ways, for example, directly using N.Q.R. techniques.

To be of interest to chemists these techniques must be related more to the atoms, molecules and crystals of which electrons and nuclei are intimate parts. Nuclei and electrons themselves produce magnetic and electric fields and it is the influence of these internal fields, which vary according to the chemical environment of the nucleus or electron under observation, on the electronic and nuclear levels and sub-levels which has made N.M.R., E.P.R. and N.Q.R. so useful to chemistry.

CHAPTER 1

THE RESONANCE CONDITION IN NUCLEAR MAGNETIC RESONANCE

1.1. Spin Angular Momentum [1]

Electrons, protons and neutrons possess intrinsic angular momenta. The angular momentum, G, associated with any of these sub-atomic particles may be written in the form

$$G^2 = G_x G_x + G_y G_y + G_z G_z$$

where G_x, G_y and G_z are its components along three mutually perpendicular axes X, Y and Z. It can be shown from the quantum mechanical properties of angular momentum operators that the eigenvalues of G^2 are given by $\ell(\ell+1)\hbar^2$ where $\hbar$ = (Planck's constant) $\times (2\pi)^{-1}$ and 2ℓ must be integral, and that eigenvalues of G_z are $m\hbar$, where m can have any of the $(2\ell+1)$ values

$$\ell, (\ell-1), (\ell-2), \text{-----}, -(\ell-1), -\ell$$

ℓ is known as the "spin quantum number" of the particle.

It has been shown experimentally that the spin quantum number of the electron, the proton and the neutron are all equal to one half and since nuclei are compounded out of these fundamental particles it follows that a nuclear spin quantum number, I, being made up of contributions from the nucleons out of which the nucleus is built, can have values of $0, \frac{1}{2}, 1, \frac{3}{2}, \ldots$ depending on how the nucleonic spins couple within the nucleus. At this point it is convenient to define dimensionless vector operators, $\underline{I}$, by the equation

$$G = \hbar I \qquad 1.1.1$$

so that I^2 has eigenvalues $I(I+1)$ and I_z has eigenvalues $I, I-1, \ldots, -I$.

A list of the nuclear isotopes of importance in the compounds under discussion in this thesis, together with their abundances in nature and their spin quantum numbers, when the nuclei are in their ground state, is given below in Table 1.1.1.

Table 1.1.1

Nucleus	abundance,%	I	Nucleus	abundance,%	I
^{1}H	99.98	$\frac{1}{2}$	^{32}S	99.3	0
$^{2}H(D)$	1.56×10^{-2}	1	^{35}Cl	75.4	$\frac{3}{2}$
^{12}C	98.9	0	^{37}Cl	24.6	$\frac{3}{2}$
^{13}C	1.1	$\frac{1}{2}$	^{39}K	93.08	$\frac{3}{2}$
^{14}N	99.64	1	^{63}Cu	69.09	$\frac{3}{2}$
^{16}O	99.95	0	^{65}Cu	30.91	$\frac{3}{2}$
^{17}O	3.7×10^{-2}		^{199}Hg	16.86	$\frac{1}{2}$
^{24}Mg	89.95	0	^{201}Hg	13.24	$\frac{3}{2}$
^{25}Mg	10.05				

1.2. Magnetic Moments of Nuclei

The spin of a charged nucleus gives rise to a magnetic moment, the relationship between the nuclear magnetic moment vector operator, $\underline{\mu}$, and the spin angular momentum operator, $\underline{G}$, being

$$\underline{\mu} = \gamma \underline{G} \qquad 1.2.1$$

where γ, the magnetogyric ratio, is a scalar quantity.

$$\gamma = g_N e/_{2Mc}$$

where e and M are respectively the charge and mass of the proton and c is the velocity of light. g_N, the nuclear g-factor, is a constant for each nucleus. 1.2.1 may be rewritten in the form

$$\underline{\mu} = g_N \beta_N \underline{I} \qquad 1.2.2$$

where β_N, the nuclear magneton, is equal to $eh/(4\pi Mc)$

The operator for the z-axis component of the magnetic moment, μ_z, is

$$\mu_z = \gamma G_z = \gamma \hbar I_z \qquad 1.2.3$$

and its eigenvalues are $\gamma \hbar m$ where m can take any of the ladder of values I, (I-1), (I-2), ---, -I.

1.3. Effect of a Static Magnetic Field on the Energy Levels of a Nucleus

The Hamiltonian which results when a magnetic field $\underline{H}$ interacts with a nuclear magnetic dipole moment $\underline{\mu}$ is given by

$$\mathcal{H} = -\underline{\mu} \cdot \underline{H} \qquad 1.3.1$$

Classically this interaction subjects the angular momentum vector to a torque causing the magnetic moment vector to precess about the field direction, and it can be shown that the angular velocity of the resultant "Larmor" precession is

$$\omega_0 = \gamma H \qquad 1.3.2$$

If the magnetic field H_0 is taken to be along the z-axis direction, then

$$\mathcal{H} = -\gamma \hbar H_0 I_z \qquad 1.3.3$$

so that the interaction energy E is given by the eigenvalues of 1.3.3. which are

$$E = -\gamma \hbar H_0 m \qquad 1.3.4$$

For a nucleus with $I = \frac{3}{2}$, $m = \frac{3}{2}, \frac{1}{2}, -\frac{1}{2}, -\frac{3}{2}$, and hence an applied magnetic field along the z-axis direction produces four equally spaced energy levels, separated by $\gamma \hbar H_0$. In general, for a nucleus of spin I, (2I+1) energy sub-levels are produced.

In order to study these sub-levels spectroscopically an interaction which can effect transitions between them is needed. The interaction most commonly used for this purpose consists of that which arises when an alternating magnetic field is applied. The Hamiltonian which represents the interaction of the nucleus with this second magnetic field is given by

$$\mathcal{H}'(t) = -\gamma \hbar \left[H_x(t) I_x + H_y(t) I_y + H_z(t) I_z \right] \qquad 1.3.5$$

where $H_x(t)$, $H_y(t)$ and $H_z(t)$ are the components of the alternating field, $2H_1 \cos \omega t$, where ω is the angular frequency of this field. It turns out that I_z can only connect states with $\Delta m = 0$ whereas I_x and I_y (or any linear combination of these) connect only states with $\Delta m = \pm 1$, so that in order to cause transitions between the energy levels of 1.3.4 the applied electromagnetic radiation must be applied in the XY plane. If this geometrical condition is obeyed then transitions between adjacent energy levels only are allowed. Transitions, in accordance with the selection rule $\Delta m = \pm 1$, will be induced only when the energy of the applied alternating field is equal to the energy separation between adjacent levels, i.e. when

$$\hbar \omega = \Delta E = \gamma \hbar H_0$$

$$\text{or} \qquad \omega = \gamma H_0 \qquad 1.3.6$$

which is the Larmor precession relationship of 1.3.2.

Therefore there is only one absorption frequency irrespective of the number of energy levels produced by interaction of the nuclear dipole and an applied static magnetic field.

Since nuclear magnetogyric ratios are of the order 10^4 - 10^5 radians sec^{-1} $gauss^{-1}$, magnetic field strengths of 3-10 K gauss require frequencies, $\omega/2\pi$, of the order of 10 - 50 Mc/s for nuclear resonance. These frequencies fall in a convenient radiofrequency band.

1.4. Nuclear Resonance in Bulk Matter

Chemists are interested in resonance phenomena in bulk matter rather than in isolated nuclei, therefore we now consider an assembly of identical atomic nuclei, with nuclear spin quantum number $\frac{1}{2}$, in a sample of matter which is subjected to a steady magnetic field H_o. The material in which the nuclei of interest are embedded is usually called the "lattice", whether it be solid, liquid or gas.

If internuclear interactions are ignored then each nucleus has two possible energy sub-levels, due to interaction with the external field separated by $\gamma \hbar H_o$. Application of radiation of the resonant frequency, polarised in a direction perpendicular to H_o, causes transitions between the two energy levels to take place. The probability of transition upwards by absorption is equal to the probability of transition downwards by stimulated emission so that if the numbers of nuclei in each level were equal, the average rates of transitions up and down would be equal and no net transfer of energy between the radiation source and the spin system would be detectable. However, the population of the lower level exceeds that of the upper level by the Boltzmann factor, exp.($\gamma \hbar H_o / kT_s$) where k is Boltzmann's constant, ($k = 1.38044 \times 10^{-16}$ erg/degree), and T_s is the equilibrium temperature of the nuclear spins. At about 300^oK this factor is $1+8 \times 10^{-6}$ for protons in a field of 10,000 gauss. Therefore, there is a net absorption of radiofrequency energy due to this small excess in the lower level.

The absorption of radiofrequency energy corresponds to the transfer of some of the excess population in the lower level to the upper level and, were it not for interaction between the spin system and the lattice, the fractional excess of population would steadily decrease to zero. This could equally well be described by imagining

the spin temperature, T_s, steadily rising as radiofrequency energy is absorbed — radiofrequency heating of the spin system — while the temperature of the lattice, on which the r.f. has no direct effect, is unaltered. Interactions between the spin system and the lattice will tend to bring both into thermal equilibrium at the same temperature. However the thermal capacity of the lattice is much greater than that of the spin system so that this common temperature is usually almost identical with the lattice temperature. Spin-lattice interactions thereforereduce the spin temperature much below $T_s = \infty$, i.e. increase the population of the lower level.

The approach of the spin and lattice systems to equilibrium can be considered a thermal relaxation process and it can be shown experimentally that equilibrium is approached exponentially with a characteristic time T_1, the spin-lattice relaxation time. T_1 is usually between 10^{-4} and 10^4 seconds. For solids it is rarely shorter than 10^{-2} seconds and may be very long at low temperatures. For pure liquids T_1 may be as short as 10^{-3} seconds and rarely exceeds 10 seconds.

A second form of interaction can affect the life-time of a spin state and thus influence the detectability of an absorption. Since each nucleus possesses a small magnetic dipole moment there is a magnetic dipole-dipole interaction between each pair of nuclei and neighbouring nuclei, in effect, produce at each nucleus a small local magnetic field. This interaction is dealt with more fully in the following chapter. The local steady field differs from nucleus to nucleus depending on their environment so that there is a distribution of Larmor precession frequencies about the ideal value ω_0, covering a range $\delta\omega_0$ which turns out to be $10^4 sec^{-1}$. If two spins have precession frequencies differing by $\delta\omega_0$ and are initially in phase, then they will be out of phase in a time $(\delta\omega_0)^{-1}$, i.e. about 10^{-4}secs. This interaction has two effects; one is that the spread of precession frequencies $\delta\omega_0$ causes the resonance to be broader than the condition defined by 1.3.6. Secondly a nucleus j produces at nucleus k a magnetic field of frequency $(\omega_0)_j$ which may induce a transition in nucleus k with a mutual exchange of energy. Since the relative phases of the nuclei j and k change after about $(\delta\omega_0)^{-1}$ secs the correct phasing for this spin exchange process should occur after this time; this should determine the life-time of a spin state. It is convenient

to introduce a spin-spin interaction, or spin-spin relaxation, time T_2 where $T_2 = 1/\delta\omega_0 \approx 10^{-4}$ secs. to describe this process. In the presence of the radiofrequency radiation, of magnitude H_1, the approach to equilibrium of the spin and lattice systems is still exponential, but the characteristic time is now T_1Z. Here Z is called the Saturation Factor and is equal to $\left[1+\gamma^2 H_1^2 T_1 T_2\right]^{-1}$. Saturation describes the state when the population of the spin energy levels become equal, so that no net resonance is detectable and it occurs when the spin-lattice exponential decay time associated with depopulation of the upper spin level is large, i.e. when T_1Z is large. Saturation can be avoided when T_1 itself is fairly large, as is the case in most solids, by ensuring that the radiofrequency power level, H_1, is kept low.

Thus in general resonances are detectable because of the small population excess of the lower spin level which persists at thermal equilibrium even in the presence of radiofrequency radiation absorption, which tends to depopulate the lower level, because of the competing process of spin-lattice relaxation which tends to populate the lower level.

1.5. Observation of Nuclear Resonances

A sample of material, containing a large number of the nuclei in which one is interested, is subjected to a steady magnetic field H_0, and then a period of time, greater than T_1, must be allowed to lapse to enable the spin system to come into equilibrium with the lattice in the field. To observe nuclear resonance absorption the sample must now besubjected to a linearly polarised radiofrequency field in a direction perpendicular to H_0. This is achieved by passing an r.f. current through a coil wound round the sample tube, the cylindrical axis of the coil being at right angles to the static field direction. Provision must be made for adjustment of either the magnitude of H_0 or of the frequency ν of the r.f. so that the resonance condition, $|\omega| = \gamma H_0$, can be achieved. Control of the magnitude of the r.f. field is also required so that a level, just low enough to avoid saturation, can be used. At resonance maximum power is absorbed from the r.f. field and this power loss can be detected electronically and a resonance signal observed on an oscilloscope or on a recorder. Fuller details of instrumentation are given in chapter three of this thesis.

1.6. Dependence of Resonance Signals on Chemical Environment

In the resonance equation, $\omega = \gamma H$, H is actually the field experienced by the nucleus, which in real situations is not quite the same as the applied field H_o, since small fields are generated by neighbouring electrons and nuclei; it is as a result of this fact that chemists have shown such an interest in the phenomenon of N.M.R.

These small internal magnetic fields are created by three different effects.

(a) The surrounding nuclei produce secondary fields at the nucleus of interest. In solids these fields are of the order of 10 gauss but in liquids and gases they are eliminated by the existence of random Brownian motions.

(b) Diamagnetic circulations induced in the electrons in the molecules by the applied magnetic field, give rise to secondary fields at the nucleus of the order of 0.1 - 0.01 gauss.

(c) Nuclear spin-spin interactions through the electrons give rise to secondary fields of the order 0.01 - 0.001 gauss.

Effects (b) and (c) are so small in comparison to (a) that, when discussing solids, they are ignored. In such cases the spectroscopy is called Broad-Line N.M.R. The compounds investigated in this thesis are solids so that it is this type of spectroscopy with which the following chapters are concerned. Effects (b) and (c), although very small, may be observed in liquids or in gases provided a high resolution N.M.R. spectrometer is available. High resolution spectroscopy will not be considered further[2,3].

If the nucleus has spin greater than $\frac{1}{2}$ then it may possess a quadrupole moment which can interact with electric field gradients generated by surrounding nuclei and electrons. Small quadrupolar interactions perturb the nuclear magnetic resonance energy, given by 1.3.4. These perturbation terms turn out to depend on m^2 and they cause the (2I+1) nuclear sub-levels to be unequally spaced. Since the normal selection rule for magnetic transition is $\Delta m = \pm 1$, 2I magnetic transitions, symmetrically distributed about the Larmor frequency, can be detected. If the perturbation is small the net result may be poorly resolved splitting or simply line broadening. Quadrupolar effects are dealt with more fully in a later chapter.

CHAPTER 2

DIPOLAR INTERACTIONS IN SOLIDS

2.1. Line Broadening

Each magnetic nucleus finds itself in a small local magnetic field, H_{local}, produced by the neighbouring nuclei. The direction of the local field differs from nucleus to nucleus, depending on the relative positions of the neighbouring nuclei in the lattice and on their quantum number m. The magnetic field of a magnetic dipole of moment μ at a distance r is of order μr^{-3} so that the field falls off rapidly with increase of r; only nearest neighbours make important contributions to H_{loc}. Hence instead of a sharp resonance, defined by 1.3.6, resonances are obtained at $\omega = \gamma(H_o \pm h_{loc})$ where h_{loc} is the field produced by each neighbouring nucleus. The net effect of many neighbouring nuclei is usally to broaden the resonance line — hence the title broad-line N.M.R. In addition to direct magnetic dipole effects other factors contribute to the width of resonance lines obtained from solids. They are the relaxation times, T_1 and T_2 and quadrupolar effects. Quadrupole interactions are discussed more fully in a later chapter. For the moment only magnetic dipole coupling between nuclei with spin quantum numbers of one half is considered.

2.2. Magnetic Dipolar Coupling of Two Identical Nuclei ($I=\frac{1}{2}$)

The classical expression for the energy of interaction between two magnetic moments μ_1, and μ_2 is [4]

$$E = \frac{\underline{\mu_1} \cdot \underline{\mu_2}}{r^3} - \frac{3(\underline{\mu_1} \cdot \underline{r})(\underline{\mu_2} \cdot \underline{r})}{r^5} \qquad 2.2.1$$

where r is the radius vector from μ_1 to μ_2.

The quantum mechanical Hamiltonian for the interaction is obtained from 2.2.1 by treating μ_1 and μ_2 as operators: $\mu_1 = \gamma_1 \hbar \underline{I}_1$ and $\mu_2 = \gamma_2 \hbar \underline{I}_2$. The angular momentum operators, $\underline{I}_1$ and $\underline{I}_2$ can be expressed in terms of their components I_x, I_y and I_z, and then I_x and I_y in terms of the shift operators I^+ and I^- which are defined by $I^{\pm} = I_x \pm iI_y$. When I^+ operates on a spin state it increases the spin quantum number, m, by one, and I^- has the effect of decreasing m by one. With these operators, the Hamiltonian corresponding to 2.2.1 becomes [5]

$$\mathcal{H}_d = \gamma_1 \gamma_2 \hbar^2 r^{-3} (A + B + C + D + E + F) \qquad 2.2.2$$

where $A = I_{z_1} I_{z_2}(1-3\cos^2\theta)$

$$B = -\tfrac{1}{4}\,(I_1^+ I_2^- + I_1^- I_2^+)(1-3\cos^2\theta)$$

$$C = -\tfrac{3}{2}(I_1^+ I_{z_2} + I_{z_1} I_2^+)\sin\theta\cos\theta . e^{-i\phi}$$

$$D = -\tfrac{3}{2}(I_1^- I_{z_2} + I_{z_1} I_2^-)\sin\theta\cos\theta . e^{i\phi}$$

$$E = -\tfrac{3}{4} I_1^+ I_2^+ \sin^2\theta . e^{-2i\phi} \qquad 2.2.3$$

$$F = -\tfrac{3}{4} I_1^- I_2^- \sin^2\theta . e^{2i\phi}$$

The energy due to interaction with the applied magnetic field, H_o, is given by the Hamiltonian

$$\mathcal{H}_z = -\gamma_1 \hbar H_o I_{z_1} - \gamma_2 \hbar H_o I_{z_2}$$

which corresponds to an interaction with a field of about 10^4 gauss in most experimental arrangements. The term $\gamma_1 \gamma_2 \hbar^2 r^{-3}$ in the dipolar expression corresponds to the interaction of a nuclear moment with a field of about 1 gauss. Hence the dipolar term can be treated as a small perturbation of the larger Zeeman term.

We are interested in this chapter in the case of two identical nuclei with spins of $\frac{1}{2}$, viz protons, in which case the direct Zeeman interaction energy is

$$E = -\gamma\hbar H_o m_1 - \gamma\hbar H_o m_2$$

where m_1 and m_2 are the eigenvalues of operators I_{z1} and I_{z2} respectively and can each be $\pm\frac{1}{2}$. There are therefore four eigenvalues of $\mathcal{H}_z$

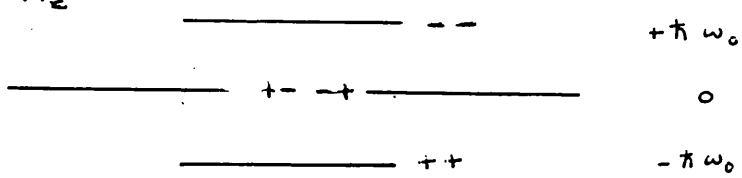

It is convenient to denote the eigenstate of $\mathcal{H}_z$ in which $m_1 = +\frac{1}{2}$ and $m_2 = -\frac{1}{2}$ by $|+-\rangle$. The two states $|+-\rangle$ and $|-+\rangle$ are degenerate with energy $E = 0$. The states $|++\rangle$ and $|--\rangle$ have respectively the energies $-\hbar\omega_o$ and $+\hbar\omega_o$, where again $\omega_o = \gamma H_o$. To determine the effect of the perturbation on each of these states we now consider each term in the perturbation expression 2.2.2. in turn.

Term A which is proportional to $I_{z1} I_{z2}$ obviously connects states $|m_1 m_2\rangle\ \langle m_1 m_2|$. Term B, proportional to $(I_1^+ I_2^- + I_1^- I_2^+)$ only connects $|m_1 m_2\rangle$ to $\langle m_1+1, m_2-1|$ and $\langle m_1-1, m_2+1|$. In other words B simultaneously flips one spin up and the other down, i.e. it connects $|+-\rangle$ and $|-+\rangle$. Terms C and D each flip one spin only and therefore join states differing by $\hbar\omega_o$. Terms E and F respectively

flip both spins up and down, connecting states separated by $2\hbar\omega_0$.

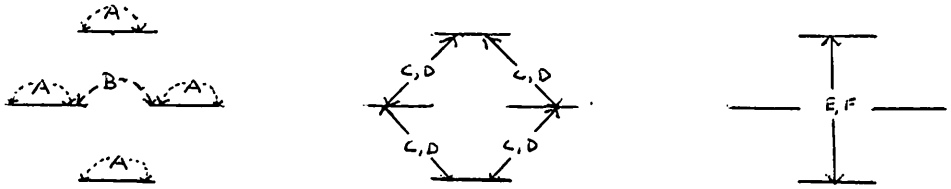

Figure 2.2.2

The effects of each perturbation term are shown in figure 2.2.2.

Terms C,D,E. and F obviously produce slight admixtures of the zero-order states into the exact states but it can be shown by second-order perturbation that the amount of admixture is small. This small admixture allows transitions which would otherwise be forbidden, i.e. transitions from $|++\rangle$ to $|--\rangle$ can take place. The situation can be summarised in figure 2.2.3.

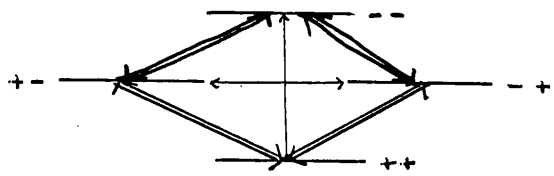

Figure 2.2.3

Strong transitions are indicated by a double arrow, the light arrows indicating the extra transition allowed due to dipolar admixture. As a consequence of this, very weak absorptions occur at $\omega=2\omega_0$ and $\omega=0$. The intensity of these absorptions is so minute, 10^{-6}% of the absorption intensity at $\omega=\omega_0$, that they may safely be disregarded, so that terms C,D,E and F can be dropped from the dipolar expression 2.2.2.

The remaining dipolar terms, A and B, can be combined to give the Hamiltonian, which can be termed $\mathcal{H}_d^0$

$$\mathcal{H}_d^0 = \gamma\hbar^2(2r^3)^{-1}(1 - 3\cos^2\theta)(3I_{z1}\,I_{z2} - \underline{I}_1\,\underline{I}_2) \qquad 2.2.4$$

Hence the total simplified Hamiltonian for an assembly of dipolar pairs is

$$\mathcal{H} = \sum_k(-\gamma\hbar H_0 I_{zk}) + \frac{1}{4}\gamma^2\hbar^2\sum_{j,k}\frac{1-3\cos^2\theta_{jk}}{r_{jk}^3}\left(3I_{zj}I_{zk} - \underline{I}_j\cdot\underline{I}_k\right) \qquad 2.2.5.$$

the factor $\frac{1}{4}$ being required since the sums over j and k would count each pair twice.

First order perturbation theory shows that, if a fixed radio-

frequency is employed, the dipolar interaction causes resonance peaks to appear at applied field strengths.

$$H = H_o \pm \tfrac{3}{2}\mu r^{-3}(3\cos^2\theta - 1) \qquad 2.2.6.$$

for a pair of identical nuclei. For non-identical nuclei the dipolar field is given by $\pm\mu r^{-3}(3\cos^2\theta - 1)$. The expression of interest in this chapter is the former; it holds exactly only for a single crystal in which the protons are paired and the pairs are remote from one another [4]. The spectrum consists of a pair of lines equally spaced about the resonance field, H_o, by an amount $\tfrac{3}{2}\mu r^{-3}(3\cos^2\theta - 1)$ where θ is the angle between the interproton vector and the magnetic field direction. From studies of angular variation of the splitting of the dipolar pair spectrum one can determine the magnitude and direction of $\underline{r}$.

2.3. Line Shape of Proton Resonance Signal of Polycrystalline Hydrates

If the specimen is polycrystalline then the interproton vectors are randomly distributed in space so that the spectrum is the sum of the spectra for the individual pairs, resulting in a smearing out of the fine structure. Since the orientation of the dipole pairs is isotropically distributed, the fraction of pairs for which θ lies in the interval $d\theta$ is $d(\cos\theta)$. Let $g(h)$ be the normalised line shape function describing the absorption signal as a function of field strength and let h be $(H-H_o)$, that is

$$h = \pm \tfrac{3}{2}\mu r^{-3}(3\cos^2\theta - 1) \qquad 2.3.1$$

The contribution of each of the two component lines for a single crystal to the spectrum for polycrystalline material is

$$g(h) = \tfrac{1}{2}\frac{d(\cos\theta)}{dh} \qquad 2.3.2$$

the factor $\tfrac{1}{2}$ entering because each of the two terms is equally probable. Expressing $\cos\theta$ as a function of h, using 2.3.1, one obtains for $g(h)$ in 2.3.2.

$$g(h) = (6\sqrt{3}\,\mu r^{-3})^{-1}\left[1 \pm h/(\tfrac{3}{2}\mu r^{-3})\right]^{-\frac{1}{2}} \qquad 2.3.3$$

The + sign is taken for $-\tfrac{3}{2}\mu r^{-3} < h < +3\mu r^{-3}$ and the − sign for $-3\mu r^{-3} < h < +\tfrac{3}{2}\mu r^{-3}$.

$g(h) = 0$ outwith the range $-3\mu r^{-3}$ to $+3\mu r^{-3}$ so that only this range needs to be considered.

The line shape obtained from 2.3.3. is shown as the dotted line in figure 2.3.1 for an isolated proton pair in a water molecule where $r = 1.58A$ and $\mu = 1.41033\times10^{-23}$ The peak separation, $3\mu r^{-3}$, is

Figure 2.3.1

Calculated proton magnetic resonance absorption line shape for a polycrystalline hydrate taking into account current neighbour interactions.

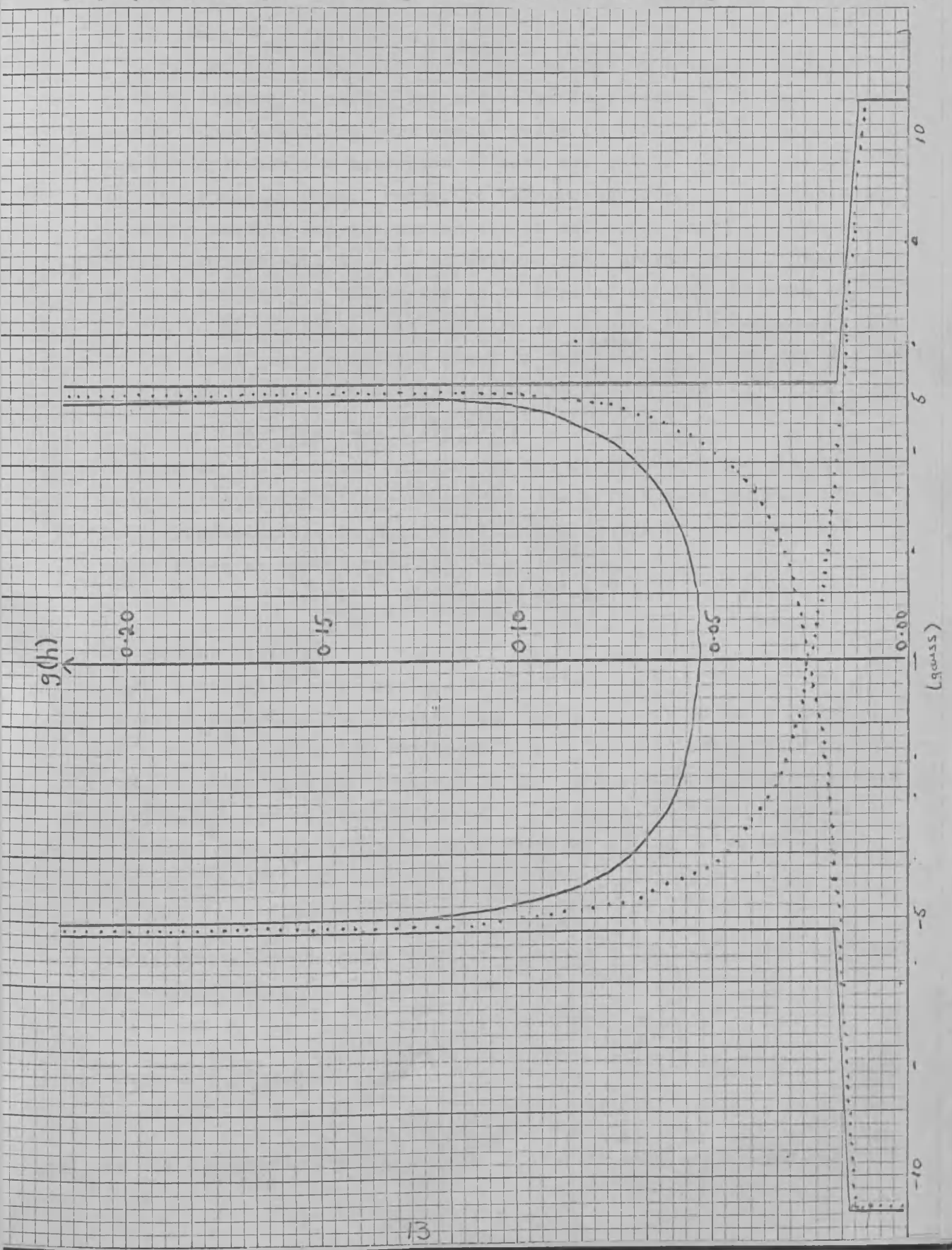

of the order of 10-20 gauss and the complete spectrum covers about 20-22 gauss in width.

So far the discussion has been confined to isolated pairs of nuclear dipoles, ignoring the effect of next nearest nuclear neighbours. This condition very nearly holds in the case of solid hydrogen[6], but for hydrates the interpair effects are not so small compared with the intrapair effects. Therefore the proton pairs are not isolated from one another and the components of each pair exert a small magnetic field, proportional to r^{-3}, at neighbouring proton pairs. The effect of each pair on its neighbours is to broaden out the spectrum defined by $g(h)$. If the broadening function is assumed to be Gaussian[7], then a line shape similar to that shown by the ~~full~~ dotted line in figure 4.3.8, say, is obtained. Gaussian distributions are of the form

$$Y = \frac{1}{\sigma\sqrt{2\pi}} \exp.\left[\frac{(X-P)^2}{2\sigma^2}\right]$$

where σ is the standard deiation of the distribution and P is the mean of the distribution. Therefore the effect next nearest neighbour broadening has is that the function $g(h)dh$ broadens out and contributes an amount equal to

$$\frac{1}{\beta\sqrt{2\pi}}\, g(h)dh.\ \exp\left\{\frac{-(h'-h)^2}{2\beta^2}\right\}$$

at another field h'.

β, the broadening parameter, is the standard deviation of the Gaussian distribution function and can be considered as a function of the splitting due to the so-far neglected next nearest neighbours. β is taken as $\frac{3}{2}\mu R^{-3}$ where R is the next nearest nuclear distance in ~~angstrom~~ centimetre units. Broadening at h increases the probability of finding a fine structure component between h' and $(h'+dh')$ by an amount

$$\frac{1}{\beta\sqrt{2\pi}}\, g(h)dh.\ \exp\left\{\frac{-(h'-h)^2}{2\beta^2}\right\}dh'$$

Therefore the total probability of finding a fine structure component between h' and $(h'+dh')$ is given by

$$C(h')dh' = C\int_{-3\mu r^{-3}}^{+3\mu r^{-3}} g(h)dh\ \exp\left\{-\frac{(h'-h)^2}{2\beta^2}\right\}dh'$$

where $C = 1/(\beta\sqrt{2\pi})$ and $\pm 3\mu r^{-3}$ are the limits of integration necessary

i.e. $$G(h') = C\int_{-3\mu r^{-3}}^{+3\mu r^{-3}} g(h).\exp\left\{-\frac{(h'-h)^2}{2\beta^2}\right\}dh \qquad 2.3.4$$

is the expression describing the absorption line shape when next

nearest neighbour broadening is considered, replacing the expression $\int_{-3\mu r^{-3}}^{+3\mu r^{-3}} g(h).dh$ before broadening. A number of acid hydrates contain the oxonium ion H_3O^+, which consists of three protons at the vertices of an equilateral triangle. The complicated theoretical analysis of the interactions of such a system has been performed[8] and the spectrum of a polycrystalline specimen of such a hydrate has a characteristic shape, from which r, the interproton vectors, can be calculated. Some "hydrates" may, in fact, contain hydroxyl groups rather than H_2O molecules and this possibility can be recognised from the line shape of the proton magnetic resonance signal. The closest H-H approach possible between hydroxyl groups is about 2.5Å, so that although the theoretical treatment is the same as for the true hydrate case the line width and peak separation, equal to $3\mu r^{-3}$, will be much less than in the H_2O case. In fact for OH dipole pairs $3\mu r^{-3}$ is about 2 gauss and this separation can seldom be detected because of next nearest neighbour broadening so that one obtains only one broad absorption signal. Fig. 2.3.2 shows spectra from polycrystalline samples of $CaSO_4 2H_2O$ [4], $HNO_3.H_2O$ [9] and β-UO_3 H_2O [10] and demonstrates that only the first compound contains discrete H_2O molecules, the others being more accurately written $H_3O^+NO_3^-$ and $UO_2(OH)_2$ respectively.

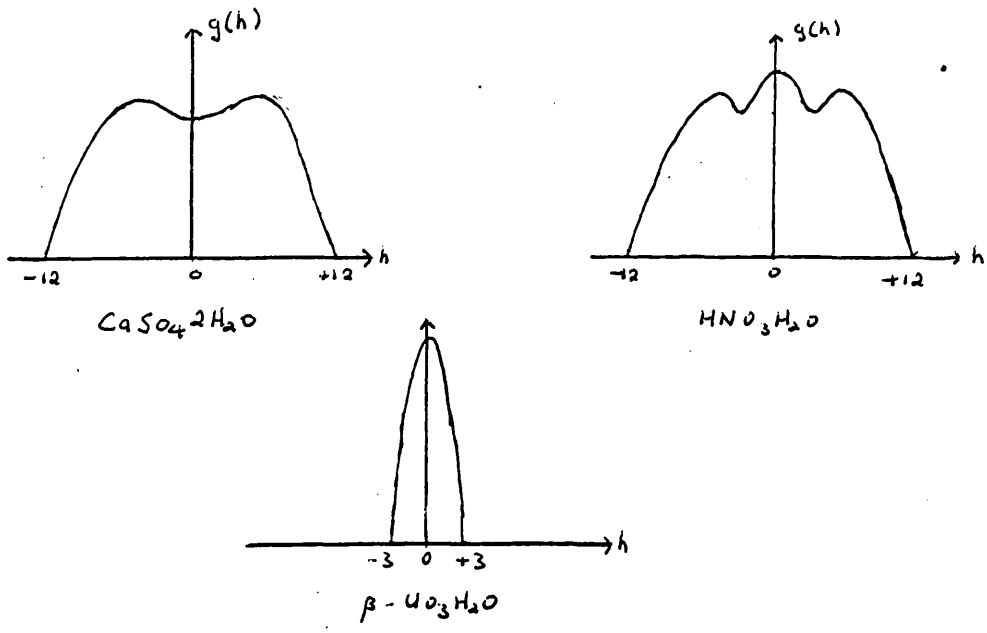

Figure 2.3.2

In more complicated systems calculation of line shapes becomes formidable and line structure becomes so complex as to be unresolved in detail . Although the line shape for general systems cannot be calculated the moments of the spectrum can be readily calculated. Clearly the width and shape of an absorption line depends on the magnetic interactions between neighbouring nuclei and hence upon the configuration of atoms in the immediate vicinity of a magnetic nucleus. Therefore not only the distances and angles characteristic of the local configuration are involved but also the motion of the nucleus and its neighbours. One can infer something about the configuration and motion near a resonant nucleus from a study of the shape of the absorption line by means of the method of moment..

2.4. Second Moment of an Absorption Line

The nth moment of an absorption line is defined as

$$S_n = \int_{-\infty}^{\infty} h^n g(h)dh \qquad 2.4.1$$

where $g(h)$ is the normalised amplitude of the curve at the position where the field strength is h gauss from the centre. Since $g(h)$ is an even function for magnetic dipolar broadening the odd numbered moments are zero. Van Vleck has calculated the second and fourth moments in the general case.[11] The fourth moment is a rather complicated expression and is not much used. For a crystal containing only one species of magnetic nucleus his result for the second moment is

$$S_2 = \frac{3}{2}\mu^2 N^{-1} \sum_{j>k} (3\cos^2\theta_{jk}-1)^2 r_{jk}^{-6} \qquad 2.4.2$$

where θ_{jk} is the angle between r_{jk}, the length of the vector joining nuclei j and k, and H_o, the applied magnetic field. N is the number of nuclei taking part in the resonance for which line-broadening is being considered, say the number of resonant nuclei per unit cell. If the specimen is polycrystalline the spectrum is the sum for the assembly of isotropically oriented constituent crystals and its second moment is therefore the average of the second moments of the individual crystals. The isotropic average of $(3\cos^2\theta - 1)^2$ is $\frac{4}{5}$, so that 2.4.2. becomes

$$S_2 = \frac{6}{5}\mu^2 N^{-1} \sum_{j>k} r_{jk}^{-6} \qquad 2.4.3$$

If the crystal contains magnetic nuclei, other than those at resonance, Van Vleck's second moment formula 2.4.2. contains the

following additional term

$$\tfrac{1}{5}N^{-1} \sum_{j,f} \mu_f^2 r_{jf}^{-6} (3\cos^2\theta_{jf} - 1)^2 \qquad 2.4.4$$

where μ_f is the magnetic moment of non-resonant nucleus, f, r_{jf} is the length of the vector joining nuclei j and f and θ_{jf} is the angle which this vector makes with the applied magnetic field, h_o. For a polycrystalline specimen , $(3\cos^2\theta - 1)^2$ is again relaced by its mean value $\frac{4}{5}$, so that the complete second moment formula becomes

$$S_2 = \frac{6}{5}\mu^2 N^{-1} \sum_{j>k} r_{jk}^{-6} + \frac{4}{15} N^{-1} \sum_{j,f} \mu_f^2 r_{jf}^{-6} \qquad 2.4.5$$

Therefore the second moment of a spectrum whose width is due to dipolar broadening can be calculated from a knowledge of the relative positions of all nuclei of non-zero spin in the crystal lattice and of their nuclear magnetic moments. Since magnetic moments are known for most nuclei, information concerning the disposition of the nuclei in the crystal lattice may be obtained from the experimentally determined spectrum, via its second moment.

The second moment of a spectrum is defined, by 2.4.1, as

$$S_2 = \int_{-\infty}^{\infty} h^2 g(h)dh \qquad 2.4.6$$

and is equivalent to the mean square width of the absorption line about its centre. If g(h) is not normalised then

$$S_2 = \int_{-\infty}^{\infty} h^2 g(h)dh \Big/ \int_{-\infty}^{\infty} g(h)dh \qquad 2.4.7$$

Because broad-line spectra are generally very broad (figs. 2.3.1 and 2.3.2), resonances can seldom be seen on an oscillograph. Most broad signals are recorded as the first derivative of the absorption signal, using audiomodulation and phase-sensitive amplification. The experimental techniques involved in the presentation of broad-line resonance spectra are the subject matter of the following chapter. The second moment of the absorption signal may, however, be computed directly from the first derivative spectrum, since partial integration of 2.4.7 gives

$$S_2 = \frac{1}{3} \int_{-\infty}^{\infty} h^2 \frac{dg(h)}{dh} \cdot dh \Big/ \int_{-\infty}^{\infty} h \frac{dg(h)}{dh} \cdot dh \qquad 2.4.8$$

where $\frac{dg(h)}{dh}$ is the amplitude of the derivative curve at the position where the field is h gauss from the centre.

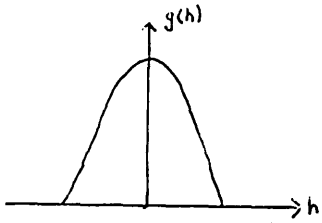

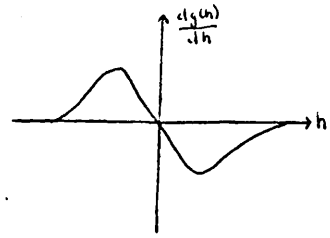

2.4.8 is approximately equal to

$$S_2 \approx \frac{1}{3} \sum_{\Delta h \to 0} h^3 \frac{dg(h)}{dh} \Delta h \Big/ \sum_{\Delta h \to 0} h \frac{dh(h)}{dh} \Delta h \qquad 2.4.9$$

where Δ h is a very small field interval, say 0.5 gauss. If Δ h is small enough then

$$S_2 \approx \frac{1}{3} \sum_{\Delta h \to 0} h^3 \frac{dg(h)}{dh} \Big/ \sum_{\Delta h \to 0} h \frac{dg(h)}{dh} \qquad 2.4.10$$

and this expression is generally used to obtain the second moment from a first derivative spectrum.

So that useful crystallographic information can be extracted from broad-line spectra, accurate values of second moments must be obtained from spectra. In this connection there are four or five notes on essentialexperimental requirements.

(i) the spectra should not be unduly broadened by magnetic field inhomogeneity.

(ii) the r.f. power level should be low enough to avoid saturation, which causes distortion, if not total loss, of the signal.

(iii) the field modulation amplitude, used to produce the first derivative line shape, must be small compared with the line width. Modulation broadening, if unavoidable, can be accounted for by using the relationship [12]

$$S_2 = S_2' - \tfrac{1}{4} h_m^2 \qquad 2.4.11$$

where S_2' is the measured second moment, S_2 is the true second moment and h_m is the amplitude of audiomodulation used in recording the derivative curve (in gauss)

(iv) the ratio of the signal intensity to the intensity of the background of random electrical fluctuations generated by the spectrometer, the signal to noise ratio, must be good since S_2 can be greatly influenced by the wings of the absorption line where the signal is weak but h^3 is relatively large.

(v) the positions of the atoms in the crystal lattice must remain fixed. The following section discusses the effects of

molecular motions on spectra and hence on their second moments. In order that 2.4.5 or the simpler 2.4.3. can be used, it is therefore essential to work at temperatures sufficiently low that such molecular motions do not take place.

2.5. Motional Narrowing of Resonance Line Widths

In solids groups of atoms usually undergo rotational motion about one or more axes with frequencies which increase with temperature. This motion modifies the interactions between nuclear dipoles and causes considerable changes in the resonance spectrum. The limit of this motion is that undergone by liquids and gases, whose random motions result in a very narrow absorption line, the dipolar interactions being eliminated. In general, motion results in narrowing of the spectrum. A narrowing of absorption lines with increasing temperature has been observed in many solids and has been ascribed to molecular motions within crystal lattices [13].

Molecules are constrained to their equilibrium positions in the crystal by intermolecular forces and rotation of any molecule from one equilibrium position to another is restricted by a potential barrier, of height U. A number of molecules, proportional to exp.(-U/RT), where R is the gas constant per mole, have sufficient energy at any one instant to surmount the barrier, so that there is a continual reorientation of all the molecules in the lattice. One can associate with this process a rate of molecular transitions from one equivalent position to another, characterised by a reorientation rate ν_c or a correlation time τ_c. These parameters are related by [14]

$$\nu_c = (2\pi\tau_c)^{-1} \qquad 2.5.1$$

τ_c and ν_c can be related to the energy barrier, U, by equations of the form

$$\tau_c = \tau_0 \exp(+U/RT) \qquad 2.5.2a \qquad \nu_c = \nu_0 \exp(-U/RT) \qquad 2.5.2b$$

where τ_0 and ν_0 are constants.

Clearly as the temperature increases, τ_c decreases and ν_c increases. The width of an absorption line can be related to the reorientation rate by the expression [15]

$$(\delta\nu)^2 = A^2(2/\pi)\tan^{-1}\left[\alpha(\delta\nu/\nu_c)\right] \qquad 2.5.3$$

$\delta\nu$ is the line width on a frequency scale. α is a factor of the

order of unity introduced to take account of inaccuracies in defining $\delta\nu$ with respect to the line shape. $\delta\nu$, or its magnetic field scale equivalent δH, is taken as the separation between outermost points of maximum and minimum slope of the absorption curve. A is the width of the absorption line for a rigid lattice, so that $\nu_c \rightarrow 0$ as $\delta\nu \rightarrow A$. As the reorientation rate increases and approaches the rigid lattice width, $\delta\nu$ decreases. Since A is usually of the order of 10^4 - 10^5 c/s, the spectrum is narrowed by molecular reorientation at frequencies which are very low on a thermodynamic scale. Hence information about energy barriers to rotations of molecules in crystals can be obtained by studying line widths as a function of temperature.

The contributions to the resonance absorption line shape from the dipolar coupling between two nuclear spins has been shown to be proportional to $(3\cos^2\theta - 1)$ where θ is the angle which the internuclear vector makes with the applied field. If the molecule of which these spinning nuclei are part is rotated around an axis ON which makes an angle α with the applied field and an angle γ with the internuclear vector, $(3\cos^2\theta - 1)$ must be replaced by $\overline{(3\cos^2\theta - 1)}$ and this average value must be taken over all the values of θ during a rotation. Using the addition theorem for spherical harmonics [16] one gets

$$\overline{(3\cos^2\theta - 1)} = \tfrac{1}{2}(3\cos^2\gamma - 1)(3\cos^2\alpha - 1)$$

Thus the spectrum consists of two lines occuring at field strengths [14]

$$H = H_0 \pm \tfrac{3}{4}\mu r^{-3}(3\cos^2\gamma - 1)(3\cos^2\alpha - 1) \qquad 2.5.4$$

rather than at fields given by 2.2.6 for a rigid system.

If the axis of reorientation ON is perpendicular to the internuclear vector, so that $\gamma = 90^\circ$, as is commonly the case, 2.5.4 becomes

$$H = H_0 \pm \tfrac{3}{4}\mu r^{-3}(3\cos^2\alpha - 1) \qquad 2.5.5$$

which is similar in form to 2.2.6; the maximum splitting, however, is only half that for the rigid system. The similarity is more complete for a polycrystalline specimen since random orientation of the constituent crystals provides all values of either θ or α. For completely random rotations as in liquids and gases it turns out that $\overline{\cos^2\theta}$ over a sphere equals $\frac{1}{3}$ so that $\overline{(3\cos^2\theta - 1)} = 0$ and only one sharp resonance line appears.

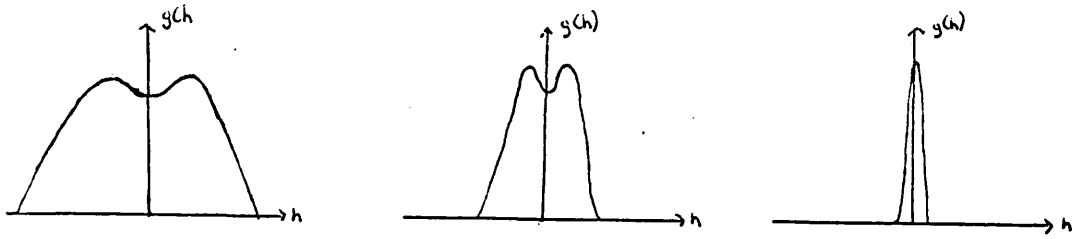

rigid system hindered rotation complete free rotation

Figure 2.5.1

For more general and complicated systems it is again necessary to turn to Van Vleck's second moment formula which for a single crystal has been shown to be

$$S_2 = \frac{3}{2}\mu^2 N^{-1} \sum_{j>k} \frac{(3\cos^2\theta_{jk}-1)^2}{r_{jk}^6} + \frac{1}{8}N^{-1} \sum_{j,f} \frac{\mu_f^2(3\cos^2\theta_{jf}-1)^2}{r_{jf}^6} \qquad 2.5.6$$

When motion occurs, 2.5.6 must be amended by averaging $(3\cos^2\theta - 1)$ as above. It is convenient at this stage to divide the second moment into an intramolecular part σ_1 and an intermolecular part σ_2. Hence, introduction of 2.5.3 into 2.5.6 leads to

$$\sigma_1 = \frac{3}{8}\mu^2 N^{-1}(3\cos^2\alpha - 1)^2 \sum_{j>k}(3\cos^2\gamma_{jk}-1)^2 . r_{jk}^{-6} + \frac{1}{12} N^{-1}(3\cos^2\alpha - 1)^2 \sum_{j,f} \mu_f^2(3\cos^2\gamma_{jf}-1)^2 . r_{jf}^{-6} \qquad 2.5.7$$

If the material is polycrystalline, there is an isotropic distribution of axes of reorientation and the factor $(3\cos^2\alpha - 1)^2$ must be replaced by its mean value of $\frac{4}{5}$, so that 2.5.7 becomes

$$\sigma_1 = \frac{3}{10}\mu^2 N^{-1} \sum_{j>k}(3\cos^2\gamma_{jk}-1)^2 . r_{jk}^{-6} + \frac{1}{15} N^{-1} \sum_{j\ f} \mu_f^2(3\cos^2\gamma_{jf}-1)^2 r_{jf}^{-6} \qquad 2.5.8$$

Comparison of 2.5.8 with 2.4.5 for a rigid structure shows that each term in the intramolecular contribution is reduced by a factor of

$$\tfrac{1}{4}(3\cos^2\gamma_{jk}-1)^2$$

This factor decreased from unity (when $\gamma_{jk} = 0^\circ$) to zero (when $\gamma_{jk} = 54^\circ 44'$) and increases again to $\frac{1}{4}$ (when $\gamma_{jk} = 90^\circ$).

Although the reduction in σ_1 caused by molecular reorientation may be calculated fairly simply, the reduction for the intermolecular contribution is more complicated since it must be remembered that during motion r_{jk} varies as well as θ_{jk}. Therefore a reduction of total second moment by a factor greater than 4 can be observed

as a particular molecular motion sets in as a result of the temperature of the polycrystalline sample being raised. Use of 2.5.2b and 2.5.3 allows the energy barrier to the motion to be calculated from a knowledge of the transition temperature and reduced line width. Frequently a large change in the second moment is witnessed as the sample temperature is increased. This can be explained by assuming that the molecules undergo reorientations which are almost isotropic. Such motions cause intramolecular local fields to average to zero, i.e. σ_1 becomes zero, but the intermolecular local fields do not average to zero, so that the resultant second moment is due to σ_2 only. The only way in which σ_2 can average to zero is for the centres of mass to move; this is the situation in liquids and gases. The resonance lines for some solids become extremely narrow at high temperature and the only explanation possible is that the molecules (or atoms) diffuse through the lattice [17].

The proton magnetic resonance spectrum of a true-hydrate has a second moment of about 28 gauss^2 when molecular motion is absent, and has a derivative line shape similar to that in figure (a) below. Should, instead, the species H_3O^+ or OH be present in the solid phase of a "hydrate", then they would contribute derivative spectra resembling those of figure (b) or (c) respectively to the overall observed spectrum. If the "hydrate" contains both H_2O and OH species in the solid state, the rigid lattice spectrum is superposition of spectra (a) and (c) in the ratio of the number of water protons to hydroxyl protons.

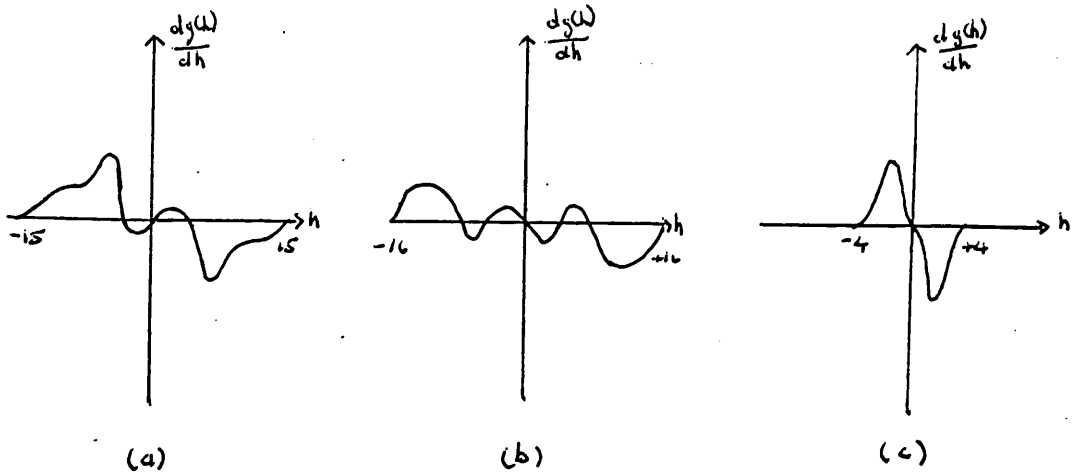

Figure 2.5.2.

β-$UO_3 2H_2O$ [19] is an example of a hydrate of this kind. The proton magnetic resonance derivative spectrum of this compound at 77°K is of the form shown by the full line in figure 2.5.3 and it shows immediately that the compound cannot be formulated as above. This conclusion is substantiated by the observation that second moment is 20 gauss, a value which is considerably less than that expected for a true hydrate, given by the dotted line of figure 2.5.3. It was shown that the spectrum obtained agrees with a ratio of (^1H in H_2O)/(^1H in OH) of 3 so that the compound is better written as $U_2O_5(OH)_2\ 3H_2O$.

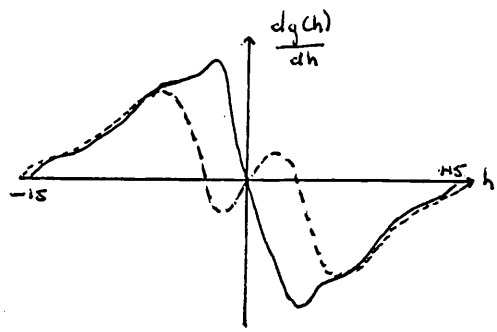

Figure 2.5.3

If the value for the ratio (^1H in H_2O)/(^1H in OH) is infinity (true hydrate case) then S_2 = 28 gauss^2. If this ratio, Q, is zero (pure OH case) then S_2 = 4 gauss^2. Obviously for values of Q between 0 and ∞, S_2 will lie between 4 and 28 gauss^2. The uranium oxide dihydrate example above has shown that for Q = 3, S_2 is about 20 gauss^2. A value of about 14 gauss^2 is expected for S_2 if Q = 1. This result can be obtained theoretically by treating the line shape function expression, 2.3.4, as a sum of two parts

$$G(h') = 0.5G_1(h') + 0.5G_2(h') \qquad 2.5.9$$

where $G_1(h')$ is the normalised line shape function for the water of crystallisation and $G_2(h')$ is the normalised line shape function for the proton in OH groups. $G_1(h')$ and $G_2(h')$ are themselves of the form of 2.3.4. and their derivatives, more useful for comparison with the experimental spectra, are given by

$$\frac{dG_1(h')}{dh'} = C_1 \int_{-3\mu r_1^{-3}}^{+3\mu r_1^{-3}} (h-h')g_1(h) \exp\left[\frac{-(h'-h)^2}{2\beta_1}\right] .dh$$

$$\frac{dG_2(h')}{dh'} = C_2 \int_{-3\mu r_2^{-3}}^{+3\mu r_2^{-3}} (h-h').g_2(h) \exp\left[\frac{-(h'-h)^2}{2\beta_2}\right] dh \qquad 2.5.10$$

The meanings of the terms in 2.5.10. are the same as given in connection with 2.3.4. r_1 is the interproton distance with the water molecules and lies within the limits $1.53A^{o} < r_1 < 1.65A^{o}$; r_2 is the interproton distance with the system (H -O ...H-) and can only have values $2.2A^{o} < r_2 < 2.7A^{o}$. R, the closest distance of approach of a neighbouring pair of protons, can have values $2.2A^{o} < R < 2.7A^{o}$. Using these parameters in equation 2.5.10 and then in 2.5.9. a line shape can be obtained for such a situation and a value for the second moment can be found in the manner described in section 2.4. The figure obtained, 12 gauss^2, is a lower limit for S_2 since intermolecular proton-proton vectors contribute to the second moment but are not included in the above theoretical treatment. Accurate knowledge of the crystal structure is required for calculation of the intermolecular contribution. This procedure is applied in reverse when one is interested in determining the value of Q and hence the correct molecular representation of a hydrate. One uses the line shape function expression

$$G(h') = w_1G_1(h') + (1-w_1)(G_2(h')) \qquad 2.5.11$$

in place of 2.5.9., where w_1 is the fraction of total protons present in water of crystallisation. Clearly $Q = \frac{w_1}{1-w_1}$. In such an experiment one has a derivative spectrum line shape and second moment and these are capable of solving 2.5.11 for w_1, r_1, r_2, β_1 and β_2. The observed derivative spectrum is scaled by integration and then normalisation of the resultant absorption line. A family of curves of $G_1(h')$ and $G_2(h')$ can now be calculated for selected values of r_1, β_1 and r_2 and β_2 within the limits given for these parameters. Now the system (H -O ...H) does not contribute to the derivative curve for $h' \geqslant 6.5$ gauss, so that by concentrating on the part of the spectrum in the range 7 gauss $\leqslant h' \leqslant$ 15 gauss, information concerning the water molecules only is obtained and hence w_1, r_1 and β_1.

Experience has shown that for chemically reasonable values of r_1 and β_1 all calculated $dG(h')/dh'$ curves pass through the point

$(h' = 11.)$ gauss ; $dG_1(h')/dh' = 0.0041 + 0.0003)$

This enables w_1 to be estimated, because from 2.5.11

$$w_1 = \frac{G(h')}{G_1(h')} \text{ in the range } 7 \text{ gauss} \leq h' \leq 15 \text{ gauss.}$$

$$\text{i.e. } w_1 = \left[dG(h')/dh'\right]_{11} / 0.0041 \qquad 2.5.12$$

where $dG(h')/dh'_{11}$ is the magnitude of the observed normalised derivative curve at $h' = 11$ gauss. Having found w_1, the curves $dG_1(h')/dh'$ calculated for a range of values of r_1 and β_1 are scaled down in the ratio w_1, compared with the observed derivative and the magnitudes of r_1 and β_1 obtained by fitting the observed curve to the collection of calculated curves.

Having thus determined the contribution from water of crystallisation to the line shape function, the contribution arising from (H-O ...H) can be obtained by subtraction from the observed normalised curve. The resultant difference curve can then be analysed in a manner similar to that outlined for w_1, r_1, and β_1, to yield r_2 and β_2.

This is the manner in which the problem of the representation of the hydrates of magnesium carbonate will be tackled. Information concerning the onset and nature of molecular motion in these hydrates and the energy barriers to their motions will also be discussed.

It is necessary, first, to deal with the instrumentation involved in detecting and presenting a broad-line resonance signal.

CHAPTER 3

INSTRUMENTATION IN BROAD-LINE NUCLEAR MAGNETIC RESONANCE

3.1. General Requirements

The resonance condition, $\omega_0 = \gamma H$, is detected by the effect of a small oscillating radiofrequency field, $2H_1 \cos \omega t$ applied to the material perpendicular to the direction of the static field, H. The frequency ω of the oscillating field is determined by the relationship

$$\omega = (LC)^{-\frac{1}{2}}$$

where L is the inductance of the sample coil and C is the capacitance of the radiofrequency generator. At resonance there is an inductance change induced in the coil which causes a change in the r.f. voltage across the coil equal to

$$\Delta V = \xi \Lambda \, 8\pi H_1 \, \omega \left(-\chi' \sin \omega t + \chi'' \cos \omega t\right) \qquad 3.1.1$$

where ξ is the filling factor denoting the proportion of the effective coil area occupied by material, Λ is the area-turns value of the coil, and χ' and χ'' are respectively the real and imaginary components of the susceptibility, χ, of the material. Bloch has derived expressions for χ' and χ'' in terms of r.f. power level, ω, T, and Z the saturation factor, and typical plots as a function of frequency are [20]

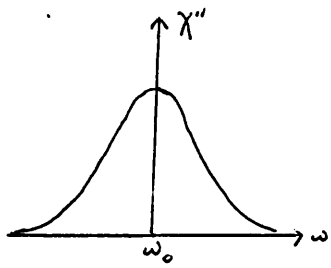

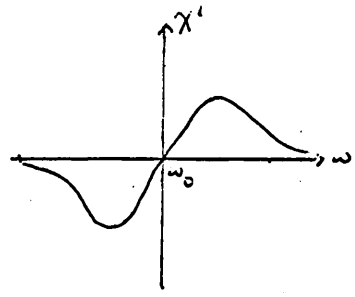

The marginal oscillator method of detection of nuclear resonances gives a pure absorption signal, proportional to χ''. The specimen is contained in a cylindrical coil placed with its axis perpendicular to the direction of the steady magnetic field. This coil and a condenser form a parallel tuned combination in the grid circuit of a radiofrequency oscillator and nuclear resonances are detected through a change in the level of oscillations.

The super-regenerative oscillator-detector which is characterised

by the repeated build-up and decay of its oscillations, also detects only changes in χ''. In this type of oscillator the change induced in the tank coil inductance at resonance causes the energy of the radiofrequency pulses to change. A simple super-regenerative oscillator is unsuitable for studies of line shapes of broad-line N.M.R. spectra since its output is complex and the detector response is not linear. Such oscillators can, however, be modified so that line shape studies can be performed [21]. More will be said about this type of oscillator in later chapters.

Other methods of detection are the bridge and the cross-coil methods, both of which require careful control to obtain a response proportional to either χ'' or χ' at resonance.

Broad-line N.M.R. signals are relatively weak and it is important that the ratio of signal strength to background oscillator and thermal "noise" be as large as possible. The following techniques are used so that the signal-to-noise ratio, S/N, of the displayed resonance is optimum.

The signal, proportional to χ'', is audiomodulated by superimposing a sinusoidal fluctuation $h_m \cos \omega_m t$ onto the static magnetic field. This field modulation is effected by passing an audiofrequency current through additional coils attached to the magnet. The modulation frequency is generally in the range 0 - 300 c/s, and if the modulation amplitude h_m is much less than the resonance absorption line width, a sinusoidal output with amplitude proportional to $d\chi''/dH$ is obtained, as the magnetic field is swept through the resonance value. An output proportional to $d\chi''/d\nu$ is obtained if frequency modulation and frequency sweep are employed. This method of modulation and sweep is generally avoided, where possible, since simultaneous optimisation of oscillator sensitivity would be required as the frequency is altered.

The audiosignal output from the oscillator, at frequency ν_m, together with the background of random r.f. and a.f. noise, is passed through a narrow-band amplifier which amplifies only frequencies in the neighbourhood of ν_m, thus rejecting a large proportion of the noise. The S/N ratio is further improved by passing the amplifier output through a phase-sensitive detector. This device

operates by mixing the amplifier output with a reference signal of frequency ν_m. The mixed d.c. output from the phase-sensitive detector can be shown to be proportional to $a_1 \cos\phi$ where a_1 is the component of signal voltage of fundamental frequency ν_m, and ϕ is the phase of this component with respect to that of the reference frequency. The maximum d.c. voltage is obtained when the two mixing signals are in phase. A phase-shifter must, therefore, be incorporated into the phase-sensitive detector. The time constant, τ secs, of the rectifying circuit imposes a bandwidth of τ^{-1} c/s on the detector so that a narrow range of noise frequencies are passed to the detector output. Thus substantial S/N enhancement results from the use of time constants of the order of 1 second. The d.c. signal, together with the much reduced level of noise, can be displayed on a d.c. meter or recorder.

3.2. The Broad-Line Proton Magnetic Resonance Spectrometer

The block diagram of the spectrometer is shown below, in figure 3.2.1. Figures 3.2.2 and 3.2.3 show some of the components of the spectrometer. The magnet, 1 of figure 3.2.3, is an A.E.I. electro-magnet capable of generating fields of up to 14,500 gauss.

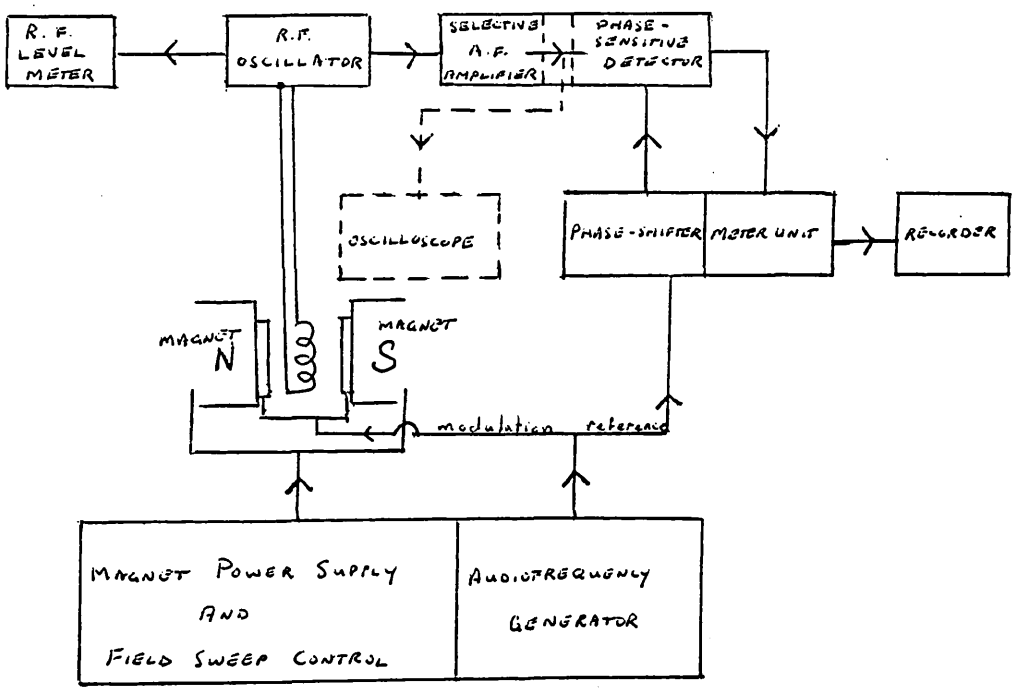

Figure 3.2.1.

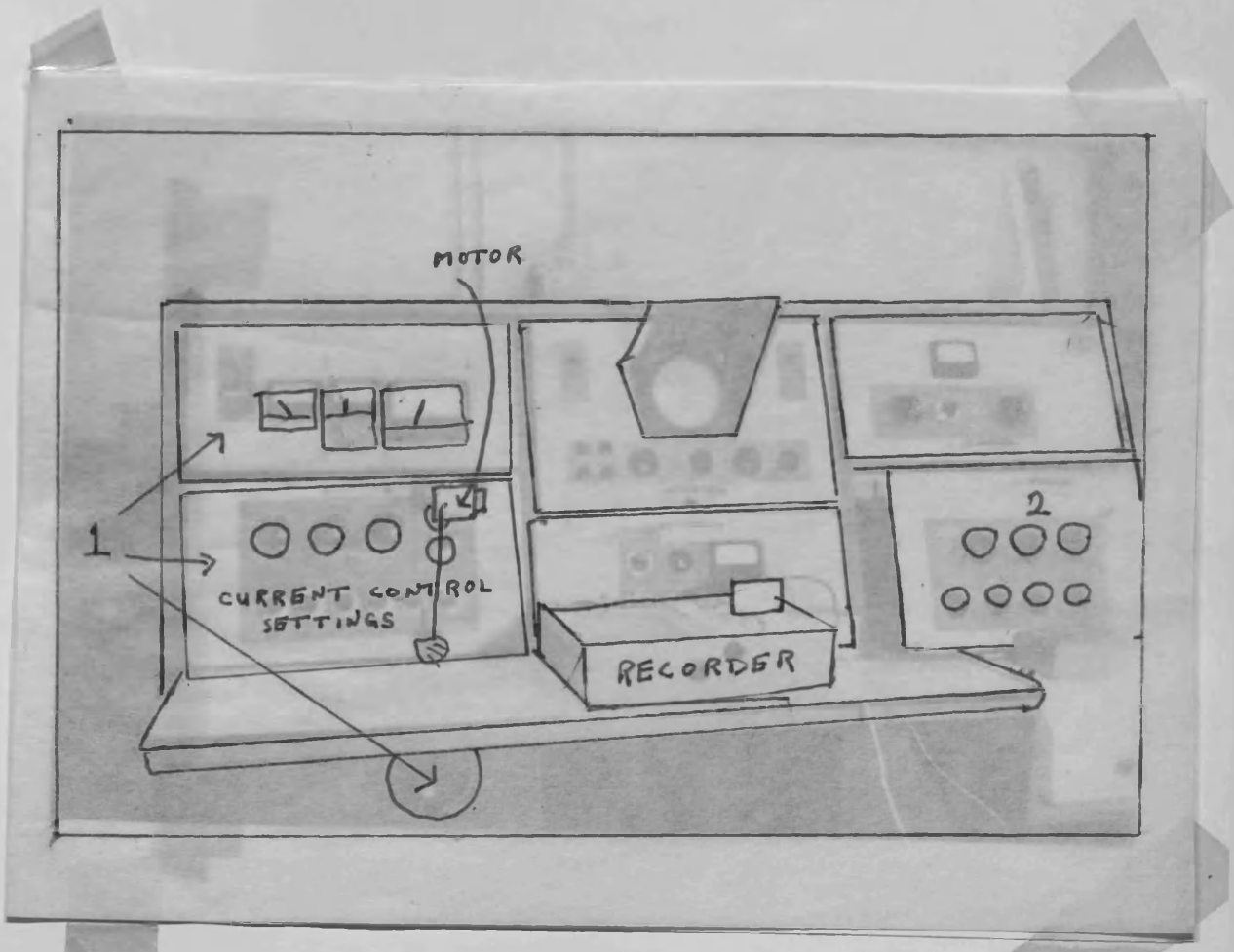

Figure 3.2.2.

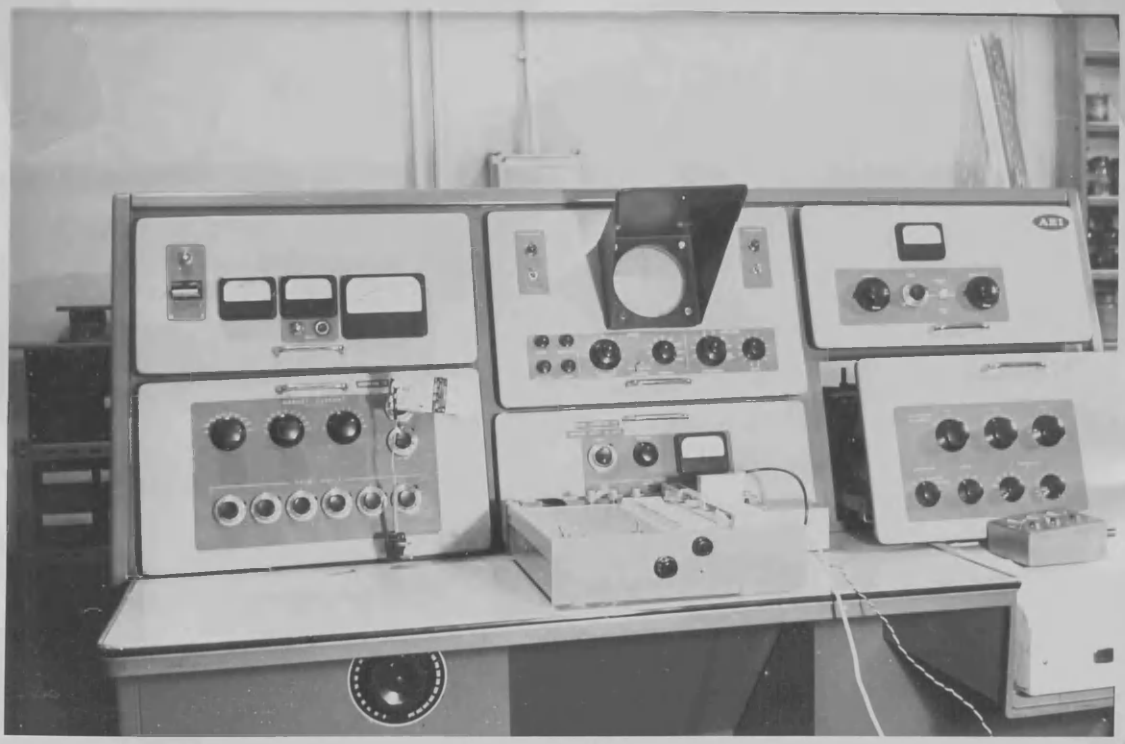

Figure 3.2.2.

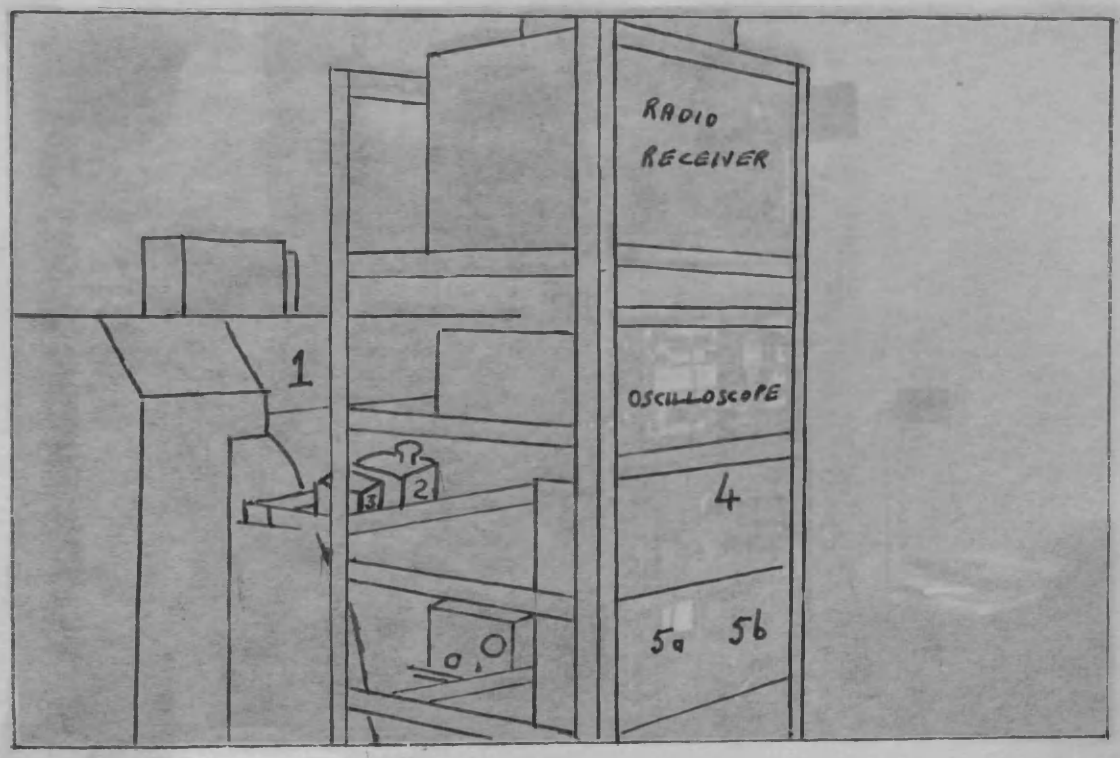

FIGURE 3.2.3.

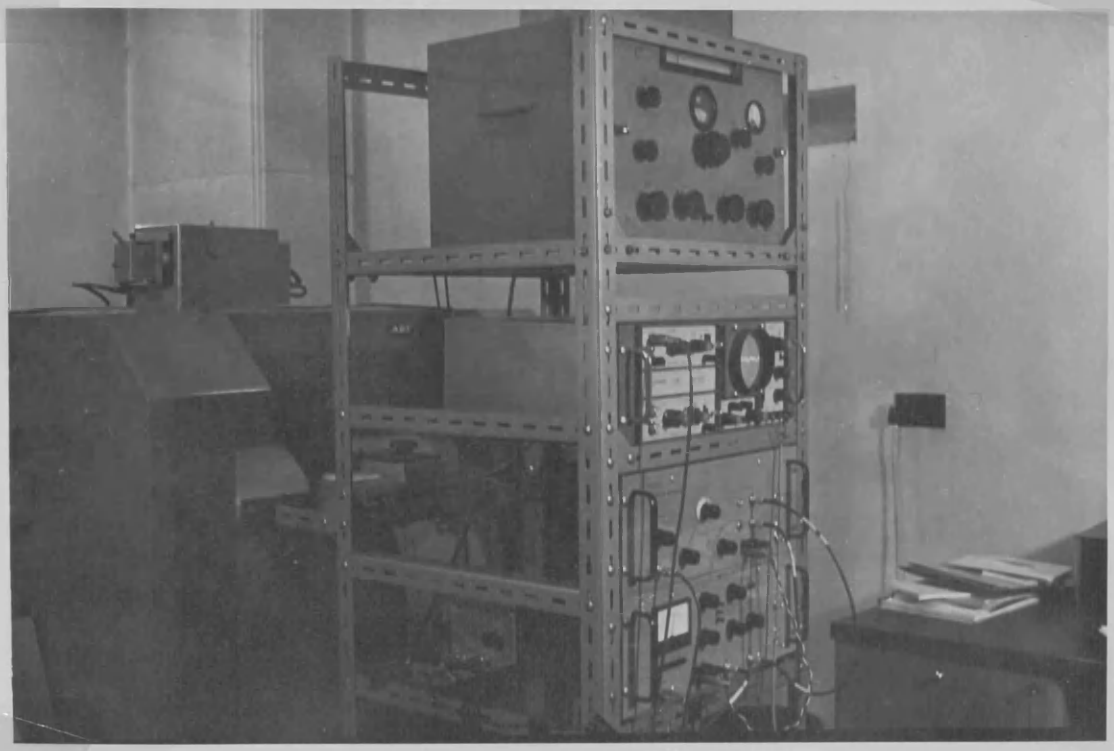

FIGURE 3.2.3.

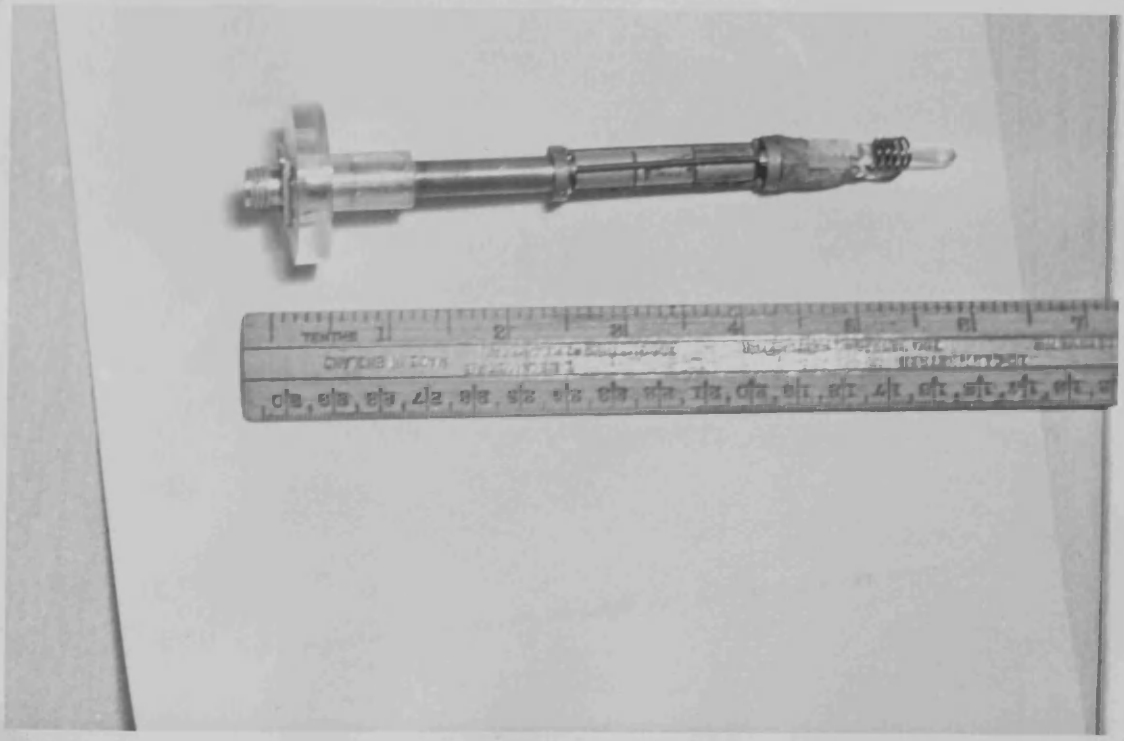

Figure 3.2.4.

Field sweep was achieved by slowly changing the current being supplied to the magnet coils. As a sweep width of 40 - 50 gauss is required to cover a broad-line proton resonance signal, a slowly rotating motor was made to drive the shaft of one of the finer field current-setting helipots, shown in figure 3.2.2. With a $\frac{1}{2}$ rev/min. motor a sweep rate of about 2 gauss/min. is obtained.

A probe insert, comprising a coil assembly, shown in figure 3.2.4, and a dewared insert, was constructed to fit exactly into the A.E.I. probe unit. The coil, five turns of enamelled copper wire of standard guage 26 is 7m.m. long and 7m.m. in diameter. A coaxial lead connects the coil assembly to the r.f. oscillator.

The oscillator, 2 of figure 3.2.3, supplied by Newport Instruments Ltd., is based on a design by Robinson [22]. It consists of an r.f. amplifier followed by a limiter, block diagram figure 3.2.5. With the probe insert described above, the oscillator could be tuned, by means of a variable condenser, over the range 16.5 - 30 Mc/s. The level of oscillation of the oscillator is controlled by varying the anode voltage of the limiter valve and is monitored on a microameter, 3 of figure 3.2.3. Resonances are detected as small changes in the r.f. level.

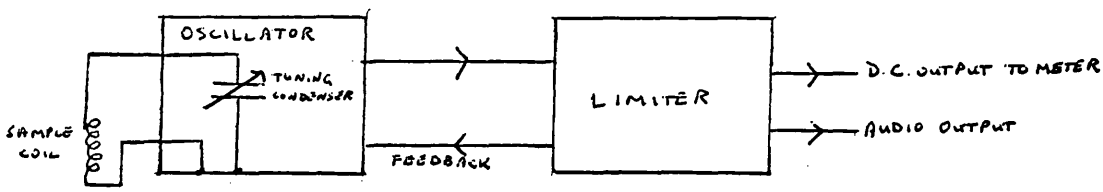

Figure 3.2.5

The output from the oscillator, comprising signal at the modulation frequency plus noise, is passed through a Brookdeal Lock-In Amplifier and Meter Unit, 4 and 5a of figure 3.2.3, in which the signal is selectively amplified and phase-sensitive detected, and the d.c. voltage output from the Meter Unit is displayed on a Servo-scribe recorder.

The audiosignal can be monitored on an oscilloscope just before the phase-sensitive detector stage. The reference for the phase-sensitive detector is taken from the A.E.I. audiofrequency generator and is passed through a Brookdeal Phase-Shifter Unit, 5b of figure 3.2.3, so that the two mixing signals can be phased for optimum output.

In most broad-line proton magnetic resonance investigations the temperature of the sample must be altered and accurately measured. In this spectrometer arrangement a stream of dry nitrogen gas is passed over the sample in the dewared probe insert. The temperature is raised by passing the gas over a heating coil and is lowered by passing the gas through a copper spiral immersed in a bath of liquid nitrogen. Control of the temperature is achieved by monitoring the rate of flow of the gas through a flowmeter. The temperature of the sample is measured by means of a copper-constantan thermocouple with its reference junction in an ice-water mixture. The other junction is attached to the sample tube in the coil assembly and the e.m.f. generated when the two terminals of the thermocouple are at different temperatures is measured by a potentiometer. By means of data supplied by Chalton and Mann[23], checked against fixed points, e.m.f. readings can be converted into temperatures.

The oscillator was tuned to about 27 Mc/s and the r.f. level could be varied between 0.5μA and 9μA. With this frequency a field of about 6360 gauss is required for proton resonance. Using a water sample the field and frequency are adjusted so that proton resonance occurs when the field-sweep helipot is in the middle of its range. The sweep width is 41.10 gauss and the sweep rate 2.055 gauss/minute. 64c/s was chosen as a suitable modulation frequency and the maximum amplitude of modulation, corresponding to 0dB on the audiofrequency generator output, was 1.0 gauss. Thus Andrew's modulation correction[12] to the second moment of broad-line spectra is not applied in most cases. A recorder chart drive speed of 3cm/minute was selected for spectral presentation.

Sample temperatures between 120°K and 360°K are obtained with the experimental arrangement of this spectrometer.

CHAPTER 4

A BROAD-LINE PROTON MAGNETIC RESONANCE INVESTIGATION OF SOME ALLEGED HYDRATES

4.1. Introduction

The term "hydrate" should, strictly speaking, be applied only to compounds whose crystals contain discrete water molecules but if the evidence on which the formulae assigned to many alleged hydrates of inorganic salts are based is examined then it becomes obvious that a large number might not be hydrates at all. For example, a compound originally given the formula $Na_2O.SnO_2.3H_2O$ and called a trihydrate was shown, after the advent of Werner's coordination theory[24] to be $Na_2[Sn(OH)_6]$. Wells mentions[25] that many other so-called hydrates may, in fact, be hydroxy salts. Copper sulphate monohydrate could be $CuSO_4.H_2O$ or $Cu(OH)(HSO_4)$; the latter representation defies no valence laws.

Information on the correct representation of a so-called hydrate can often be obtained from a study of the conditions required for dehydration[25]. Several hydrates retain their water molecules above 200°C while others readily lose theirs on heating to 100°C. Some even undergo decomposition before complete dehydration. The more vigorous treatment is often required for true hydrates if a transition metal is present, because the latter can bond to their water molecules very strongly as a consequence of the available d-orbital vacancies of such metals[26]. With ions of the inert gas configureation s^2p^6, such as Na^+ and Mg^{2+} true hydrates would be expected to dehydrate fairly readily. Some do not, so these may be hydroxy-salts.

Only physical techniques however, can supply conclusive proof of the correct formulation of an alleged hydrate. X-ray crystallography, where applicable, usually solves problems of structure determination but protons, because of their low X-ray scattering power[27], can only be positioned accurately on an electron density map after a great deal of effort. The related techniques of electron[28] and neutron[29] diffraction are able to locate the protons with the same amount of effort as is required to locate heavier nuclei, ~~because~~ in the latter the scattering is produced by interaction of the particles with the nucleus and not with the extra nuclear electrons. It is simpler to apply one or other

of these diffraction methods only when the crystal has already been investigated using X-rays and the positions of the other atoms are already known. The dihydrate of oxalic acid was investigated using neutron diffraction[30] together with the information supplied by X-ray analysis[31] and it was found that the species H_3O^+ was not present in the crystal but that the dihydrate contains almost unperturbed water molecules. This conclusion had been arrived at two years earlier[9] by means of broad-line proton magnetic resonance studies, together with the result that the crystalline hydrates of nitric, perchloric and sulphuric were more correctly represented by $H_3O^+NO_3^-$, $H_3O^+ClO_4^-$ and $H_3O^+HSO_4^-$ respectively. Infrared analysis[32] can supply information on the type of O-H bonds present in an alleged hydrate and on the hydrogen bonding involved.

N.M.R. can supply the answer to the question of the correct representation of an alleged hydrate in a shorter time and with less effort than are involved in the diffraction methods although the latter supply fuller structural information such as all the bond angles and lengths in the unit cell of the crystal specimen. Broad-line N.M.R. is able to supply the required data from a single crystal or a polycrystalline study. In general when little is known about the crystal structure of the compound it is better to examine the polycrystalline material first.

Only a small amount of chemical information is available for the magnesium carbonate hydrates formulated empirically as $MgCO_3 3H_2O$ and $MgCO_3 H_2O$. The trihydrate is converted to the monohydrate on heating at 100°C. Further heating of the monohydrate results in decomposition at about 250°C to magnesium oxide with loss of carbon dioxide. These observations might suggest that at least the third molecule of water is actually "tied up" with the crystal structure and that the compounds might be better formulated as $Mg(OH)(HCO_3).2H_2O$ and $Mg(OH)(HCO_3)$ respectively.

If both are indeed true hydrates one would expect their magnetic resonance spectra, when motions are frozen out, to resemble that of $CaSO_4.2H_2O$, for example, (see Figure 2.5.2a) but to be quite different if they are hydroxy-bicarbonates (see figure 2.5.2c).

This chapter deals with the experimental details of how the spectra of these hydrates were obtained at a number of temperatures and how

the spectra at the lowest temperature employed distinguish between the different representations. In addition a discussion is given of the types of motions which take place within the "hydrate" crystals when their temperature is altered.

4.2. Preparation of the "Hydrates"

It has been reported[33] that when a solution of magnesium bicarbonate is recrystallised at 50°C then crystals of the trihydrate, $MgCO_3.3H_2O$ are obtained. Japanese workers[34] have extensively studied the preparation of the "bicarbonate" and give the following relevant information concerning the reaction.

$$MgO+H_2O+2CO_2 \rightleftharpoons Mg(HCO_3)_2$$

They state that when carbon dioxide is passed into a basic solution, three competing reactions take place.

a. $CO_2 + OH^- \rightleftharpoons HCO_3^-$

b. $HCO_3^- + OH^- \rightleftharpoons CO_3^{2-} + H_2O$

c. $CO_2 + H_2O \rightleftharpoons H_2CO_3$

Inorder to prepare magnesium bicarbonate reaction a. must predominate and the Japanese workers report that this is the case only if the rate of flow of CO_2 and the agitation of the magnesium oxide suspension are correctly adjusted. They give as optimum conditions, at 25°C, the rate of stirring = 1000 r.p.m., CO_2 flow rate = 5l./min. and the ratio of oxide to water = 30 g./l.

Carbon dioxide was passed into a suspension of stock magnesium oxide using these "optimum" conditions but the milky colour of the suspension did not disappear and no reaction appeared to occur. It was realised that possibly the stock MgO had formed a coating of impervious magnesium carbonate on standing and so it was decided to perform the reaction on freshly prepared magnesium oxide. Standard sodium hydroxide solution was added to a weighed amount of magnesium sulphate heptahydrate and the resultant precipitate of magnesium hydroxide quickly filtered, washed thoroughly with water then suspended in water and allowed to react with gaseous CO_2 under the conditions quoted above. The solution became clear almost at once. After reaction for 30 mins. the solution was left for several days after which time crystals had formed on the side of the reaction vessel. These were collected and analysed for magnesium and carbonate;

they proved to be the required $MgCO_3 3H_2O$.

Some of the trihydrate was converted to the monohydrate by heating a known amount in an oven at 100°C until constant weight was obtained. The resultant loss in weight was consistent with the formation of $MgCO_3H_2O$ from the trihydrate. Standard methods of magnesium and carbonate analysis confirmed this empirical formula.

Both samples were kept in sealed containers to prevent any absorption or loss of moisture.

4.3. Investigation of the Tri- and Mono-hydrates of Magnesium Carbonate

The proton magnetic resonance spectra of $MgCO_3 3H_2O$ and $MgCO_3H_2O$ were investigated over the temperature range 140° - 350°K. The signal-to-noise ratiosof many of the spectra were enhanced using a Cumputer of Average Transients, a C.A.T. Figures 4.3.1, 4.3.2 and 4.3.3 show the derivative spectra of the trihydrate at, respectively 141°K, 271°K and 315°K. The derivative spectra of the monohydrate species at 153°K, 300°K and 347°K, are shown in figures 4.3.4, 4.3.5 and 4.3.6, respectively. The variation of the observed second moments of the proton absorption curves over the temperature range studied is shown in figure 4.3.7.

The curves of second moment against temperature show that in both compounds there is unlikely to be any motions which affect the shape of the absorption curves below about 190°K. Consequently, the derivatives of the absorption curves at about 150°K represent the "rigid lattice" spectra. These curves, figures 4.3.1 and 4.3.4, are not typical of simple hydrates. The proton magnetic resonance spectrum of a simple hydrate is of the form shown by the dotted curves in figures 4.3.8 and 4.3.9. The observed "rigid lattice" spectra, shown by the solid curves in figures 4.3.8 and 4.3.9 and obtained as an average of a number of spectra, are clearly quite different from those which would be expected if all the protons were present in water molecules. Hence some of the protons in both these compounds are in environments different from water of crystallisation.

This is further borne out by the magnitude of the observed second moments at 150°K; these are 25 ± 1 gauss^2 and 23.5 ± 1 gauss^2 respectively for the tri- and mono-hydrates whereas the second moment of the proton magnetic resonance absorption spectrum characteristic of rigid water

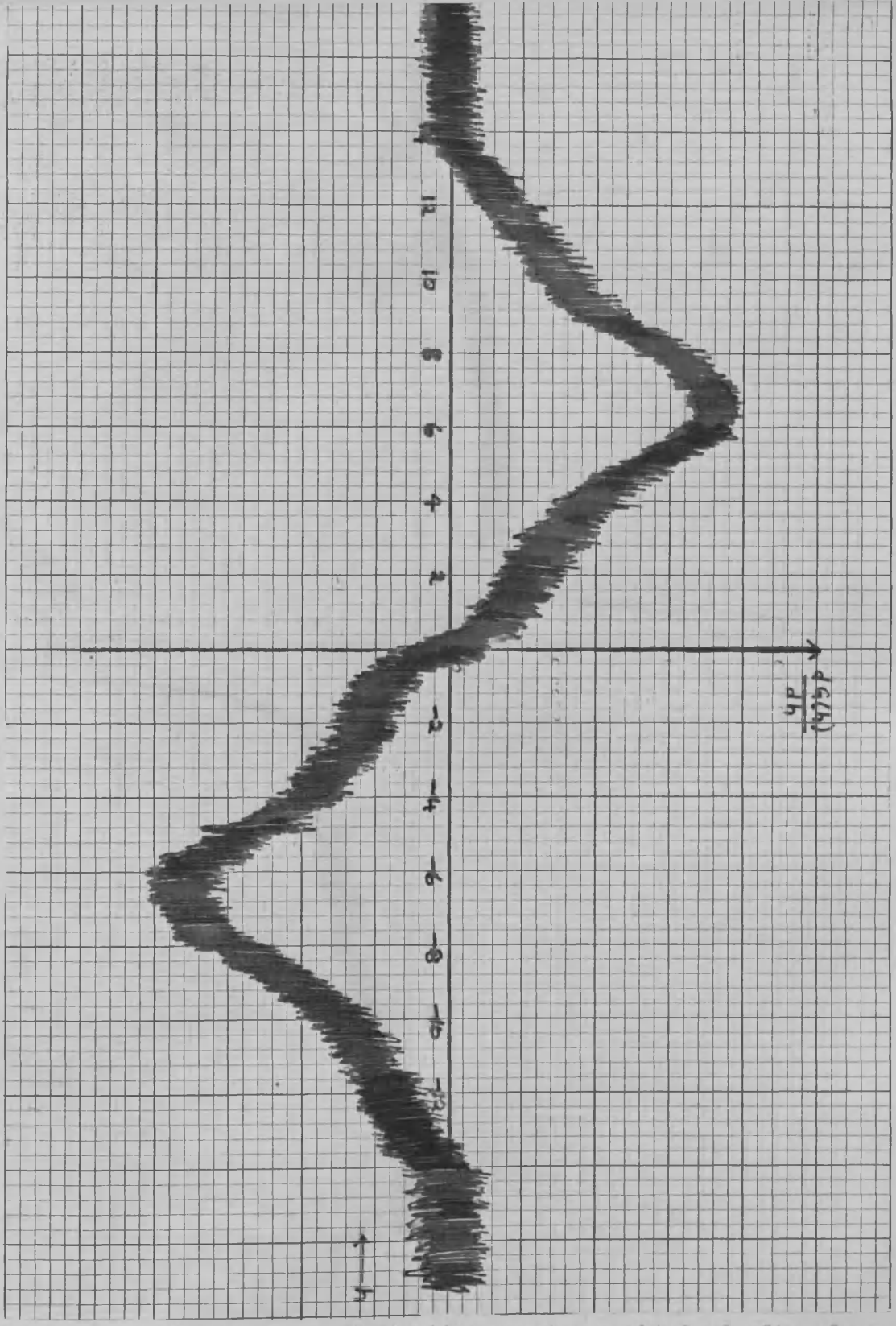

Proton magnetic resonance derivative spectrum, obtained after four accumulations in the C.A.T., of polycrystalline $MgCO_3 3H_2O$ at 141°K. The second moment of the absorption spectrum is 25 ± 0.7 gauss^2.

Figure 4.3.1

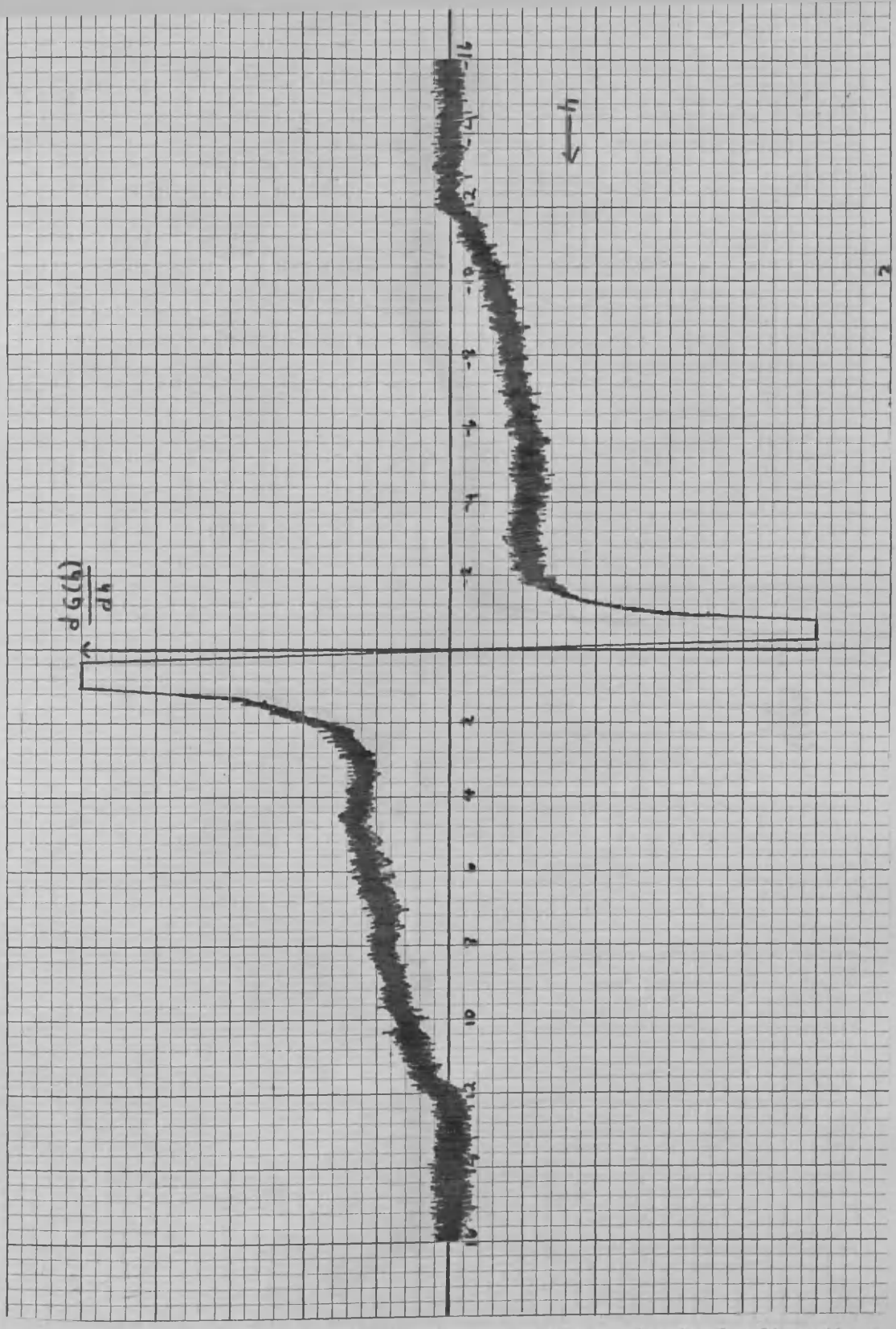

Proton magnetic resonance derivative spectrum, obtained after three accumulations in the C.A.T., of polycrystalline $MgCO_3 \cdot 3H_2O$ at 271°K. The second moment of the absorption spectrum is 17.1±0.6 gauss^2.

Figure 4.3.2

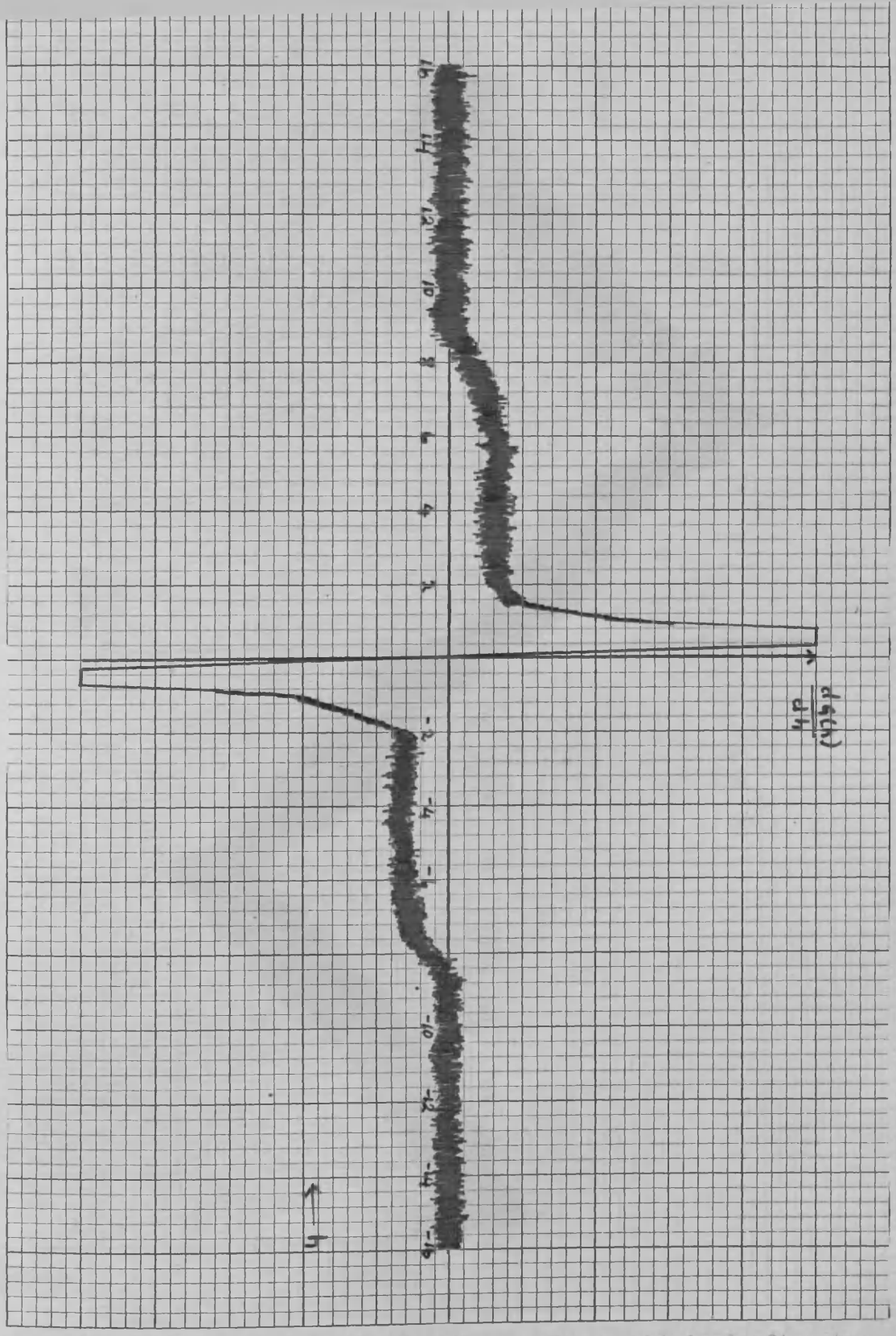

Proton magnetic resonance derivative spectrum, obtained after two accumulations in the C.A.T., of polycrystalline $MgCO_3 3H_2O$ at 315°K. The second moment of the absorption spectrum is 9.2±0.5 gauss^2.

Figure 4.3.3

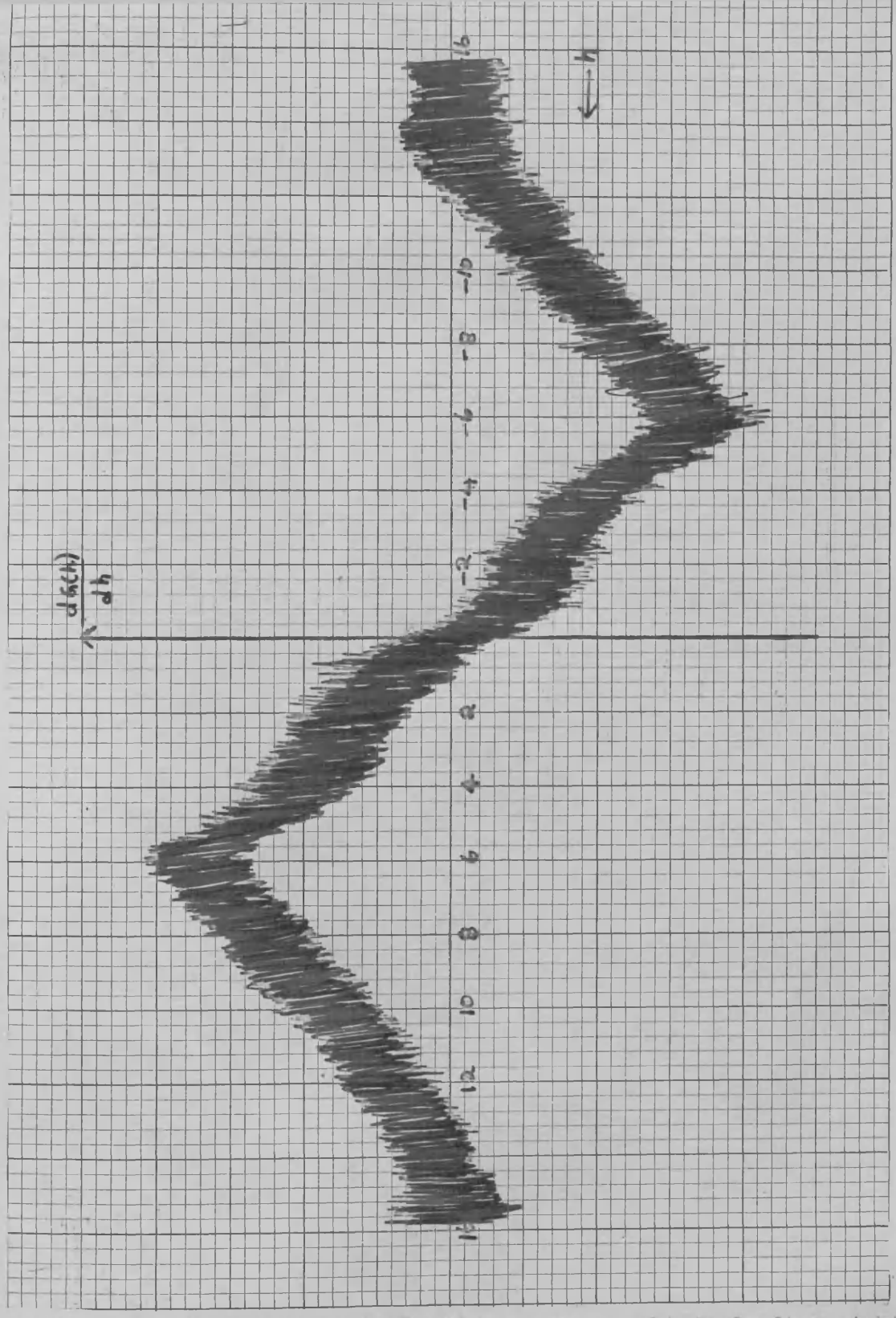

Proton magnetic resonance derivative spectrum, obtained after eight accumulations in the C.A.T., of polycrystalline $MgCO_3 \cdot H_2O$ at 153°K. The second moment of the absorption spectrum is 25.4±0.8 gauss^2.

Figure 4.3.4

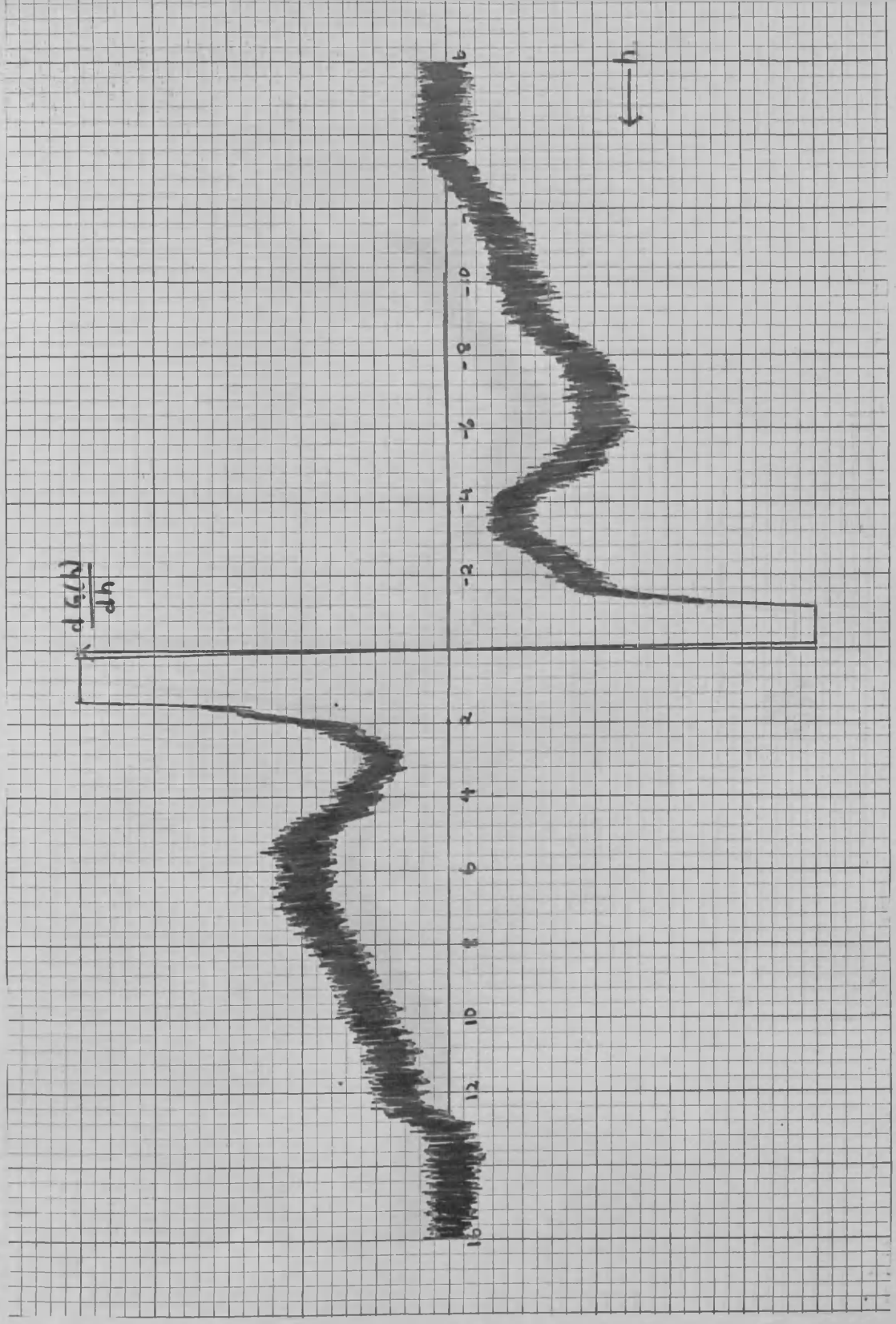

Proton magnetic resonance derivative spectrum, obtained after four accumulations in the C.A.T., of polycrystalline $K_2CO_3 \cdot H_2O$ at 300°K. The second moment of the absorption spectrum is 20.4±0.4 gauss^2.

Figure 4.3.5

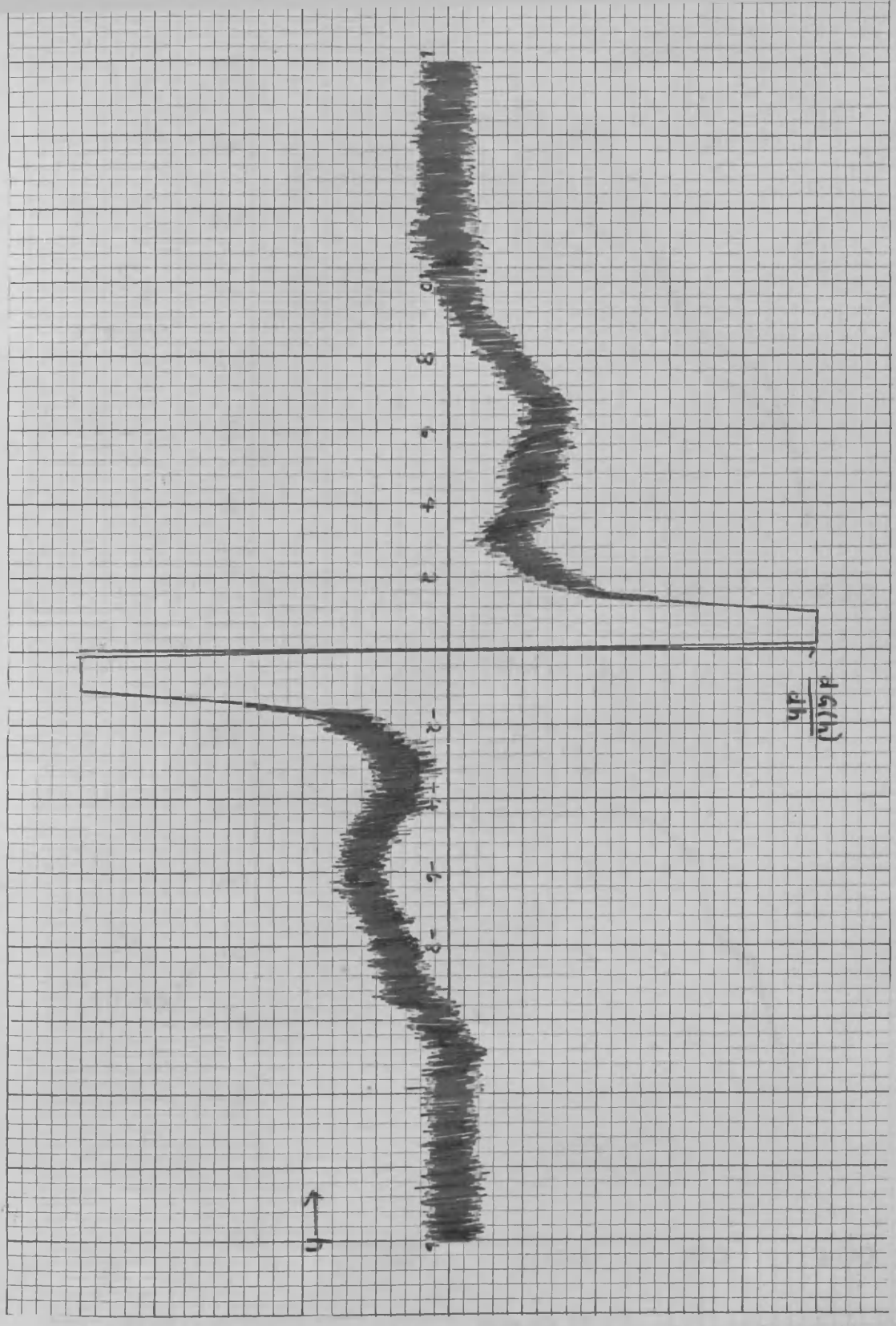

Proton magnetic resonance derivative spectrum, obtained after two accumulations in the C.A.T., of polycrystalline $MgCO_3H_2O$ at 347°K. The second moment of the spectrum is 11.7±0.4 gauss^2.

Figure 4.3.6

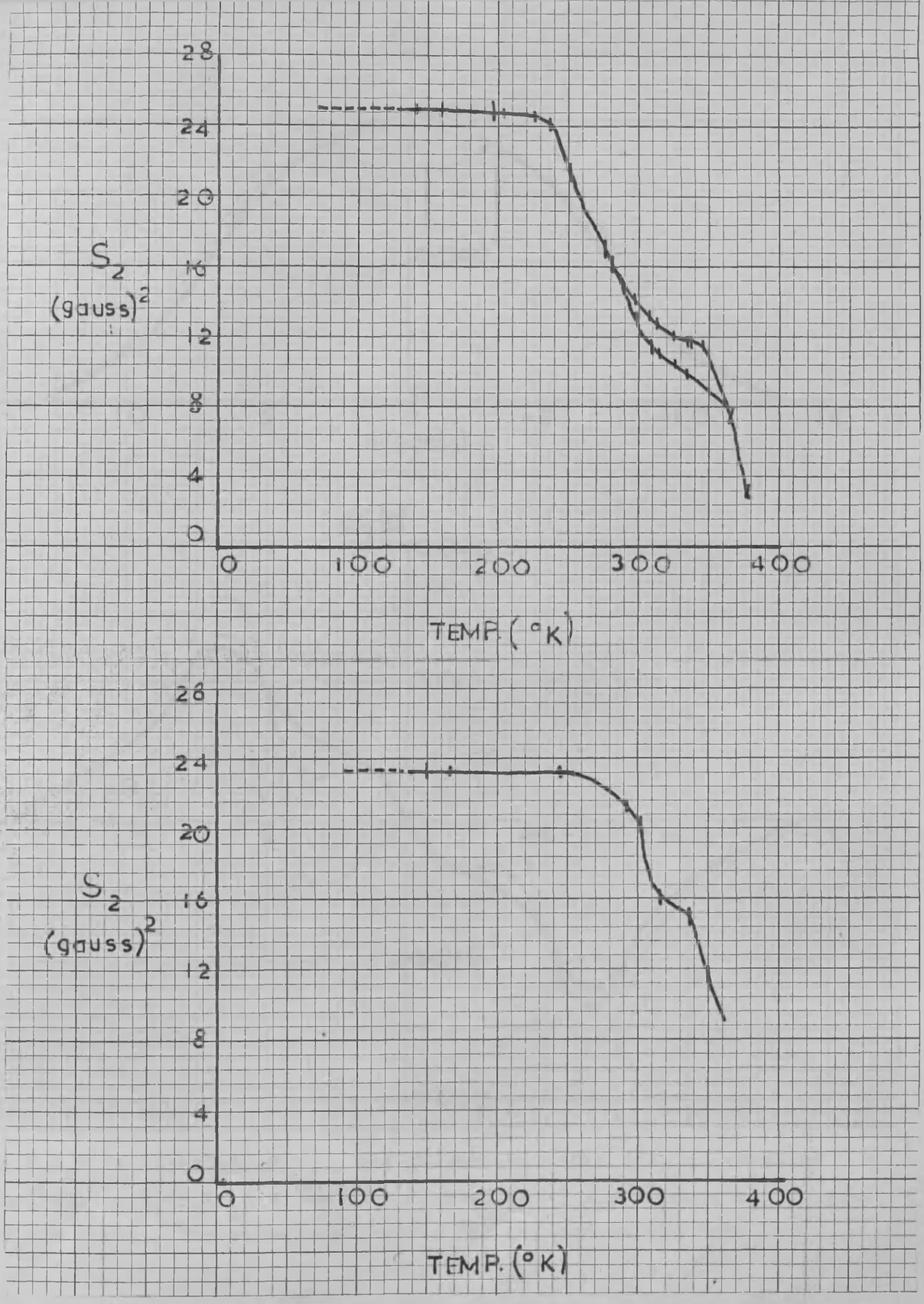

Second moment, S_2 gauss^2, of the proton magnetic resonance spectra observed as a function of temperature, T°K, in $MgCO_3 3H_2O$ (top) and $MgCO_3 H_2O$ (bottom). Figure 4.3.7

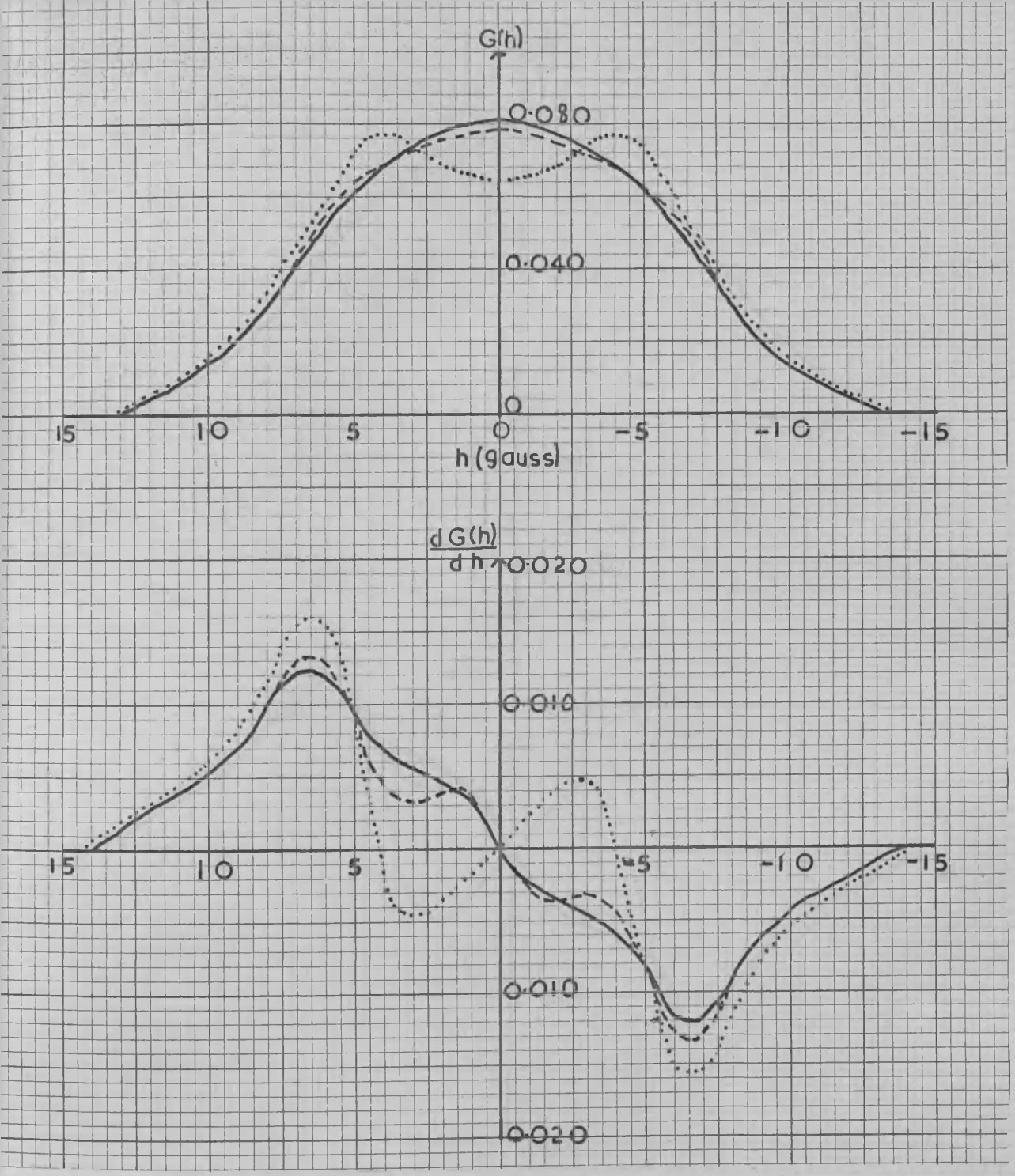

Proton N.M.R. absorption, $G(h')$, and derivative, $dG(h')/dh'$, curves of polycrystalline $MgCO_3 3H_2O$ at 141°K. Observed (---) and calculated (...;---) curves are shown. The calculated curves are defined in the text.

Figure 4.3.8

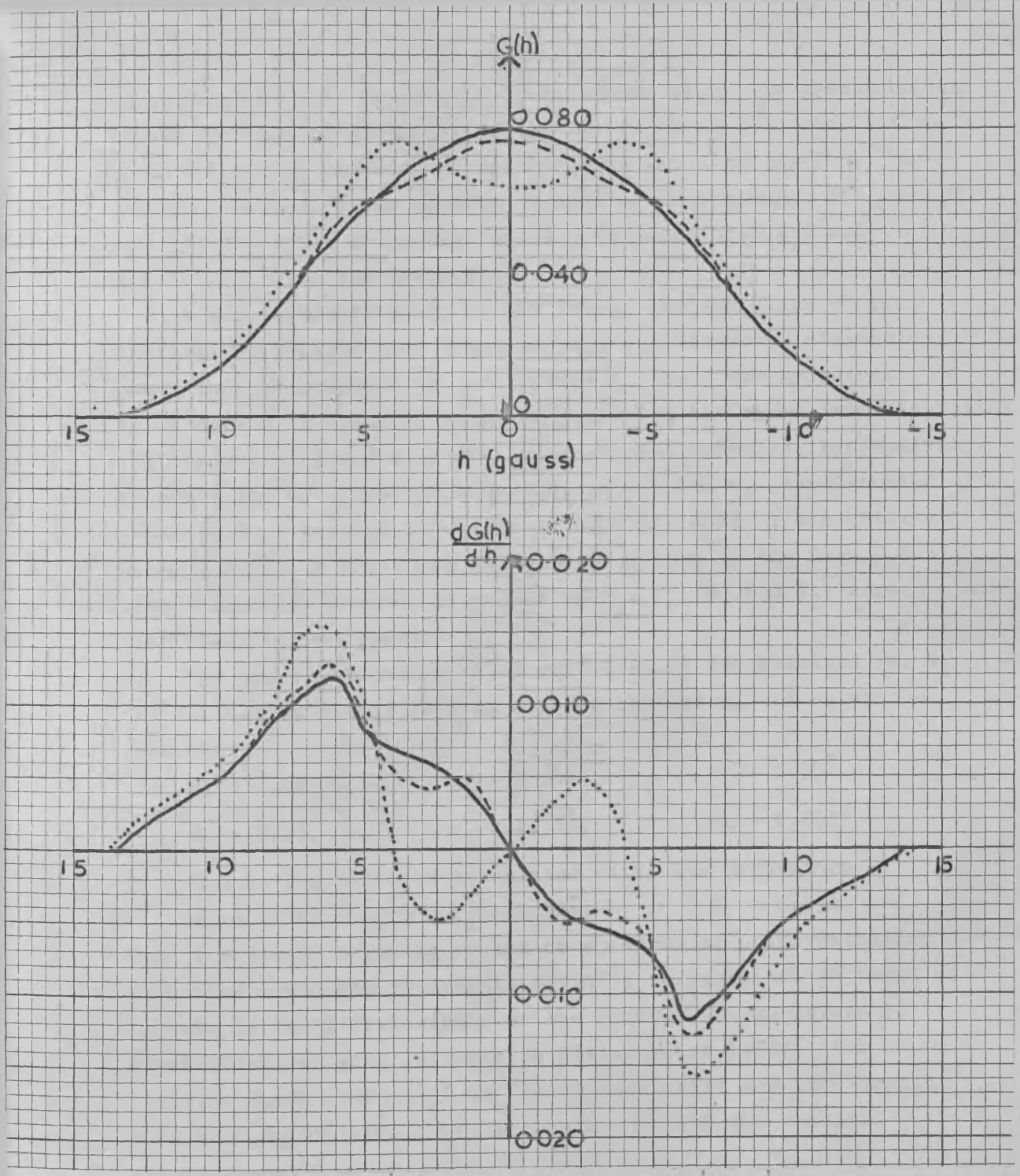

Proton N.M.R. absorption, $G(h')$, and derivative, $dG(h')/dh'$, curves of polycrystalline $MgCO_3H_2O$ at $\frac{153}{11}$ K. Observed (---) and calculated (...;---) curves are shown. The calculated curves are defined in the text.

Figure 4.3.9

molecules is about 28 gauss^2. Furthermore since the second moment characteristic of protons in OH groups is about 3-4 gauss^2, the observed second moments are too large to arise solely from such groups. Therefore the observed second moments exclude the formula $MgCO_3 3H_2O$ for the trihydrate and the formulae $MgCO_3 H_2O$ and $Mg(OH)(HCO_3)$ for the monohydrate.

A more complete study of the "rigid lattice" line shapes, as outlined in section 2.5, provides more quantitative information about the environments of the protons in these two hydrates. The solid curves in figures 4.3.8 and 4.3.9 are the normalised absorption and derivative spectra of the tri- and mono-hydrates, respectively, at about 150°K. From these curves, values for w_1, the fraction of total protons present in waters of crystallisation, are obtained using 2.5.12. A series of calculated spectra of the form 2.5.11, with chemically reasonable values of r_1, r_2, R_1 and R_2, were compared with the observed spectra.

For the trihydrate a value of 0.84 ± 0.03 was obtained for w_1 and the dashed curves in figure 4.3.8 are calculated using the parameters

$w_1 = 0.84$, $r_1 = 1.58$Å, $R_1 = 2.35$Å

$w_2 = 0.16$, $r_2 = 2.35$Å, $R_2 = 2.43$Å

The dotted curve is calculated using the parameters

$w_1 = 1.00$, $r_1 = 1.58$Å, $R_1 = 2.35$Å

Thus the proton magnetic resonance spectrum of polycrystalline magnesium carbonate trihydrate at 140°K is explained in terms of a formula in which five-sixths of the protons are in waters of crystallisation with interproton distances of 1.58Å. The representation $Mg(OH)(HCO_3)2H_2O$ is clearly not valid but the formula $MgCO_3 3H_2O, Mg(OH)(HCO_3)2H_2O$ is consistent with the spectral observations.

From analysis of the normalised curve for the monohydrate, solid line of figure 4.3.9, w_1 was found to be 0.80 ± 0.03. The dashed curves of figure 4.3.9 are calculated using the parameters

$w_1 = 0.80$, $r_1 = 1.58$Å, $R_1 = 2.35$Å

$w_2 = 0.20$, $r_2 = 2.35$Å, $R_2 = 2.43$Å.

Table 4.3.1

Infra-red absorption frequencies of magnesium carbonate tri- and mono-hydrate and of some other carbonates and bicarbonates.

	$4MgCO_3 \cdot H_2O \cdot Mg(OH)(HCO_3)$	$MgCO_3 \cdot 3H_2O \cdot Mg(OH)(HCO_3) \cdot 2H_2O$	$KHCO_3$	$NaHCO_3$	NH_4HCO_3	$PbCO_3$	$CoCO_3$	$BaCO_3$	$CaCO_3$	$3MgCO_3 \cdot Mg(OH)_2 \cdot 3H_2O$	K_2CO_3	Na_2CO_3	Li_2CO_3
3500		s b								m vb			
3400	s b						m vb						
3300											m vb		
3200					vs sp								
3100					vs sp								
3000												m vb	
2900			m	m									
2800													
2700			s vb									vw	
2600					m				vw				
2500				s vb								m	
2400													
2300			m	m									
2200													
2100													
2000				vw									
1900													
1800				m	m								
1700									vw			m sp	
1600	m	m	vs	ss	ss								
1500	s	s								vs.vs.			ss
1400	s	vs	vs m sh	ms vs sp sp	vs vs sp b	vs	vs	vs	vs		vs	vs	
1300													
1200	m												
1100	m	m	ss	ms ms sp sp	ms ms sp sp								
1000													
900	m	m	ss sp	s s sp	s s sp	vw m	m vw	s sp m	s sp m	vw vw	vw m	svw m m	m
800													
700	m	m b	s	s s	s s								
600	m												
500	m b												

The "simple hydrate" spectrum, with $w_1 = 1.00$, $r_1 = 1.58\mathring{A}$ and $R_1 = 2.35\mathring{A}$ is again shown, as the dotted curves in figure 4.3.9. In the representation $MgCO_3H_2O, Mg(OH)(HCO_3)$, $w_1 = w_2 = 0.50$ and this is inconsistent with the observed "rigid lattice" spectrum. The representation $4MgCO_3H_2O, Mg(OH)(HCO_3)$ has the required w_1 value.

The proton magnetic resonance results can be explained by assuming that when the trihydrate is prepared from the bicarbonate by the method outlined in the previous section then a 50:50 mixture of the species $MgCO_3 3H_2O$ and $Mg(OH)(HCO_3)2H_2O$ is obtained. Heating at 100°C converts the "trihydrate" to "monohydrate", the $MgCO_3 3H_2O$ being dehydrated to $MgCO_3H_2O$ and the $Mg(OH)(HCO_3)2H_2O$ being converted to a mixture of $Mg(OH)(HCO_3)$ and $MgCO_3H_2O$.

Infra-red absorption spectra of the two hydrates of magnesium carbonate were recorded over the frequency range 4000 — 300cm^{-1} as KBr discs. The spectra of the "tri- and mono-hydrates" are very similar. Table 4.3.1 shows the infra-red absorption frequencies and relative intensities of a number of carbonates and bicarbonates [35], together with those of the "magnesium carbonate hydrates". The symbols vs, s, m, w, vw denote the intensities of the absorptions as, respectively, very strong, strong, medium, weak, very weak. Some absorptions are further qualified as broad (b), very broad (vb), spur (sp), or shoulder (sh). Infra-red absorptions in the range 1700 — 1500cm^{-1} in the "hydrate spectra" are consistent with the presence of bicarbonate in these compounds.

The graphs of second moment versus temperature for the two hydrates show that, above 240°K, internal motions set in in the crystals and some of thewater molecules start to rotate about axes perpendicular to the H-H vectors. This causes the rigid lattice spectra to collapse. Figures 4.3.2 and 4.3.5 show the recorded derivative spectra of the "trihydrate" and "monohydrate" respectively, at temperatures where such motions are present. For the trihydrate at 271°K the line width of the absorption spectrum, measured as the separation between outermost points of maximum and minimum slope of the absorption curve, is 13 ± 0.5 gauss, so that, using 2.5.3 and 2.5.1, the correlation time, τ_c, characteristic of the motion present at this temperature turns out to be 6.2 ± 2 μsecs, using a value of 15 ± 0.5 gauss for the line width of the "rigid lattice" absorption spectrum. At

250°K the line width is 14±0.5 gauss so that τ_c for the motion at this temperature is 11.6±3.3 μ secs. The energy barrier, U, to the motions present at these temperatures is found from the relationship

$$\frac{\tau_c(T_1)}{\tau_c(T_2)} = \exp\left\{\frac{U}{R}\left(\frac{1}{T_1} - \frac{1}{T_2}\right)\right\}$$

to be 4.0±1 k cals.

A similar analysis of the monohydrate spectra at 270°K and 300°K shows that the correlation times of 11.6±3.3 μ secs and 4.4±1 μ secs. respectively, are associated with the motions present in this compound at these temperatures. The energy barrier to these motions is 5.0±1.3 k cals.

Further motions set in in these compounds at temperatures above 320°K resulting in further collapse of the spectra. The spectra displayed in figures 4.3.3 and 4.3.6 were recorded at temperatures where these motions exist. At 335°K the line width of the absorption spectrum of the trihydrate is 11±0.5 gauss so that τ_c for the motions present at this temperature is 3.4±0.5 μ secs., using a value for A, the line width of the "rigid lattice" spectrum, of 15±0.5 gauss. The line width of 12±0.5 gauss for the spectrum at 315°K indicates a correlation time of 4.4±1 μ secs. The energy barrier to the motions present at these temperatures is found to be 2.7±1.0 k cals. The spectra of the monohydrate at 337°K and 347°K show that the correlation times associated with the motions present at these temperatures are, respectively, 4.4±1 μ secs and 3.4±0.5 μ secs. so that the energy barrier to these motions is 6.0±1.7 k cals.

In order to study the energetics involved in the decomposition

$$\text{"}MgCO_3 3H_2O\text{"} \longrightarrow \text{"}MgCO_3 H_2O\text{"} \longrightarrow MgCO_3 \longrightarrow MgO,$$

thermogravimetric studies were carried out on the two hydrates at a series of fixed temperatures within the range 100° — 300°C. It was found that both "hydrates" decompose according to second-order kinetics with two distinct stages. Second order reactions obey the relationship

$$k = \frac{1}{at}\,\frac{x}{(a-x)}$$

where k is the rate constant, a is the initial quantity of substance present and (a-x) is the quantity present after time t(secs). The rate constant is related to the energy of activation involved in

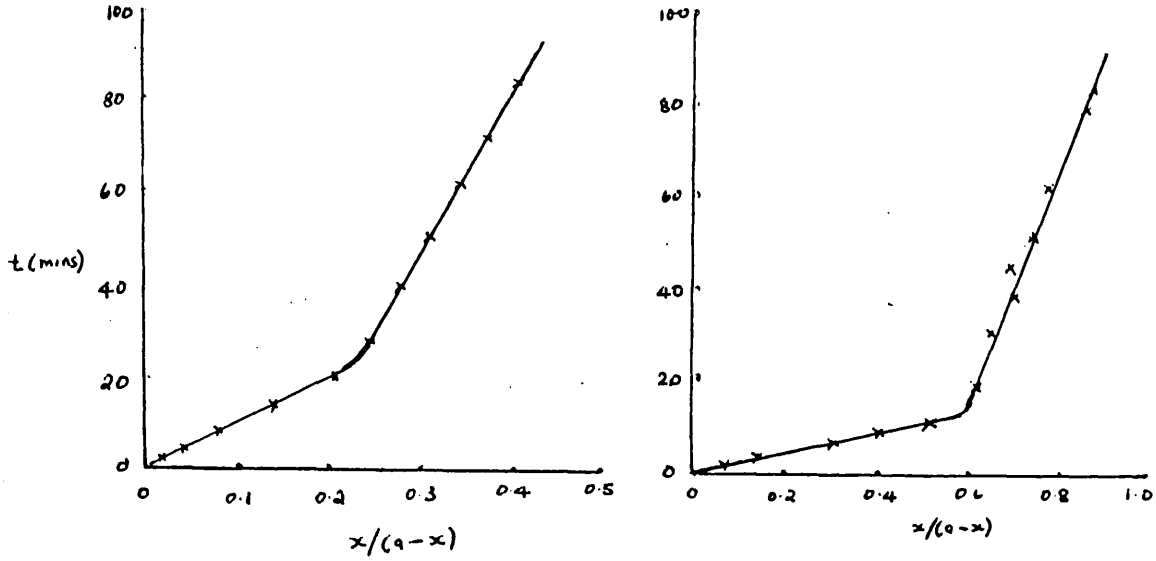

Decomposition of Magnesium Carbonate Trihydrate as a Second Order Rate Process.

Figure 4.3.10

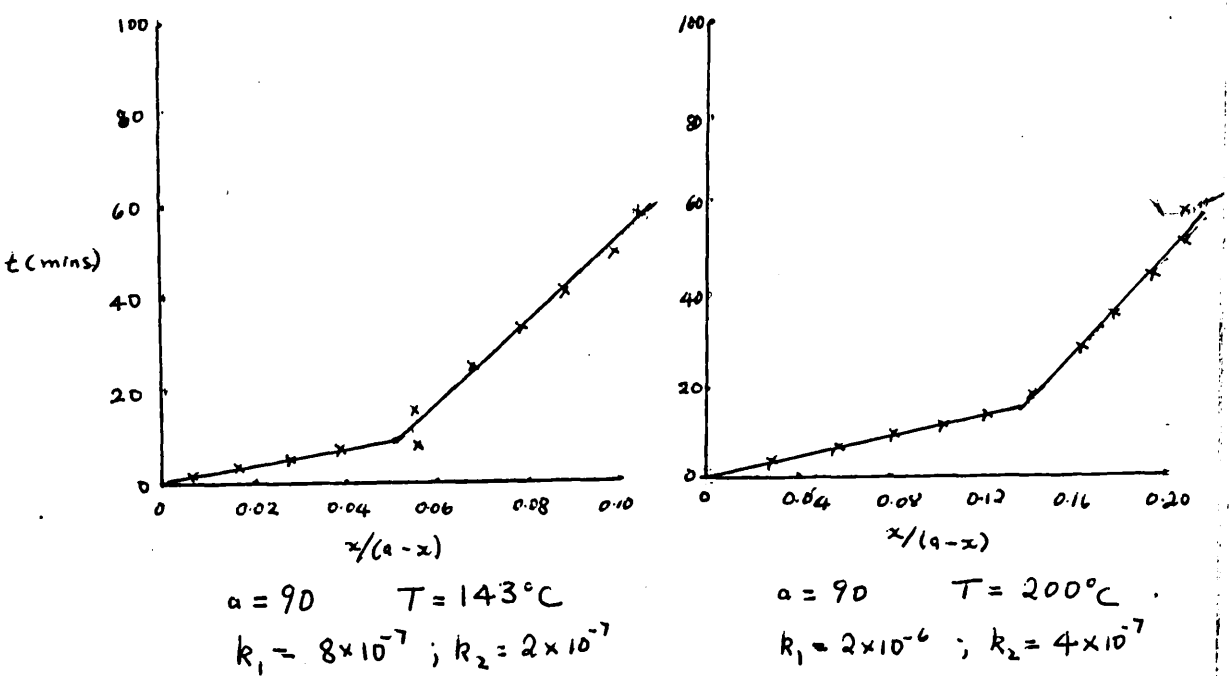

Decomposition of Magnesium Carbonate Monohydrate as a Second Order Rate Process.

Figure 4.3.11

the reaction, by the Arrhenius equation

$$k = Ae^{-E/RT}$$

where A is a constant for each reaction.

Figures 4.3.10 and 4.3.11 show the graphs of x/(a-x) versus time (minutes) at two temperatures, for respectively the "tri-" and "mono-hydrates". From the Arrhenius equation a plot of log k against $T^{-1}(^{o}K)$ gives a straight line of gradient -E/2.303R. From such plots of log k_1 and log k_2 against (temperature, $^{o}K)^{-1}$ for the tri- and mono-hydrate decompositions, activation energies of (12.9±8.6) k cals/mole and (6.3±5.4) k cals/mole are found for the reactions

$$\text{"}MgCO_3 3H_2O\text{"} \longrightarrow MgO + 3H_2O + CO_2$$

and

$$\text{"}MgCO_3 H_2O\text{"} \longrightarrow MgO + H_2O + CO_2$$

respectively.

CHAPTER 5

QUADRUPOLE INTERACTIONS

A nucleus whose quantum number I obeys the condition $I \geq 1$, possesses, in addition to a magnetic dipole moment, a nuclear electric quadrupole moment which can interact with electrostatic field gradients. In chemically interesting systems, these field gradients are produced by electrons and nuclei close to the quadrupolar nucleus of interest.

When the quadrupolar interaction is small compared with the magnitude of the nuclear magnetic interaction energy, 1.3.4, then the former interaction can be treated as a perturbation on the ~~eigenfunctions~~ ~~and~~ eigenvalues ~~of~~ 1.3.4. In this "high field" case the N.M.R. experiment is performed in a conventional manner and a number of resonance lines are detected, the number of lines providing a determination of the value of I and the separation between the lines yielding information concerning the quadrupole moment-field gradient interaction.

On the other hand, when the nuclear quadrupole interaction is very large compared with the magnetic interaction, the "low field" case, then the magnetic interaction is considered as a perturbation acting on the quadrupolar eigenvalues and eigenfunctions. This magnetic perturbation can be made zero so that transitions between the energy levels which arise from the interaction of an electric quadrupole moment with an electric field gradient can be studied.

Detection of transitions between pure nuclear quadrupole energy levels or "low field" perturbed quadrupole energy levels may require instrumental arrangements which differ from those used in pure N.M.R. or "high-field" cases.

Since the energy of transition between pure nuclear quadrupole levels depends on the interaction of the quadrupolar nucleus with the electrons and nuclei around it, information concerning the structure of a compound may be obtained by measuring the energy of separation of the quadrupolar levels of one of the constituent nuclei. The second topic in this thesis is an attempt to measure the quadrupolar transition energies of the chlorine nuclei, spin $\frac{3}{2}$, in a series of complexes of mercuric chloride with a view to relating the measured transition energies to structural changes throughout the series.

It is necessary, in this connection, to deal, at some length, with the theory of nuclear quadrupole resonance spectroscopy, which

is concerned with the nature and detection of interactions between a quadrupolar nucleus and its environment.

CHAPTER 6

NUCLEAR QUADRUPOLE RESONANCE SPECTROSCOPY

6.1. Introduction

Nuclei with spin quantum number $I = 0$ behave as charged stationary spheres, and nuclei with $I = \frac{1}{2}$ behave as if they are charged spinning spheres. To an external observer the electrical properties of such nuclei are equivalent to those which he would experience from a point charge equal to the total charge on the nucleus concentrated at the centre of the sphere. Nuclei with $I > \frac{1}{2}$ behave like charged spinning ellipsoids. Since they are spinning they possess magnetic moments and since they are ellipsoidal they possess electrical properties of interest. This is illustrated by considering the arrangements shown in figure 6.1.1. In this figure a non-spherical nucleus experiences four charges, +q on the $\pm$ x-axes and -q on the $\pm$ y-axes. Clearly configuration 6.1.1.(b) is energetically more favourable.

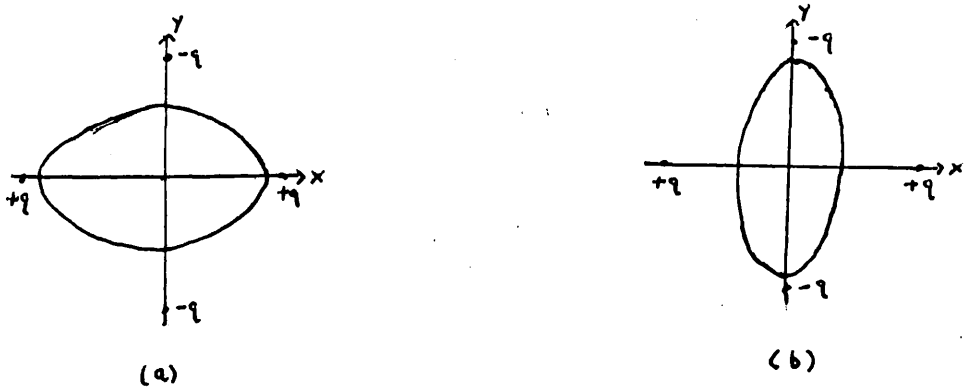

Figure 6.1.1

There is, therefore, a contribution to the potential energy of the system which arises through the electrostatic interaction between the nucleus and the environment, and which varies with nuclear orientation. Spherical nuclei are obviously unaffected by such charge distributions.

6.2. Electrostatic Interaction of a Nucleus with Environment [36,37]

To develop a more quantitative theory it is useful to begin by describing the interaction in terms of the classical interaction of the charge of the nucleus, charge density $\rho(r)$, and an electrostatic potential $V(r)$ and then, at a later stage, to insert appropriate operators into the classical expressions in order to obtain a quantum mechanical picture.

Classically, the interaction energy, E, of a charge distribution of density $\rho(r)$ with a potential $V(r)$ due to external sources is

$$E = \int_{\substack{\text{nuclear}\\ \text{volume}}} \rho(r)\, V(r)\, d\tau \qquad 6.2.1$$

The potential $V(r)$ can be expanded in terms of the potential at the nuclear centre of mass ($r=0$) by means of Taylor's theorem, thus

$$V(r) = V(o) + x\left(\frac{\partial V}{\partial x}\right)_{r=0} + y\left(\frac{\partial V}{\partial y}\right)_{r=0} + z\left(\frac{\partial V}{\partial z}\right)_{r=0}$$

$$+\tfrac{1}{2}\left[x^2\left(\frac{\partial^2 V}{\partial x^2}\right)_{r=0} + y^2\left(\frac{\partial^2 V}{\partial y^2}\right)_{r=0} + z^2\left(\frac{\partial^2 V}{\partial z^2}\right)_{r=0} + xy\left(\frac{\partial^2 V}{\partial x \partial y}\right)_{r=0}\right.$$

$$= V_o + \sum_{\alpha} x_\alpha \left(\frac{\partial V}{\partial x_\alpha}\right)_{r=0} + \tfrac{1}{2}\sum_{\alpha\beta} x_\alpha x_\beta \left(\frac{\partial^2 V}{\partial x_\alpha \partial x_\beta}\right)_{r=0} + \cdots\cdots \qquad 6.2.2$$

in which, when $\alpha, \beta = 1,2,3$, x_α or $x_\beta = x, y, z$ respectively.

Now define

$$\left(\frac{\partial V}{\partial x_\alpha}\right)_{r=0} = V_\alpha = -(\text{electric field component in the } x_\alpha \text{ direction at the origin})$$

and

$$\left(\frac{\partial^2 V}{\partial x_\alpha \partial x_\beta}\right)_{r=0} = V_{\alpha\beta} = -(\text{the gradient of the electric field component with direction } x_\alpha x_\beta \text{ evaluated at the centre of the nucleus})$$

Then 6.2.1. becomes

$$E = V(o)\int \rho(r)\, d\tau + \sum_{\alpha} V_\alpha \int x_\alpha \rho(r)\, d\tau + \tfrac{1}{2}\sum_{\alpha\beta} V_{\alpha\beta}\int x_\alpha x_\beta \rho(r)\, d\tau + \cdots \qquad 6.2.3$$

$$= E_o + E_1 + E_2 + \cdots\cdots$$

Taking the origin of the coordinate system at the centre of mass of the nucleus, then E_o is that energy which would arise from the interaction of a point charge, equal in magnitude to the total charge on the nucleus, with the potential at the origin. E_1 arises from the interaction of the components of the nucleus's electrical dipole moment

with the electric field components at the nucleus. If the nucleus is centrosymmetric then it follows that the contribution of $+x\rho(r)d\tau$ to E_1 exactly counterbalances the contribution from $-x\rho(r)d\tau$, and so on, i.e. if nuclei are centrosymmetric then they cannot possess electric dipole moments; experiments devised to detect electric dipole moments in nuclei have all failed so that it seems that all nuclei are centrosymmetric. Hence $E_1 = 0$.

E_2 is the energy due to the quadrupolar term with the components of the gradient of the electric field at the centre of the nucleus.

Terms beyond E_2 are due to interaction of higher electric multipole moments of the charge with higher derivatives of the electric field. The contribution of the next highest term, electric octopolar interaction, in the expansion for E is zero, but the electric hexadecapole moment interaction is non-zero. In fact it turns out that the even electric multipole moments are finite, the odd multipole moments are zero. Similar arguments involving generalised interactions with a magnetic field show that nuclei can possess magnetic dipole moments and magnetic octupole moments but not magnetic quadrupole moments. The even nuclear moments are electric moments, the odd nuclear moments are magnetic moments. It is worthwhile at this point commenting on the orders of magnitude of successive terms in the expansion 6.2.3. V_0 is of the order of e/r_e where r_e is a typical atomic dimension, say 10^{-8}cm. E_0 is the electrostatic energy Ze^2/r_e which is equal to about $10^5 cm^{-1}$, corresponding to an ultraviolet frequency. $E_1 = 0$ as do E_3, E_5 etc. E_2 is of the order of $er_n^2(e/r_e^3)$ where r_n is the nuclear radius ($\approx 10^{-12}$cm) Hence the quadrupolar interaction is of the order of $(r_n/r_e)^2 \approx 10^{-8}$ times the electrostatic energy, i.e. of the order of $10^{-3} cm^{-1}$ or 30 Mc/s. Similarly the next non-zero term, E_4, the hexadecapole term, is of the order $(r_n/r_e)^2 \approx 10^{-8}$ that of the quadrupolar term, i.e. of the order of 1c/s. Hexadecapolar interactions are ordinarily outside the range of experimental detectability and shall be neglected henceforth.

$$E_2 = \frac{1}{2}\sum_{\alpha\beta} V_{\alpha\beta} Q'_{\alpha\beta} \qquad 6.2.4.$$

where $Q'_{\alpha\beta} = \int x_\alpha x_\beta \rho(r) d\tau$

Both $V_{\alpha\beta}$ and $Q'_{\alpha\beta}$ are second rank tensors and, by their definition, are symmetric. Therefore there are six independent components of both these tensors. The tensor $V_{\alpha\beta}$ can be diagonalised by choosing a

particular set of axes, X, Y and Z, principal axes, of the potential V(r). Also V(r) must satisfy LaPlace's equation $\nabla^2 V = 0$ so that at the centre of the nucleus

$$\sum_{\alpha} V_{\alpha\alpha} = V_{XX} + V_{YY} + V_{ZZ} = 0 \qquad 6.2.5$$

in terms of the principal axes X,Y,Z.

Hence two parameters are required to specify the field gradient in the principal-axes system. A convenient choice of the two parameters is the following. One can choose to orient the principal axes so that the Z-axis lies along the direction of maximum field gradient and the X-axis along the direction of minimum gradient, i.e. such that

$$|V_{ZZ}| \geq |V_{YY}| \geq |V_{XX}| \qquad 6.2.6$$

One defines the two parameters q and η by

$$q \equiv V_{ZZ} \qquad 6.2.7$$

$$\eta \equiv (V_{XX}-V_{YY})/V_{ZZ} \qquad 6.2.8$$

By 6.2.5. $|V_{ZZ}| = |V_{XX}+V_{YY}|$ so that 6.2.6. shows that V_{XX} and V_{YY} must have the same sign.

Thus 6.2.5 and 6.2.6 show that η has the property $0 \leq \eta \leq 1$.

Hence field gradient is specified by the orientation of the principal axes of the field gradient tensor and by two parameters, q and η. If the field gradient is axially symmetric, $V_{XX}=V_{YY}$ and $\eta=0$. Therefore η can be called an "asymmetry parameter" and measures the departure of the field gradient from cylindrical symmetry. If the field gradient is spherically symmetric, or has cubic symmetry, $V_{XX}=V_{YY}=V_{ZZ}$ so that by 6.2.5 each component equals zero and the quadrupolar interaction vanishes.

The tensor $Q'_{\alpha\beta}$ also has six independent components and it is advantageous to define a simpler tensor, which is not only symmetric but traceless (i.e. the sum of the diagonal components is zero) so that this new tensor $Q_{\alpha\beta}$ has only five independent components. This is achieved by defining

$$Q_{\alpha\beta} = \int (3x_\alpha x_\beta - \delta_{\alpha\beta} r^2)\, \rho(r)\, d\tau \qquad 6.2.9$$

where $\delta_{\alpha\beta}$ is the Krönecker delta, i.e. where $\delta_{\alpha\beta} = 1$ for $\alpha=\beta$ and is zero for $\alpha \neq \beta$.

6.2.9 can be re-written

$$\int x_\alpha x_\beta \rho(r) d\tau = Q'_{\alpha\beta} = \tfrac{1}{3}\left[Q_{\alpha\beta} + \int \delta_{\alpha\beta} \rho(r)\, d\tau\right]$$

Hence the quadrupolar contribution to the energy of the nucleus in an electric field is given by

$$E_Q = E_2 = \frac{1}{6} \sum_{\alpha\beta} \left[V_{\alpha\beta} Q_{\alpha\beta} + V_{\alpha\beta} \delta_{\alpha\beta} \int r^2 \rho(r) d\tau \right] \qquad 6.2.10$$

The second term on the right hand side of 6.2.10 involves only traces. If $Q_{\alpha\beta}$ is defined relative to the principal axes of V(r) - it involves an integral over the total nuclear volume and is therefore independent of the choice of axes - then this second term vanishes since $V_{XX}+V_{YY}+V_{ZZ}$ equals zero.

Therefore, in terms of the principal axes of the potential V(r)

$$E_Q = \frac{1}{6}\left[V_{ZZ}Q_{ZZ} + V_{XX}Q_{XX} + V_{YY}Q_{YY} \right]$$

where, for example,

$$Q_{ZZ} = \int (3z^2 - r^2) \rho(r) d\tau$$
$$= \sum_{k \text{ protons}} -e(3Z_k^2 - r_k^2)$$

6.3. The Quadrupolar Hamiltonian

In order to go from this classical description to a quantum mechanical description of the system, the following procedure is employed.

The Hamiltonian, $\mathcal{H}_Q$, describing the quadrupolar interaction is given by

$$\mathcal{H}_Q = \frac{1}{6} \sum_{\alpha\beta} V_{\alpha\beta} Q_{\alpha\beta} \qquad 6.3.1$$

The quadrupolar contribution to the energy of a nucleus in an electric field now becomes

$$E_Q = \int_{\text{nucleus}} \psi^*_{\text{nucleus}} \mathcal{H}_Q \psi_{\text{nucleus}} \, d\tau \qquad 6.3.2$$

where ψ_{nucleus} is the eigenstate of the nucleus.

Solution of this equation seems to require that the nucleus be treated as a many-particle system. However, in chemistry one is generally concerned with the ground state of a nucleus in which the eigenstates are characterised by a total angular momentum, I, of each state, (2I+1) values of a component of angular momentum, m_I, and a set of other quantum numbers, ϵ. Since nuclear quadrupole resonance spectroscopy is concerned only with the spatial reorientation of the nucleus for the nuclear ground energy level, I and ϵ are constant. The expression 6.3.2. for E_Q can now be re-written in the form

$$E = \frac{1}{6}\left[V_{ZZ}\langle I, m_I, \epsilon | Q_{ZZ} | I, m_I, \epsilon \rangle + V_{XX}\langle I, m_I, \epsilon | Q_{XX} | I, m_I, \epsilon \rangle + V_{YY}\langle I, m_I, \epsilon | Q_{YY} | I, m_I, \epsilon \rangle \right. \qquad 6.3.3$$

using the notation $\langle a,b,c|O\Gamma|a,b,c\rangle$ for $\int \psi^*_{a,b,c}(O\Gamma)\psi_{a,b,c}\, d\tau$

At this point use is made of the theorem that the corresponding matrix elements of all traceless, symmetric, second-rank tensors are proportional [38]. $Q_{\alpha\beta}$ is such a tensor and using the components of the total nuclear spin $\underline{I}$ another such tensor can be constructed. 6.3.3 can be written in the form

$$\frac{1}{6}\sum_{\alpha\beta} V_{\alpha\beta}\langle I,m_I,\epsilon|\, Q_{\alpha\beta}\,|I,m_I,\epsilon\rangle$$

or

$$\frac{1}{6}\sum_{\alpha\beta} V_{\alpha\beta}\langle I,m_I,\epsilon|\, c\sum_{k\,\text{protons}}(3x_{\alpha k}x_{\beta k}-\delta_{\alpha\beta}r_k^2)\,|I,m_I,\epsilon\rangle$$

By making use of the above theorem this can be shown to equal

$$\frac{c}{6}\sum_{\alpha\beta} V_{\alpha\beta}\langle I,m_I,\epsilon|\tfrac{3}{2}(I_\alpha I_\beta + I_\beta I_\alpha)-\delta_{\alpha\beta}\underline{I}^2|I,m_I,\epsilon\rangle \qquad 6.3.4$$

where C is a constant, different for each set of the quantum numbers I and ϵ.

Assuming nuclear spin to be quantised along the Z-axis, nuclear quadrupole moment Q is defined as the expectation value, in units of proton charge e, of Q_{ZZ} in the state in which the component of I along the Z-axis is a maximum.

$$\begin{aligned}
\text{i.e. } eQ &= \langle I,I,\epsilon|\, Q_{ZZ}\,|I,I,\epsilon\rangle \\
&= \langle I,I,\epsilon|\, e\sum_{k\,\text{protons}}(3z_k^2-r_k^2)\,|I,I,\epsilon\rangle \qquad 6.3.5\\
&= C\langle I,I,\epsilon|\,3I_z^2-\underline{I}^2\,|I,I,\epsilon\rangle \\
&= C\left[3I^2-I(I+1)\right] \\
&= CI(2I-1)
\end{aligned}$$

That is

$$C=\frac{eQ}{I(2I-1)} \qquad 6.3.6$$

so that all components $Q_{\alpha\beta}$ can be related to the one scalar quantity Q.

Note that if I = 0 or $\frac{1}{2}$, the nuclear quadrupole moment must be zero. Only nuclei with spin quantum number $I \geqslant 1$ can possess quadrupole moments. It should also be noticed that for points on the surface of a sphere $x^2 = y^2 = z^2 = \frac{1}{3}r^2$ so that if a nucleus is spherically symmetrical $\langle Z^2\rangle = \frac{1}{3}\langle r^2\rangle$ and therefore the quadrupole moments will be zero. One can visualise, in physical terms, the nuclear electric quadrupole moment as defined by 6.3.5 as being a measure of the departure of the nuclear charge distribution from spherical symmetry. Q = 0 for spherical symmetry. If the nuclear charge distribution is elongated along the nuclear spin axis, figure 6.3.1(a), then Q is

positive; if it is flattened along this axis as in figure 6.3.1(b), then Q is negative.

Nuclei with spin quantum numbers I = 0 and $\frac{1}{2}$ show no orientation dependent electrostatic interaction and so can be considered as spheres; those with zero-spin have no axis of nuclear spin and those with spin $\frac{1}{2}$ have two possible spin orientations of the nucleus but they differ only by reversal of the spin direction and thus correspond to the same effective nuclear charge distribution.

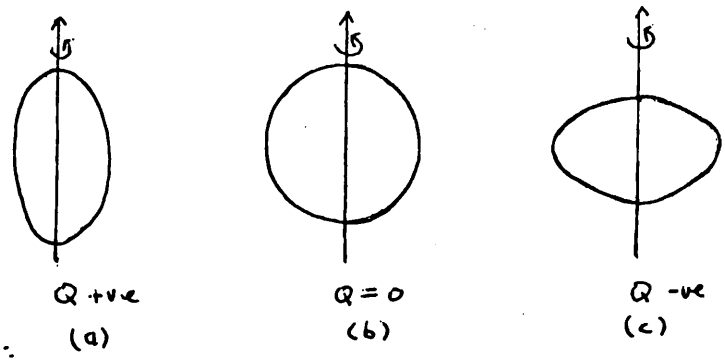

Figure 6.3.1.

If, therefore, an assembly of nuclei with $I \geq 1$ is placed in an electric field then each nucleus interacts with the electric field gradient and the quadrupolar contribution to the total energy of the system is given, for an arbitary (i.e. non-principal) set of axes, by

$$E_Q = \frac{C}{6} \sum_{\alpha\beta} V_{\alpha\beta} \langle I, m_I \epsilon | \tfrac{3}{2}(I_\alpha I_\beta + I_\beta I_\alpha) - \delta_{\alpha\beta} \underline{I}^2 | I, m_I, \epsilon \rangle \qquad 6.3.7$$

It is useful to write 6.3.7. in terms of I_Z, I^+ and I^- for an arbitary set of axes.

By defining

$$V_0 = V_{zz}$$
$$V_{\pm 1} = V_{xz} \pm iV_{yz} \qquad 6.3.8$$
$$V_{\pm 2} = \tfrac{1}{2}(V_{xx} - V_{yy}) \pm iV_{xy}$$

it turns out, after suitable algebraic manipulation, that

$$E_Q = \frac{eQ}{4I(2I-1)} \left\{ V_0(3I_z^2 - \underline{I}^2) + V_{+1}(I^- I_z + I_z I^-) + V_{-1}(I^+ I_z + I_z I^+) + V_{+2}(I^-)^2 + V_{-2}(I^+)^2 \right\} \qquad 6.3.9$$

In terms of the principal axes (X, Y and Z), when terms of the type $V_{\alpha\beta}$ with $\alpha \neq \beta$ vanish, 6.3.9 simplifies to

$$E_Q = \frac{eQ}{4I(2I-1)} \left\{ V_{zz}(3I_z^2 - \underline{I}^2) + (V_{XX} - V_{YY})(I_X^2 - I_Y^2) \right\}$$
$$= \frac{eQq}{4I(2I-1)} \left[3m_I^2 - I(I+1) + \eta(I_X^2 - I_Y^2) \right] \qquad 6.3.10$$

in terms of the two parameters q and η defined earlier. eQq is termed the quadrupole coupling constant for the nucleus in the particular environment under consideration.

6.4. Quadrupolar Energy Levels and Production of Spectra

For an axially symmetric field gradient this equation simplifies to

$$E_Q = \frac{eQq}{4I(2I-1)}\left[3m_I^2 - I(I+1)\right] \qquad 6.4.1$$

Therefore the effect of an axially symmetric electric field gradient on a quadrupolar nucleus of spin I is to produce a number of energy levels of energy given by 6.4.1. Each of these energy levels, except $m_I = 0$, is doubly degenerate since E_Q depends on m_I^2 and not m_I. For half-integral spins there are $(I+\frac{1}{2})$ groups of energy levels, all doubly degenerate, while for integral spins there are (I+1) groups, of which I of these are doubly degenerate.

Transitions between the energy levels given by 6.4.1 can be produced by applying an oscillating magnetic field which interacts with the magnetic dipole moment which is always associated with a quadrupolar nucleus. Transitions could be brought about by applying oscillating inhomogeneous electric fields with which the nucleus's electric quadrupole moment would interact. But electric field gradients too large for generation in the laboratory would be required to induce a sufficient number of transitions by this procedure. Thus transitions in nuclear quadrupole resonance spectroscopy are caused by means of the interaction which is used to induce transitions in N.M.R. (see section 1.3 of this thesis). Similar selection rules hold for the detection of transitions between quadrupole energy levels. That is, if an alternating magnetic field is applied with a non-vanishing component in the XY plane, it produces transitions governed by $\Delta m_I = \pm 1$. If the small perturbating field is applied in the XY plane the intensity of $\Delta m_I = \pm 1$ transition is maximum, whereas if it is applied parallel to the Z-axis the intensity of these transitions is zero. Therefore transitions of energy $(E_{m_I+1} - E_{m_I})$ are involved and are induced by an oscillating field of angular frequency ω such that

$$\hbar\omega = E_{m_I+1} - E_{m_I}$$

$$\text{i.e.} \quad \nu = \frac{3eQq}{4I(2I-1)}(2|m_I| + 1) \qquad 6.4.2$$

is the frequency of the radiation at which absorption of power occurs for an axially symmetric field gradient. There are $(I-\frac{1}{2})$ different absorption frequencies for half-integral spins and I different frequencies for integral spins. The quantity eQq can be obtained very accurately by measuring these resonance frequencies and assigning each transition frequency correctly to its m_I value. For spin $I = \frac{3}{2}$ and 1 there is only one transition frequency in each case so that the problem of assignment does not arise. These resonances occur at frequencies given by

$$\nu_1 = \frac{3eQq}{4h} \quad \text{for } I = 1$$

and

$$\nu_{3/2} = \frac{eQq}{2h} \quad \text{for } I = \frac{3}{2}$$

For I = 2 there are two resonance frequencies $(\nu' \equiv \pm 1 \leftrightarrow 0;\ \nu'' \equiv \pm 2 \leftrightarrow \pm 1)$

$$\nu_2' = \frac{eQq}{8h} \quad \text{and} \quad \nu_2'' = \frac{3eQq}{8h} = 3\nu_2'$$

while $I = \frac{5}{2}$ has two frequencies, also, $(\nu' \equiv \pm\frac{3}{2} \leftrightarrow \pm\frac{1}{2};\ \nu'' \equiv \pm\frac{5}{2} \leftrightarrow \pm\frac{3}{2})$

$$\nu_{5/2}' = \frac{3eQq}{20h} \quad \text{and} \quad \nu_{5/2}'' = \frac{3eQq}{10h} = 2\nu_{5/2}'$$

More generally, for two lines corresponding to transitions between $|m_I|$ and $|m_I+1|$ and $|m_I'|$ and $|m_I'+1|$, the ratio of their frequencies is

$$\frac{2|m_I|+1}{2|m_I'|+1}$$

The orientation of the axis of symmetry of the field gradient tensor (Z) could be found by studying the dependence of the intensity of the resonance lines on the orientation of the applied oscillating field with respect to axes fixed in the crystal in which the nuclei are contained. The intensity vanishes when the perturbation is applied along the symmetry axis and becomes maximum when applied in a plane perpendicular to the symmetry axis.

So far in this section η has been taken as zero. It is now necessary to consider the effect of asymmetry on the electric field gradient at the nucleus. The quadrupole energy levels are given, by

$$E_Q = \frac{eQq}{4I(2I-1)}\left\{\left[3m_I^2 - I(I+1)\right] + \eta\left(\langle I_x^2\rangle - \langle I_y^2\rangle\right)\right\} \qquad 6.3.10$$

When deviation from cylindrical symmetry is small then the second term is small compared with the first term and the second term can be treated as a perturbation on the first.

The outcome of such perturbation treatment is a mixing of some of the "pure" energy states whose energies were given by 6.4.1 for $\eta = 0$. This alters the energies of the states and causes the selection rule $\Delta m_I = \pm 1$ to break down. It proves more manageable at this stage to treat separately nuclei with half-integral spins and nuclei with integral spins. This part of the thesis is concerned with complexes of mercuric chloride, $HgCl_2$, and the nuclei ^{201}Hg, ^{35}Cl and ^{37}Cl all have $I = \frac{3}{2}$. For this reason much more emphasis will be placed on the discussion relevant to half-integral spins.

For half-integral spins the effect of the asymmetry term of 6.3.10 is to cause the "pure" energies

$$\langle m_I' | \mathcal{H}_Q | m_I \rangle = A \left[3m_I^2 - I(I+1)\right] \delta_{m_I', m_I} \qquad 6.4.3$$

to be altered by amounts given by [39]

$$\langle m_I' | \mathcal{H}_Q | m_I \rangle = \tfrac{1}{2} A \eta f_I(\pm m_I) f_I(1 \pm m_I) \delta_{m_I', m_I \pm 2} \qquad 6.4.4$$

where

$$A = \frac{eQq}{4I(2I-1)}$$

and $$f_I(\pm m_I) = f_I(-m_I - 1) = \left[(I-m_I)(I+m_I+1)\right]^{\frac{1}{2}}$$

The presence of η mixes states ψ_{m_I} which differ by $\Delta m_I = \pm 2$. Also the degeneracy of $\pm m_I$ is not removed by the presence of an asymmetric field gradient. This is not the case with integral spins whose $\pm m_I$ degeneracy is completely removed when $\eta \neq 0$. This result is an example of Kramers' theorem which states that for a system of angular momentum $M = n + \frac{1}{2}$ where n = 0,1,2, etc. the degeneracy of any state can never be completely lifted by electric fields.

In an asymmetric field gradient the eigenfunctions are linear combinations of the basis funcations $| I, m_I, \epsilon \rangle$ with functions whose m_I' values are $(m_I \pm 2)$ and, using these and the matrix elements 6.4.3 and 6.4.4, the secular equations for the system can be worked out. Table 6.4.1 tabulates the secular equations for spins $\frac{3}{2}, \frac{5}{2}, \frac{7}{2}$. [40]

I	Secular Equation	Units of
$\frac{3}{2}$	$x^2 - 3\eta^2 - 9 = 0$	E/A
$\frac{5}{2}$	$x^3 - 7(3+\eta^2)x^2 - 20(1-\eta^2) = 0$	E/2A
$\frac{7}{2}$	$x^4 - 42(1+\frac{1}{3}\eta^2)x^2 - 64(1-\eta^2)x + 105(1+\frac{1}{3}\eta^2)^2 = 0$	E/3A

Secular Equation for Pure N.Q.R. when $\eta \neq 0$.
Table 6.4.1.

For $I = \frac{3}{2}$ the solutions are

$$E_{\pm\frac{3}{2}} = 3A\,(1+\tfrac{1}{3}\eta^2)^{\frac{1}{2}}$$

$$E_{\pm\frac{1}{2}} = -3A\,(1+\tfrac{1}{3}\eta^2)^{\frac{1}{2}}$$

the suffices of E refer to the pure states to which they reduce when $\eta = 0$. The single resonance frequency becomes

$$\nu_{3/2} = \frac{eQq}{2h}\,(1+\tfrac{1}{3}\eta^2)^{\frac{1}{2}} \qquad 6.4.5$$

Therefore both $|eQq|$ and η cannot be obtained from a quadrupole resonance spectrum alone since there is only one absorption frequency.

An expansion of the energy levels for $I = \frac{5}{2}$, limited to the lowest power in η^2 (which is valid for $\eta < 10\%$) gives

$$E_{\pm\frac{5}{2}} \approx A(10+\tfrac{5}{9}\eta^2), \quad E_{\pm\frac{3}{2}} \approx A(-2+3\eta^2), \quad E_{\pm\frac{1}{2}} \approx A(-8-\tfrac{32}{9}\eta^2)$$

The frequencies of the two transitions governed by the rule $\Delta m_I = \pm 1$ become

$$\nu'_{5/2} \approx \frac{3eQq}{20h}\,(1+\tfrac{59}{54}\eta^2) \qquad \nu''_{5/2} \approx \frac{3eQq}{10h}\,(1-\tfrac{11}{54}\eta^2) \qquad 6.4.6$$

whence

$$\nu''_{5/2} \big/ \nu'_{5/2} \approx 2(1-\tfrac{35}{27}\eta^2)$$

Therefore for a nucleus with spin $\frac{5}{2}$ the asymmetry of the electric field gradient can be determined from the ratio of the two resonance frequencies.

For higher spins $|eQq|$ and η can be determined if two of the numerous resonance lines can be found and identified.

The transitions other than those corresponding to $\Delta m_I = \pm 1$ are forbidden for axial symmetry and are weak except for large values of η These need not be considered further.

For integral spins the $\pm m_I$ degeneracy of the axially symmetric case is removed when $\eta \neq 0$. For $I = 1$ the $m_I = 0$ remains unaffected, with energy

$$E_0 = -\tfrac{1}{2}eQq$$

and the $m_I = \pm 1$ level is split by the anisotropy of the field gradient, into[39]

$$E_{\pm} = \tfrac{1}{4}\,eQq(1\pm\eta)$$

The values of $|eQq|$, the quadrupole coupling constant, and η, the asymmetry parameter — both functions of the electrostatic potential experienced by the quadrupolar nucleus and generated by surrounding charges in the molecule and environment — can be determined, in all

cases except $I = \frac{3}{2}$ by measurement of the frequencies at which quadrupole resonances occur. The axis of symmetry of the field gradient, or the axis from which small deviations from axial symmetry are measured, can be estimated by studying the dependence of the intensity of resonance lines on the orientation of the applied oscillating field. A superior method of obtaining the direction of this axis is outlined in section six of this chapter.

6.5. Detection of Nuclear Quadrupole Resonances

It turns out that the frequency, ν, of the applied perturbing field, $\mathcal{H}'(t)$, which is required to cause transitions between adjacent quadrupolar energy levels is, for a large number of quadrupolar nuclei in normal chemical situations, in the range $1-10^3$ Mc/s.[41] Therefore, again, as in N.M.R., a radiofrequency field can be used to induce the transition described by 6.4.2 for $\eta = 0$ and equations similar to 6.4.5 and 6.4.6 for $\eta \neq 0$. It will be shown in a later section that quadrupole resonance experiments cannot be performed in liquids or in solids near the melting point because the continual tumbling of the molecules produces an effective electric field gradient at the nucleus of zero. Quadrupole resonance may be observed in gases at low pressures, when the probability of intermolecular collision is greatly reduced and the field gradients at the nuclei do not average out to zero. Most work in nuclear quadrupole resonance spectroscopy is performed in the solid state. For pure N.Q.R. either a powdered sample or a single crystal is used.

6.6. The Effect of a Small Applied Magnetic Field on Quadrupole Resonance Spectra

A small magnetic field, through interaction with the magnetic dipole moment of the quadrupolar nucleus, causes the pure quadrupole energy levels, defined by 6.3.10, to be perturbed. This is the "low field" situation mentioned in chapter five.

If, for simplicity, the electric field gradient at the nucleus is assumed to have axial symmetry, $\eta = 0$, then the effect of the Zeeman interaction is to produce energy levels defined by

$$E_{m_I} = \frac{eQq}{4I(2I-1)}\left[3m_I^2 - I(I+1)\right] - \gamma\hbar H m_I \cos\theta \qquad 6.6.1$$

where γ is the magnetogyric ratio of the quadrupolar nucleus, H is the Zeeman field magnitude, θ is the angle between the field and the

symmetry axis of the field gradient and $m_I > \frac{1}{2}$. Thus the degeneracy of the $\pm m_I$ levels is removed by this perturbation. The $m_I = \pm\frac{1}{2}$ states are unique. They have identical energies in the absence of the Zeeman field but when the Zeeman perturbation is applied, the two states mix, to form new states $|+\rangle$ and $|-\rangle$ whose energies are found to be described by[39]

$$E_{\pm} = \frac{eQq}{4I(2I-1)}\left[\frac{3}{4} - I(I+1)\right] \mp \frac{1}{2} f \gamma \hbar H\cos\theta \qquad 6.6.2$$

where $f = \left[1 + 4\tan^2\theta\right]^{\frac{1}{2}}$

The states $|+\rangle$ and $|-\rangle$ which reduce to $|+\frac{1}{2}\rangle$ and $|-\frac{1}{2}\rangle$ respectively when $H = 0$ or when $\theta = 90°$, are given by

$$|+\rangle = |+\tfrac{1}{2}\rangle \cdot \sin\alpha + |-\tfrac{1}{2}\rangle \cos\alpha$$

$$|-\rangle = |-\tfrac{1}{2}\rangle \sin\alpha - |+\tfrac{1}{2}\rangle \cos\alpha \qquad 6.6.3$$

where $\tan^2\alpha = (f+1)/(f-1)$.

The single resonance line obtained for a nucleus of spin $\frac{3}{2}$ at a frequency

$$\nu_Q = eQq/2h$$

in zero magnetic field is replaced as a result of Zeeman perturbation by four lines at frequencies

$$\nu_\alpha = eQq/2h - \frac{3-f}{4\pi} \cdot \gamma H\cos\theta$$

$$\nu_\beta = eQq/2h - \frac{3+f}{4\pi} \cdot \gamma H\cos\theta \qquad 6.6.4$$

$$\nu_{\alpha'} = eQq/2h + \frac{3-f}{4\pi} \cdot \gamma H\cos\theta$$

$$\nu_{\beta'} = eQq/2h + \frac{3+f}{4\pi} \cdot \gamma H\cos\theta$$

where the α-type lines are due to the transitions, $|+\frac{3}{2}\rangle \leftrightarrow |+\rangle$ and $|-\frac{3}{2}\rangle \leftrightarrow |-\rangle$ and the β-lines arise from $|+\frac{3}{2}\rangle \leftrightarrow |-\rangle$ and $|-\frac{3}{2}\rangle \leftrightarrow |+\rangle$ transitions. Figure 6.6.1 shows the effect of a Zeeman field on the resonances of nuclei with $I = \frac{3}{2}$.

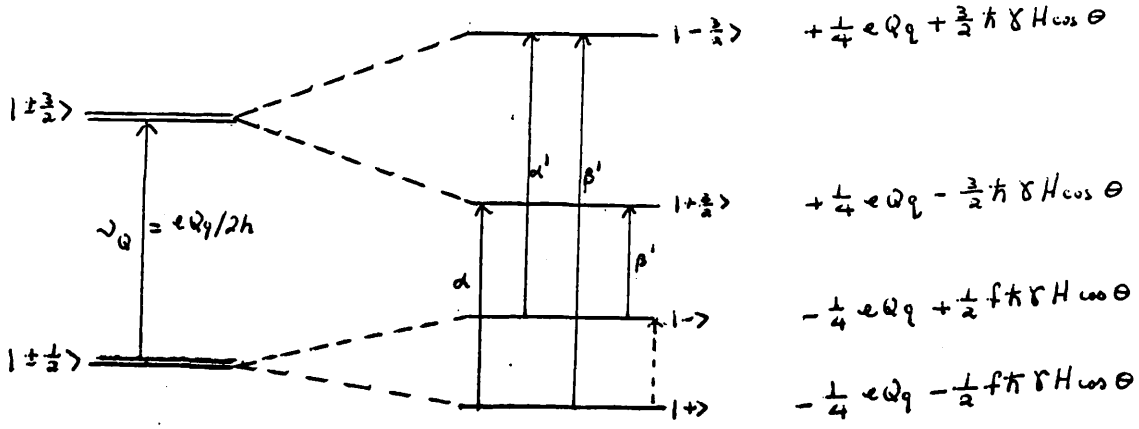

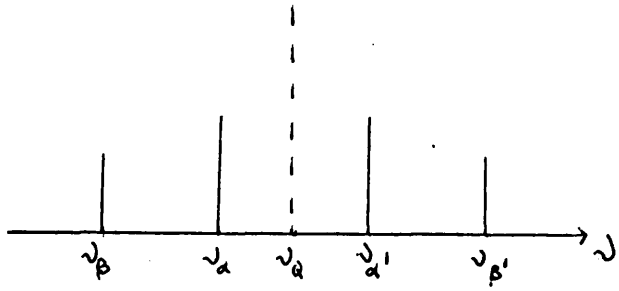

Figure 6.6.1

The intensity ratio of the outer, β, pair of resonance lines to the inner, α, pair turns out to be $(f-1)/(f+1)$. When $\theta = 0°$ the separation between the α lines is $\frac{2\gamma H}{2\pi}$ c/s and the β lines vanish, since $f = 1$. At $\theta = 90°$ only two lines are observed, again at $\nu_Q \pm \gamma H(2\pi)^{-1}$ c/s due to overlap of the α and β lines. Further to these transitions, there is the low frequency transition $|+\rangle \longleftrightarrow |-\rangle$, shown by the dotted line in figure 6.6.1. The frequency of this transition is, to first order,

$$\nu = f\gamma H\cos\theta/2\pi \qquad 6.6.5$$

In general, for any I, the effect of a Zeeman field on a quadrupole resonance is to split each line in the pure spectrum, which arises from the allowed transitions $\pm m_I \rightarrow \pm(m_I+1)$, into two lines when $m_I > \frac{1}{2}$ and into four lines when $m_I = \frac{1}{2}$.

The effect of a Zeeman field on the quadrupole resonance spectrum of a nucleus in an asymmetric field gradient has been investigated by a number of workers [42, 43] and is not given here. However for nuclei with integral spins the $\pm m_I$ energy levels are not degenerate even in the absence of a small magnetic field, so that the Zeeman field simply displaces each spectral line without introducing extra absorptions. If there are two lines in the pure N.Q.R. spectrum of a nucleus with spin 1, they may be due to two resonant nuclei experiencing non-equivalent symmetric field gradients or to all nuclei experiencing identical asymmetric field gradients. Application of a Zeeman field would produce four lines if the former were the case but would simply shift the two lines if all the nuclei were in identical environments.

For nuclei with spin $\frac{3}{2}$ it is impossible to establish the magnitudes of both eQq and η from a pure N.Q.R. experiment since only one resonance

line occurs. In many cases η is expected to be small and, in these instances, it can be neglected. However both these quantities can be obtained from measurements of the four-lined spectrum obtained in the presence of a small magnetic field. Normally a field of about 100 gauss is used in Zeeman N.Q.R. experiments and single crystal speciments are required. Powder or polycrystalline samples are not suitable because the random orientation of the constituent crystals produces a spread in θ values, resulting in a spread of absorption frequencies about each pure resonance frequency.

By observing the frequencies of nuclear quadrupole Zeeman resonance lines as a function of the orientation of a single crystal in the magnetic field the direction of the field gradient symmetry axis and the magnetogyric ratio of the quadrupolar nucleus can be determined.

6.7. Factors affecting N.Q.R. Line Widths and Frequencies

The magnetic effects of neighbouring nuclei, or the effects of molecular motions and crystal imperfections have not so far been considered. Magnetic interactions, dipole-dipole and spin-spin, can occur between the resonant quadrupolar nucleus and neighbouring nuclei.

Magnetic dipole-dipole interactions between neighbours cause a fine splitting of the quadrupole spectrum, proportional to the factor $\mu_A \mu_B r_{AB}^{-3}$ where μ_A and μ_B are the magnetic moments of the neighbouring nuclei and r_{AB} is their separation. As in N.M.R., such dipolar interactions cause a general broadening of a quadrupole spectrum [44] unless there is a particularly close neighbour, whose dipolar contribution is relatively large.[45] Magnetic spin-spin interactions take place between two nuclei through the interaction of their nuclear spins with the electrons forming the chemical bond between them. If the effect of this interaction is sufficiently strong to overcome the direct dipolar interaction then splitting of the resonance spectrum can be observed [46].

Broadening due to this interaction is expected only if it occurs with equal strength between the resonant nucleus and a large number of neighbouring nuclei and such a situation, although possible in metals and ionic crystals, is unlikely to exist in molecular solids, where there is usually little direct bonding between molecules.

Dislocations and strains in crystals and powders broaden quadrupole spectra [47] because they produce random distributions of field gradients

at nuclear sites. Strains can be introduced into crystals and powders as a result of random distributions of intermolecular interactions, by cooling as well as by the processes of crystal growth.

The presence of impurities also leads to broadening of N.Q.R. lines as a result of random distribution of environments around different nuclei.

Molecular motions in solids have a profound effect on quadrupole resonances, just as they have in nuclear magnetic resonances. The torsional motions of molecules inside crystals cause the nuclei to be agitated at a rate which is very fast compared to the quadrupole resonance frequencies of the nuclei ($10-100cm^{-1}$ against $0.1-0.01cm^{-1}$). This has been shown [48] to have two effects. Firstly there is a shift in N.Q.R. frequencies since the nuclei see temperature-dependent averaged field gradients which are different from those they would see if the molecules were stationary. Secondly resonance lines are broadened due to the natural line width being affected by the effect of the motion on the relaxation mechanisms and due to random fluctuations in the field gradients caused by torsional motions interacting with other vibrational and rotational degress of freedom of the molecules.

Rotational motions of the molecules themselves in the molecular crystal, or of groups within each molecule relative to the rest of the molecule, have been shown to markedly affect N.Q.R. spectra.[49] If rotation occurs about an axis θ degrees away from the symmetry axis of the field gradient then the net field gradient experienced at the nucleus is given by

$$q' = \tfrac{1}{2}\, q(3\cos^2\theta - 1)$$

The effective field gradient at a nucleus is, therefore, always less than that experienced in the absence of rotation unless the axis of rotation is itself the symmetry axis of the field gradient. Additional rotations about other axes reduce the effective field gradient even more. In a liquid where the axis of rotation is continually changing the effective field gradient is averaged to zero. N.Q.R. experiments cannot be performed in liquids or in solids at temperatures close to their melting point.

CHAPTER 7

USES OF NUCLEAR QUADRUPOLE RESONANCE IN CHEMISTRY: APPLICATION TO MERCURIC CHLORIDE COMPLEXES

7.1. Contributors to Electric Field Gradient at a Quadrupolar Nucleus[50]

The energy levels and transition frequencies derived in the previous chapter are determined by the interaction of a nucleus of quadrupole moment Q with the electric field gradient generated by a non-spherical, or non-cubic, distribution of charge around it. This field gradient is described by the parameters q and η, the Z-axis component of the field gradient at the nucleus and the field gradient asymmetry parameter, respectively. In a crystal the extra-nuclear charge distribution arises from the atom's inner core of electrons, valence and bonding electrons and from the charges exerted by neighbouring nuclei in the molecule and crystal and their electrons. Thus q and η depend on both the intra- and inter-molecular bindings in the crystal. In molecular crystals, generally, the intramolecular binding is much stronger than the intermolecular binding so that q's for free molecules in the gaseous state do not differ very much from the q's of molecules in the solid state.

Measurements of quadrupolar absorption frequencies of a nucleus in a crystalline compound yield values for the parameters eQq and η so that the field gradient parameter q can only be determined if the quadrupole moment of the nucleus is known. Accurate values of Q for a large number of nuclei, including the halogens and the isotopes of mercury, are available from other sources.

Before considering how quadrupole coupling constants, eQq, can be interpreted to give information about molecular and crystal structure it is best to see what factors determine the field gradient at a nucleus. A charge i at distance r_i from nucleus, Q, gives rise to a potential $V = e/r_i$ at the nucleus and a field gradient.

$$q_i = \left(\frac{\partial^2 V}{\partial z^2}\right)_i = \frac{\partial^2}{\partial z^2}\left(\frac{e}{r}\right)_i = \frac{e(3\cos^2\theta_i - 1)}{r_i^3} \qquad 7.1.1$$

where θ_i is the angle between r_i and the symmetry axis Z.

To obtain the contribution of the ith electron in a molecule containing nucleus Q the above expression must be averaged over the orbital of the electron in the molecule. Therefore the total electronic

contribution of the molecule to the field gradient at Q is q_{el}.

$$q_{el} = \sum_i -e \int \psi_i^* (3\cos^2\theta_i - 1)\, r_i^{-3}\, \psi_i \, d\tau \qquad 7.1.2$$

where ψ_i is the normalised wave function describing the orbital of the ith electron in the molecule. The total contribution to the field gradient q at the nucleus is the sum of the electronic contributions, 7.1.2, together with the contribution of the other nuclei in the crystal, a sum, of which 7.1.1 is the ith member. Clearly there are far more electrons and nuclei in the molecule that there are observables, and the correct wave function of the electrons are not known, so that an exact solution is not possible. Assumptions must be made to simplify 7.1.2. Firstly only intra-molecular contributors need be considered, that is contributions from nuclei and electrons of neighbouring molecules can be ignored. The r^{-3} dependence of q also makes it reasonable to neglect all charges within the molecule except those electrons in orbitals which are close to nucleus Q.

These simplifications are so sweeping that the normal electronic charge distribution around nucleus Q in the free atom can be regarded as being perturbed by all other charges, the greatest perturbation arising from direct bonding of atom Q to other atoms. Thus charge distribution data can be expressed in terms of free atom information.

$$q_{crystal} \approx q_{mol} = f\, q_{atom} \qquad 7.1.3$$

where f is a quantity depending largely on the electronic configuration around the nucleus Q and hence on the bonding involving Q.

q_{at} can be regarded as being made up of a contribution from the inner "closed shell" electrons around nucleus Q and a contribution from the electrons in the outer, valence shell. The former contribution is very small, although not zero. Closed shells of electrons are assumed to a first approximation to have spherical symmetry so that their effect on q_{at} is nearly zero. That the effect is not exactly zero is due to the fact that an aspheric nucleus, such as Q must be, induces an aspherical distribution of electronic charge around it, and also to the fact that the non-spherically symmetric electron distribution of the outer valence electrons also destroys the ideally symmetrical distribution of charge in the inner shells. This effect has been analysed by Sternheimer [51]. The valence electrons of atoms

can be in s,p,d,f - etc. - type orbitals. An s-electron orbital has spherical symmetry around the atomic nucleus and so is not expected to contribute to q_{at}, except for contributions from the Sternheimer effect. Townes and Dailey [52] computed the relative values of field gradients generated at the nucleus by electrons in various electronic orbitals, defined by the quantum numbers n, l and m, with m = 0. Those orbitals whose regions of maximum electron density are closest to the central nucleus, because of the r^{-3} term in 7.1.1, have the greatest effect. It turns out that the effect of a d-electron is only about 10-15% that of a p-electron with the same n quantum number, and a 4p electron has only a small effect on q compared with a 3p electron. Thus to a reasonable approximation only p-electrons in the valence shell of an atom need to be considered. Taking the chlorine atom as an example, the electronic configuration is $1s^2 2s^2 2p^6 3s^2 3p^5$. Only the five 3p-electrons significantly contribute to q_{Cl}. The configuration $3p^6$ would have spherical symmetry and the field gradient would be zero, neglecting the Sternheimer polarisation factor. One can assume that the actual q_{at} for chlorine is caused by a lack of one 3p electron in an otherwise spherical environment, that is, equals the value for a single electron in the 3p orbital, but with opposit sign,

i.e. $q_{at} = -q_{3p}$ for chlorine.

q_{at} can often be calculated from experimental data because quantities such as the nuclear magnetic hyperfine structure [53] and the fine-structure splitting of atomic spectra [54] depend upon $\langle \phi_i | r_i^{-3} | \phi_i \rangle$ where ϕ_i is the wave-function for the ith electron in the atom. Also, for atoms of known quadrupole moment, Q, the field gradient at the nucleus can be determined from the value of the atomic coupling constant, eQq(atom) [55].

Returning to the example of chlorine, one can determine q at the chlorine nucleus when the atom is involved in bonding. If, for simplicity, the "electon hole" in the chlorine valence electron shell is in the $3p_z$ orbital then formation of a σ-bond between Cl and X involving the $3p_z$ orbital will cause the effect of this "hole" to be spread over the bonding molecular orbital ψ compounded out of the two atomic orbitals ϕ_{Cl} and ϕ_x.

Therefore $\psi = a\psi_{Cl} + b\psi_x$ 7.1.4

where a^2 and b^2 represent the relative importance of the original atomic orbitals ϕ_{Cl} and ϕ_x in this new bonding molecular orbital (m.o.). The total contribution of the two electrons in this m.o. to q at the chlorine nucleus is found, by substitution of 7.1.4 into 7.1.2, to be

$$(q_{bond})_{Cl} = 2a^2 \langle \phi_{Cl} | q_1 | \phi_{Cl} \rangle + 4ab \langle \phi_{Cl} | q_1 | \phi_x \rangle + 2b^2 \langle \phi_x | q_1 | \phi_x \rangle \qquad 7.1.5$$

The contribution of the non bonding $3p_x^2$ and $3p_y^2$ electrons of chlorine is assumed to be the same in the molecule as in the atom and the other non bonding electrons of X can be taken as having little effect on the total q at the chlorine nucleus, because of the r^{-3} term in 7.1.1. The first term on the right of 7.1.5 is $2a^2$ times the gradient produced by one electron in the atomic orbital ϕ_{Cl}, the second is the gradient produced by the electron density in the overlap region and the third term is $2b^2$ times the contribution from an electron in the original X atomic orbital ϕ_x. Because of the r^{-3} dependence of q, the last term and even the middle term can be neglected relative to the first term, so that

$$(q_{bond})_{Cl} \cong 2a^2 q_1 \qquad 7.1.6$$

The total contribution to q at the chlorine nucleus from the molecule Cl-X is therefore approximately equal to 7.1.5 plus the contributions from the two $3p_x$ and the two $3p_y$ electrons. This is equivalent to the field gradient which would be experienced at the chlorine nucleus from $(2 - 2a^2)$ electrons in an atomic $3p_z$ orbital but with opposite sign. Thus the one "electron hole" in the chlorine atom's 3p orbitals has been replaced by $(2-2a^2)$ "electron holes" in the 3p atomic orbital by the perturbing effect of bonding the atom X. Therefore one can write

$$q_{mol} = (2-2a^2)\, q_{at} = -(2-2a^2) q_{3p} \qquad 7.1.7$$

If the molecular orbital ψ is normalised then

$$a^2+b^2+2abS = 1 \qquad 7.1.8$$

The ionic character of a bond can be defined [56] as

$$i = a^2-b^2 \qquad 7.1.9$$

so that $1 \geq i \geq -1$. i=1 corresponds to the fully ionic structure $Cl^- X^+$, the orbital ψ being identical with the atomic orbital ϕ_{Cl}. i = 0 corresponds to the case when a = b that is when the bond is homopolar. i = -1 corresponds to the situation when a = 0 and ψ is

identical with atomic orbital ϕ_x. Normally a bond is intermediate in type so that one can consider ϕ_{Cl} to contain (1+i) electrons and ϕ_x as having (1-i) electrons, ignoring overlap between the orbitals. From 7.1.8 and 7.1.9 it can be shown that

$$a^2 \approx \frac{1+i}{2(1+S)}$$

and it is generally accepted that the overlap integral, S, can be neglected. Therefore 7.1.6 becomes

$$q_{mol} = (1-i)q_{at} = -(1-i)q_{3p} \qquad 7.1.10$$

The quantity f introduced in 7.1.3 has thus been related to the parameter i, the ionic character of the bond.

If bonding between Cl-X is described not in terms of a combination of pure atomic orbital as in 7.1.4 but as a combination of hybrid atomic orbitals, possessing some s and d character then ϕ_{Cl} in 7.1.4 must be replaced by

$$\phi_{Cl} = s^{\frac{1}{2}}\phi_s + p^{\frac{1}{2}}\phi_p + d^{\frac{1}{2}}\phi_d \qquad 7.1.11$$

so that the orbital has s-character of amount s and d character of amount d. Clearly, since "s-electrons" and d-electrons" contribute much less to q than do "p-electrons", q_{mol} will be smaller than given by 7.1.10. It can be shown using 7.1.11 in place of 7.1.4. that for a covalently bound chlorine atom

$$q_{mol} \approx \left[1-s+d-i(1-s-d)\right] . q_{3p} \qquad 7.1.12$$

Since the quadrupole moment Q is a constant for a given nuclear state

$$eQq_{mol} \approx \left[1-s+d-i(1-s-d)\right] . eQq_{at} \qquad 7.1.13$$

A direct measure of eQq_{mol}, together with its sign, can frequently be obtained from studies of the rotational spectra of molecules in the gas phase using microwave spectroscopy [57] and from molecular beam experiments [58]. eQq_{mol} has also been obtained for one or two molecules by the method of pure N.Q.R. spectroscopy in gases at low pressures. Measurement of the experimental eQq, which approximates fairly well to eQq_{mol}, can yield information about the character of the bonding involving the quadrupolar nucleus by comparison with the atomic coupling constant obtained by other techniques or, in simple cases, with values calculated for pure p-electrons. Unfortunately 7.1.13 contains three unknown parameters, s,d and i and only one measurable quantity, (eQq_{mol}/eQq_{at}). This difficulty can be reduced if measurements are made of

the eQq for extensive series of related compounds because on this basis conclusions can be drawn about the nature of the bonding from the trend in the coupling constant values.

In the above discussion it has been assumed that the $3p_x$ and $3p_y$ atomic orbitals remained virtually unaffected by the attached X atom. This corresponds to the case where the field gradient is cylindrically symmetric, about the σ-bond direction, Z. If $\eta \neq 0$ then this means that no longer are the contributions of the $3p_x$ and $3p_y$ electrons equal, due presumably to the involvement of these atomic orbitals in some sort of π-bonding to atom X. It turns out that, for nuclei with $I = \frac{3}{2}$ such as ^{35}Cl, ^{37}Cl, ^{201}Hg,

$$\eta = \frac{3(N_x - N_y)eQq_{at}}{4\nu}$$

where N_x and N_y are the populations of $3p_x$ and $3p_y$ orbitals of the chlorine atom in the molecule and ν is the frequency of quadrupole transition between the $m_I = \pm\frac{1}{2}$ and $m_I = \pm\frac{3}{2}$ states. Hence information on the difference in population of the $3p_x$ and $3p_y$ states of the atom can be obtained by a measure of the asymmetry parameter η.

Despite the existence of the approximation of 7.1.3., $q_{crystal} \approx q_{mol}$, useful information, other than that just outlined, can be procured from measurements of eQq in the solid state. The number and symmetry of chemically inequivalent lattice sites in the unit cell of a crystal which are occupied by the same quadrupolar atomic species but generally do not have identical q_{zz} values can be obtained by studying the number of resonance lines and the relative frequencies. For nuclei with $I = \frac{3}{2}$ one resonance line is expected for each inequivalent lattice site. Nuclear positions which are equivalent in the free molecule may be rendered inequivalent in the crystalline lattice due to intermolecular forces.

Zeeman patterns of quadrupole spectra in single crystals enable the asymmetry parameter to be determined and also the orientation of the principal axes of the field gradient tensor with respect to axes fixed in the crystal. The direction of these principal axes with respect to axes in the free molecules can be obtained approximately from considerations of the molecular structure. Therefore Zeeman studies in N.Q.R. can determine the orientations of molecules in the crystalline lattice.[59]

It was mentioned briefly in the previous chapter how resonance frequencies, ν, and line widths, $\delta\nu$, can change with temperature, being related to the torsional and rotational motions of the molecules within the crystal. Informations about these molecular motions can be obtained by studying the changes in ν and $\delta\nu$, as well as T_1, as functions of temperature [49,60,61]. Graphs of, say, ν (c/s) against T (^{o}K) are usually smooth curves and can be related approximately to the internal motions of the molecules in the crystal lattice.

Occasionally such a graph of experimental frequency against temperature shows abrupt changes in resonance frequency at unique temperatures. These temperatures have been shown to involve phase transitions [62,63]. The sudden change in crystal structure which takes place at a transition point causes the inter-molecular binding forces of the crystal to alter so that the electric field gradient, and therefore eQq, at a resonant nucleus abruptly alters at this temperature. Thus N.Q.R. is a sensitive method of detecting phase changes in crystals and many studies of such phenomena have been made.

The intermolecular contribution to the field gradient at a nucleus in a molecular crystal has two components, a direct and an indirect. The direct contribution is due to charge distributions in neighbouring molecules. Due to the large intermolecular distances and the r^{-3} relationship of distance with q this direct effect has practically no effect on the field gradient at the nucleus within the central molecule. In ionic crystals, however, this is not the case because of large electric charge on the neighbouring ions: the difference in ^{35}Cl resonance frequencies of 29.93 and 28.10 Mc/s for $NaClO_3$ and $KClO_3$ respectively could be attributed [44] to the direct effects of their respective cationic neighbours. The neighbouring molecules in a molecular crystal can affect the field gradient in an indirect manner. These molecules are held together by electrostatic forces which cause the ionic character of the intramolecular bonds in solids to differ from that present in free molecule.

Differences in eQq_{mol} obtained in the solid state using N.Q.R. and in the gaseous state, using microwave spectroscopy, have been "explained" in terms of a change in the ionic character of bonds within the molecule.

In order to extract information concerning molecular and crystal structure using N.Q.R. absorption frequencies, it is most advantageous, because of the complex relationship between the quadrupole coupling constant and the electrical environment of a quadrupolar nucleus, to investigate an extensive series of related compounds. In this way trends in the absorption frequencies of the series may be related to structural differences among the members of the series.

The following section is concerned with the possibility of extracting information concerning the structure of a series of complexes of mercuric chloride using N.Q.R. spectroscopy.

7.2. Mercuric Chloride and Some of its Complexes

Atomic mercury has an electronic configuration $1s^2 2s^2 2p^6 \ldots 5s^2 5p^6 5d^{10} 6s^2$ in its ground state. Like other s^2p^0 atoms mercury should be expected to form linear diatomic molecules with monovalent atoms or radicals, such as the halides and the methyl radical, by making use of collinear sp hybrids. The molecules $HgCl_2$, $HgBr_2$ and HgI_2 have been shown by electron diffraction [64] to be linear in the vapour state, the Hg-Cl bond distance in the mercuric chloride being 2.34Å. Even "HgX", the mercurous halides, were shown [65] to consist of linear X-Hg-Hg-X molecules in which the mercury atoms are again bonding with their sp hybrid orbitals.

In the crystalline state, however, the situation is less straightforward. Mercuric chloride is the only simple halide known to exist essentially on the form of simple molecules, with the Hg-Cl bond length now 2.25Å [66]. It could be described as an infinite network of mercury and chlorine atoms with each mercury surrounded by six chloride ions in a grossly distorted octahedral arrangement such that the discrete molecules of $HgCl_2$ appear in plan to have the arrangement in figure 7.2.1. where the atoms shown as dotted circles lie in planes above and below that of the atoms indicated by full circles.

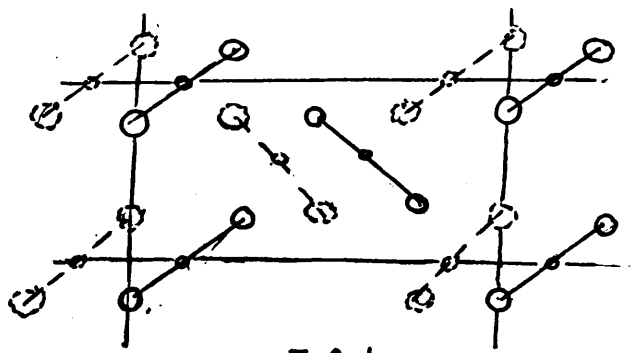

Figure 7.2.1

The distances between the mercury atoms and the four "out-of-plane" neighbouring chlorides are 3.34Å for one pair and 3.63Å for the other pair.

The hydrate $K_2HgCl_4H_2O$ has been shown [67] to be built up from chains of $HgCl_6$ octahedra as shown in figure 7.2.2.

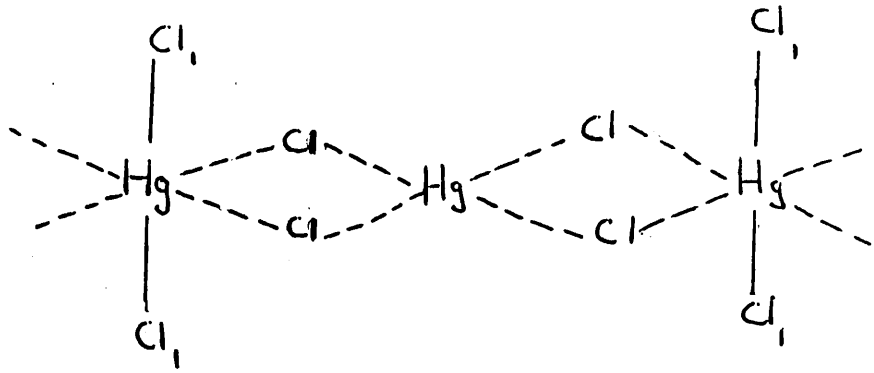

Figure 7.2.2.

with the $HgCl_1$ distances 2.4Å; two Hg-Cl distances are 2.8Å and the other two are 3.15Å in length. The chains are held together by the K^+ ions and the water molecules. The $(HgCl_4)^{2-}$ chains may be visualised as being equivalent to a pair of chloride ions suitably placed between pairs of $HgCl_2$ molecules.

NH_4HgCl_3 has been assigned the structure shown in figure 7.2.3.[68] in which layers of $HgCl_6$ octahedra are linked such that the composition is $(HgCl_3)_n^{n-}$.

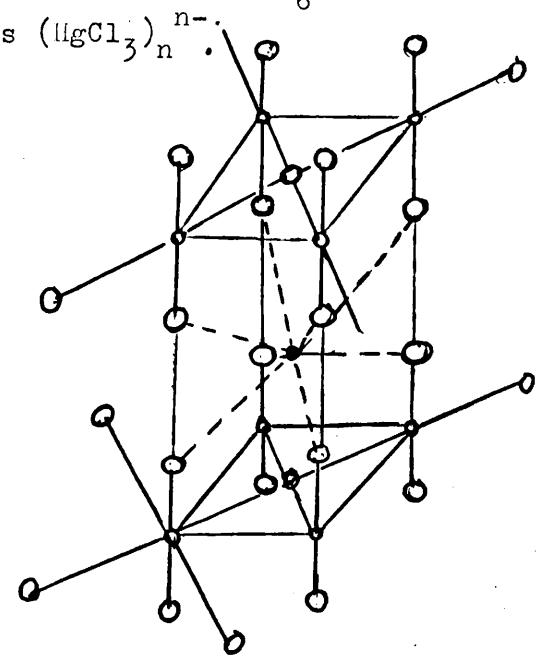

Figure 7.2.3.

The layers are held together by the NH_4^+ ions. Again the bond-lengths are such that essentially an aggregate of $HgCl_2$ molecules, Cl^- and NH_4^+ ions is present. The Hg-Cl bond length in the $HgCl_2$ molecular component is 2.34Å, the Hg-Cl^- bond lengths are 2.96Å.

The evidence so far suggests that in the crystalline state mercuric chloride can be considered as complexing so that the chlorine environment of the mercury is a distorted octahedral arrangement, with two short strong and four longer weaker Hg-Cl bonds.

However complexes are known in which the mercury is approximately tetrahedrally co-ordinated. The bis(mercuric chloride) complex of 1,6, - dithia-cyclodeca-cis 3-, cis 8-, diene, 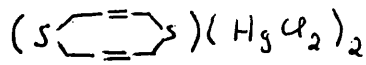

has been investigated by X-ray analysis and the following structure found [69].

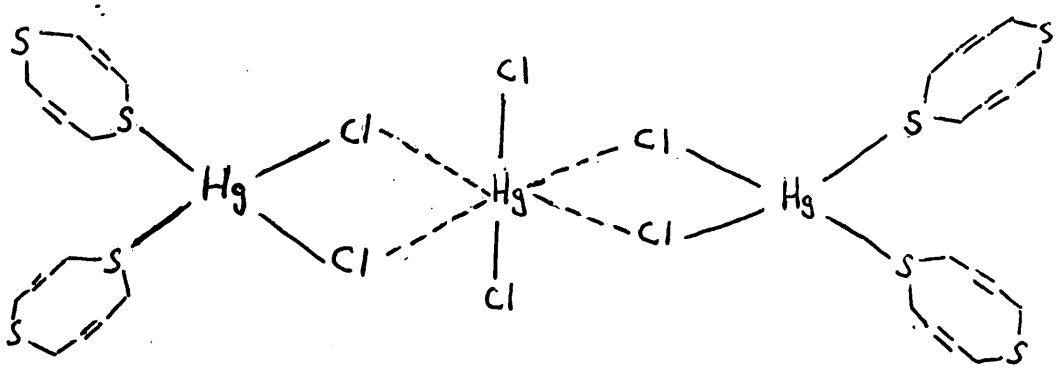

Figure 7.2.4

Figure 7.2.4. shows that there are two types of mercury environment; one is the distorted octahedron of chlorines similar to those already described and the other is a distorted tetrahedron involving two chlorine and two sulphur atoms.

Bisarsine tris (mercuric chloride), $(R_3As)_2\ (HgCl_2)_3$, is a member of the series $(R_3As)_nHgCl_2$ where n can be $\frac{2}{3}$, $\frac{1}{2}$, 1 or 2, and has been shown [70] to be as in figure 7.2.5. where again two mercury sites are present, the planar $HgCl_2$ or distorted octahedron of $HgCl_6$ and the distorted tetrahedron of $HgCl_3As$.

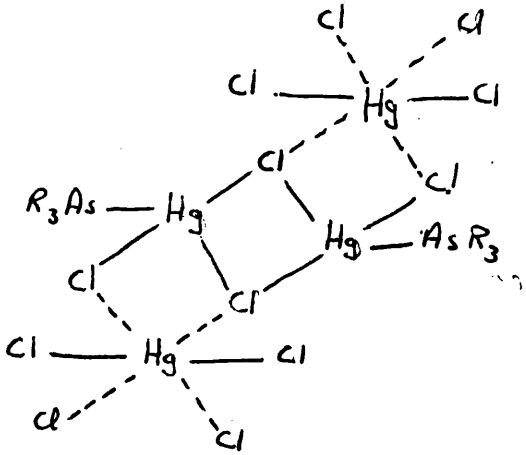

Figure 7.2.5.

It is generally accepted that the other members of this series have the mercury at the centre of a distorted tetrahedron, although X-ray analyses have not been performed. The n = 2 and n = 1 members are assumed to have the structures 7.2.6 and 7.2.7 respectively.

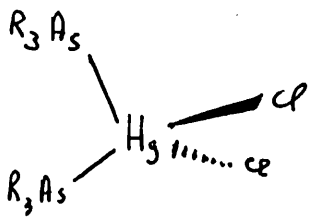

Figure 7.2.6

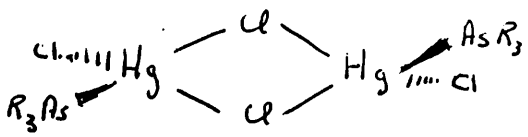

Figure 7.2.7

The fourth member of the series, the n = ½ member, is thought by the authors of reference 70 to have a structure analogous to figure 7.2.5, made up from two $HgCl_2$ "molecules" and one "molecule" of 7.2.7.

$K_2HgCl_4H_2O$ does not possess discrete $HgCl_4^{2-}$ tetrahedra but if a sufficiently large cation is substituted for K, the crystal is forced to adopt the $HgCl_4^{2-}$ tetrahedral arrangement. Perloline, $C_{20}H_{17}N_2O_3Z.yH_2O$ where Z = $\frac{1}{2}HgCl_4$, has been shown [71] to have discrete $HgCl_4^{2-}$ anions.

Mercuric chloride forms a number of stable complexes with sulphur-containing ligands, the dithiacyclodecadiene complex shown in figure 7.2.4 being one example. Thiourea and $HgCl_2$ form a series of complexes $HgCl_2.nSC(NH_2)_2$ where n = 1,2,3 and 4. All four complexes are white

solids. Only the dithiourea complex has been analysed by X-ray techniques[72] and it has been found to contain the system shown in figure 7.2.8.

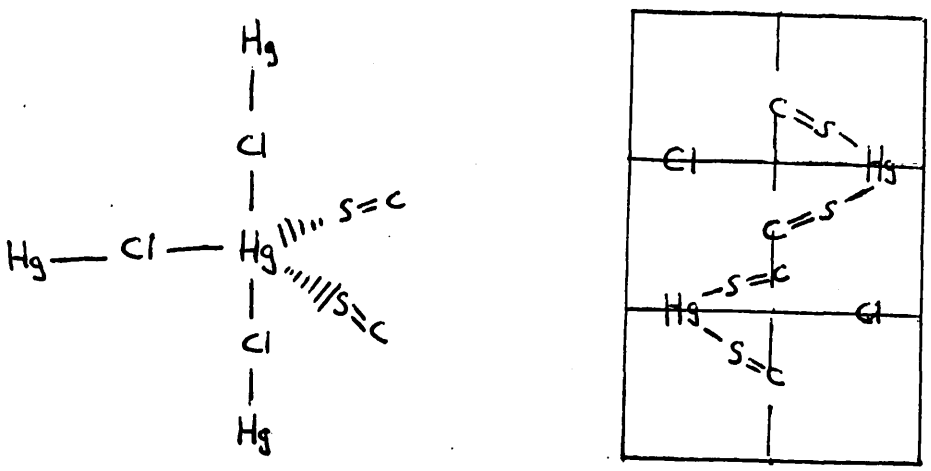

Figure 7.2.8.

Here the mercury is approximately penta-co-ordinated in a distorted trigonal bipyramidal arrangement involving three chlorines and two sulphurs.

Clearly these X-ray results indicate that it is not possible to use analogies to predict the structures of complexes of mercuric chloride. Each complex must be treated separately since it seems that different ligands force the mercury atom to adopt different stereochemistries. Information concerning the structures of these complexes could be obtained from ^{201}Hg, ^{35}Cl and ^{37}Cl nuclear quadrupole resonance investigations of polycrystalline speciments of the complexes.

Mercuric chloride has been thoroughly investigated using N.Q.R. and Table 7.2.1. shows the resonance frequencies for the ^{201}Hg, ^{35}Cl and ^{37}Cl nuclei.[73]

The structure of mercuric chloride is such that the two chlorine atoms of the linear $HgCl_2$ molecules within the planar sheets of figure 7.2.1. have slightly different surroundings so that two chlorine quadrupole resonance frequencies are observed for each chlorine isotope. Dehmelt, Robinson and Gordy[73] interpreted the values for the (eQq) for ^{201}Hg in terms of the two HgCl bonds being made up of $6s-6p_z$ hybrids on the mercury atom, each bond having 50% p_z-character.

Table 7.2.1.

Nucleus	Abundance	Spin	Temp.	Frequency(Mc/s)
^{201}Hg	13.24%	$\frac{3}{2}$	83°K	361.966
^{35}Cl	75.4%	$\frac{3}{2}$	room	22.2303 22.0503
^{37}Cl	24.6%	$\frac{3}{2}$	room	17.5197 17.3789

The ionic characters of the Hg-Cl bonds were estimated from the coupling constants for the two chlorine nuclei. Using these data together with a value for the field gradient produced per 6p electron a value for the quadrupole moment of ^{201}Hg was obtained and compared favourably with the value obtained from hyperfine structure of optical spectra; its sign, however, cannot be determined from N.Q.R. measurements.

The environment around each mercury and chlorine atom will differ from complex to complex so that the number and frequency of the quadrupole resonance is expected to reflect these environment changes. For example, by comparing the ^{35}Cl resonances of $HgCl_2$ and $K_2HgCl_4H_2O$, one would expect in both cases two resonance frequencies from the two chemically inequivalent chlorine sites in these crystalline compounds. The resonances from the $K_2HgCl_4H_2O$ sample are expected to occur at much lower frequencies than those from $HgCl_2$ because of the added negative charges in the $HgCl_4^{2-}$ chains. The effect of this additional charge is to increase the coefficient $2a^2$ of 7.1.6 to $(2+\delta)a^2$ for each nucleus where δ is the amount of extra electronic charge associated with the bonding orbital ψ so that instead of the field gradient at the chlorine nucleus being equivalent to $(2-2a^2)$ electron holes, the field gradient is produced by $(2-2a^2-\delta a^2)$ electron holes, effectively.

A ^{201}Hg N.M.R. spectrum of the complex 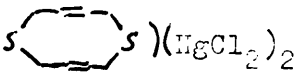 $(HgCl_2)_2$ would be expected to show two resonance frequencies due to the two inequivalent mercury sites in the compound, the octahedral $HgCl_6$ and the tetrahedral $HgCl_2S_2$ arrangements.

A ^{35}Cl or ^{37}Cl N.Q.R. investigation of the mercuric chloride dithiourea compound should yield two resonance frequencies, not far removed from the frequencies for $HgCl_2$ itself. The presence of a

Hg-S bond should affect the electron density around the chlorines so that the two frequency shifts with respect to $HgCl_2$ would not be expected to be the same. If the structure was assumed to approximate to the ionic species, then the chlorine nucleus in the cationic species would be expected to absorb at a greater frequency than in the "neutral" $HgCl_2$ since additional contribution δ is now negative, and the Cl^- ion would absorb at a very low frequency indeed, cf. NaCl.

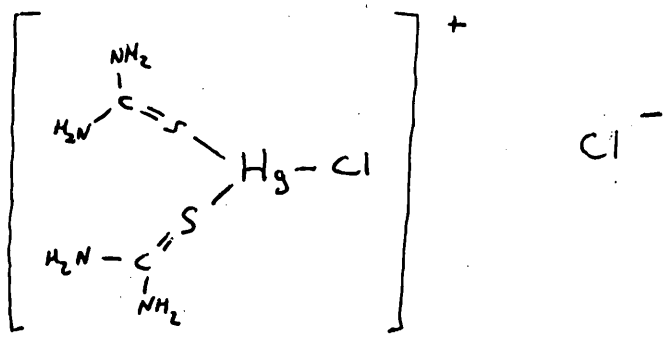

These examples illustrate qualitatively the kind of information one can associate with the relative frequencies of mercuric chloride and its complexes. It should be possible to distinguish between a neutral species, as in $HgCl_2$ and $HgCl_2 2SC(NH_2)_2$, a uninegative species, as in NH_4HgCl_3, a dinegative species, as in $K_2HgCl_4H_2O$, and positive species, as $HgCl_2 2SC(NH_2)_2$ might have been. It is also not unreasonable that a distinction can be made between an octahedral (or nearly so,) arrangement and a tetrahedral (or nearly so) arrangement, using N.Q.R. techniques. Of the large number of compounds mentioned in this section only a few could be investigated in the time available. Six compounds were selected for study, $HgCl_2$, $K_2HgCl_4H_2O$ and the four members of the mercuric chloride-thiourea series. The structures of three of these members are presently unknown and only the quadrupole resonance of the parent, $HgCl_2$, has been reported.

Clearly the most sensitive probe to the steriochemistry and charge distribution around the central mercury nuclei in these compounds is the ^{201}Hg N.Q.R. spectrum. However, since the quadrupole coupling constant of ^{201}Hg in $HgCl_2$ itself is 723.932 Mc/s, a spectrometer is required which operates at a frequency of 362 Mc/s. Chlorine N.Q.R. absorptions generally occur within the frequency range 10-60Mc/s; $Hg^{35}Cl_2$ resonates at about 22 Mc/s, $Hg^{37}Cl_2$ at about 17.4Mc/s.

The N.Q.R. spectrometer available to the author was designed to operate in the range 20-70 Mc/s so that it was decided to investigate the mercuric chloride complexes using the chlorine nuclei as the probes for structural information.

CHAPTER 8

A NUCLEAR QUADRUPOLE RESONANCE SPECTROMETER

8.1. Introduction

The detection of quadrupole resonances in solids requires the application of a radiofrequency magnetic field, of suitable amplitude, at a frequency determined by 6.4.2. This is achieved, as in most N.M.R. detection systems, by winding the oscillator coil, which generates the r.f., around a tube containing the solid of interest. The r.f. field H_1 should not be so large that saturation results nor so small that the signal is undetectable. Because in general the spin-lattice relaxation times are smaller, the nuclei can, after all, relax from higher to lower nuclear energy levels by both dipolar and quadrupolar interactions, larger r.f. power levels than in N.M.R. can be tolerated in N.Q.R. spectroscopy.

At resonance the magnetic susceptibility χ of the sample changes and this change can be detected by techniques similar to those discussed in connection with the detection of broad-line N.M.R. signals. It can be shown [61] that the cross-coil method of Bloch cannot in principle be used to detect pure N.Q.R. signals because the degeneracy of the oppositely-oriented nuclear spin states, such as $\psi_{\pm\frac{3}{2}}$ causes zero E.M.F. to be induced in a coil perpendicular to the r.f. field. The application of a small Zeeman field to the system removed the degeneracy of the spin states $\psi_{\frac{3}{2}m}$ so that the second coil no longer experiences zero E.M.F. and the cross-coil method becomes a possibility. However for the detection of zero-field N.Q.R. signals, only the one-coil methods of detection can be employed. The three most widely used single-coil techniques are the bridge-type, the regenerative continuous wave type and the super-regenerative type of oscillator detector.

A suitable N.Q.R. detection apparatus must have sufficient sensitivity so that the nuclear quadrupole signals exceed the background noise levels. In general N.Q.R. signals are weaker than N.M.R. signals. The frequencies to be detected fall into a rather wide range depending on the nucleus, described by Q and I, its electrical environment, determined by q and η, and the nuclear orientation with respect to its environment, described by m_I. In order to search for resonances over a limited frequency range the applied frequency must be changed continuously, without seriously affecting the stability

and sensitivity of the apparatus. Herein lies the most important difference in the technique of detecting N.Q.R. signals and N.M.R. signals. In N.M.R. the frequency of the perturbing r.f. field may be held fixed while the resonance condition is achieved by slowly changing an applied steady magnetic field. This is not possible in N.Q.R. since the frequency required to induce resonance is determined by the internal electric field gradient within the molecule and crystal.

Methods which use radiofrequency bridges are unsuitable for N.Q.R. signal detection because they require simultaneous tuning of a number of circuits.

The regenerative and super-regenerative oscillator detectors, however, may be used to detect N.Q.R. absorptions in the frequency range $0 \leq \nu \leq 100$ Mc/s. Regenerative detectors provide a simple signal output suitable for the measurement of line shape or the observation of close-lying multiplets. A disadvantage of this type of detector is that the maintainance of conditions of high sensitivity over a long period and at variable frequency is rather difficult.

In a super-regenerative oscillator the application of a periodic voltage to one of the electrodes of the oscillator valve of an r.f. oscillator causes it to alternately go in and out of oscillation. The periodic voltage, or quench voltage, can be generated by a separate oscillator or by suitably biasing the r.f. oscillator valve.

The sample coil and a variable condenser form a parallel tuned circuit which determines the frequency of the oscillator. During the "on" period the mutual conductance of the valve is large enough to allow sufficient feedback to cause the valve to operate as an oscillator, oscillations building up exponentially to a limiting amplitude determined by the curvature of the valve characteristic. During the "off" period the conductance of the valve becomes low enough to prevent sufficient feedback to sustain oscillations so that the oscillations decay exponentially. The time constant for the build-up and decay of oscillations if 2RC where C is the capacity and R is the resultant resistance of the tuned circuit. R is positive in the "off" periods and negative in the "on" periods, due to the large feedback during these periods.

At resonance the net positive resistance of the tuned circuit decreases. This increases the time constant for build-up of

oscillations due to the larger negative value for the resultant R and reduces the time constant for the decay process since R is now the less positive resistance of the tuned circuit. These effects cause a reduction in the total energy of the r.f. pulse.

If the period of the quenching oscillations is not long compared with the spin-spin interaction time T_2 the effect of the previous r.f. pulse on the nuclear spin levels will not have been completely destroyed by the time of commencement of the next "on" period. Thus the build-up at the next "on" period starts from this small residual voltage level resulting in the integrated pulse energy being increased at resonance. The relative importance of these two opposing effects is determined by the conditions of operation of the oscillator and by the nature of the sample.

Frequency sweep and frequency modulation must be employed in pure N.Q.R. spectroscopy to produce an audiofrequency signal output from the oscillator. This audiosignal can be extracted from the background noise and displayed on a d.c. recorder by means of selective audioamplification and phase sensitive detection. With a super-regenerative oscillator a quench frequency of the order of 10^4 c/s is often employed and the radiofrequency generated by such a quenched oscillator is complex, consisting of the central radiofrequency ν together with a number of sidebands of frequency $\nu \pm n\nu_Q$ where $n\nu_Q$ are harmonics of the quench frequency ν_Q. These sidebands can also satisfy the resonance condition so that an N.Q.R. spectrum obtained using a super-regenerative oscillator contains a number of responses, the intensities of each component decreasing as the value of n increases.

The super-regenerative oscillator has the advantage that very high r.f. voltages can be employed without much danger of saturating the spin system and detection occurs at the threshold of oscillation where sensitivity is maximum. On account of the high r.f. power levels which can be used, super-regenerative oscillators are suitable for observing resonances with large line widths. Also reasonable sensitivity can be maintained for long periods and over wide frequency ranges with only a minimum of adjustment.

For these reasons the super-regenerative oscillator is suitable for the purpose of this investigation of mercuric chloride and its complexes. A fuller account of the theory of super-regenerative

oscillators is given by Whitehead[74].

8.2. The Spectrometer

The 20 - 70 Mc/s N.Q.R. spectrometer, whose construction is due largely to Wallace[75] employs a self-quench super-regenerative oscillator-detector, similar to that proposed by Dean[76]. The spectrometer layout is shown in figure 8.2.1. A schematic representation of the way in which the signal is developed by this spectrometer is shown in figure 8.2.2.

The crystalline specimen to be investigated is placed in the tank coil of the self-quenching super-regenerative oscillator (1) which is tunable between 20 and 50 Mc/s. The grid RC network of the oscillator generates a quench frequency of between 10 and 40 Mc/s. A large audiomodulation amplitude of frequency 150c/s is superimposed on the oscillator radiofrequency so that as the latter is swept through a resonance, the output from the oscillator contains audio-signal at 300 c/s together with r.f., quench frequency and random noise at all frequencies. An r.f. filtering network and an a.f. preamplifier (1) remove the r.f. output and reduce the amount of quench frequency and noise frequency relative to the audiosignal and audionoise components of the output. A narrow-band amplifier (2) sharply tuned to 300c/s amplifies by a factor of about 200 the audiosignal plus noise of frequencies in the immediate vicinity of 300c/s, all other frequencies being suppressed by this network. A phase-sensitive detector (3), whose reference frequency of 300c/s is obtained by frequency doubling an output from the modulation frequency generator (5), converts the audio-signal together with a very small amount of noise into a d.c. output, suitable for display on a recorder (4).

Details of the circuitry of these components of the spectrometer are given in the paper by Dean and the thesis of Wallace. Changes were made in the method of frequency sweep, since in the Wallace arrangement 1 Mc/s could be swept in about 24 hours. So that the method of sweep used can be explained, the circuitry of the oscillator (and preamplifier) and modulation unit (6) is included, figure 8.2.3. The d.c. bias to the diode, HC 7001, is fixed at 30 volts and frequency modulation is achieved by superimposing a voltage of 150c/s upon this d.c. bias, the modulation amplitude being controlled by the switch and the 10K potentiometer in the figure 8.2.3. The quench

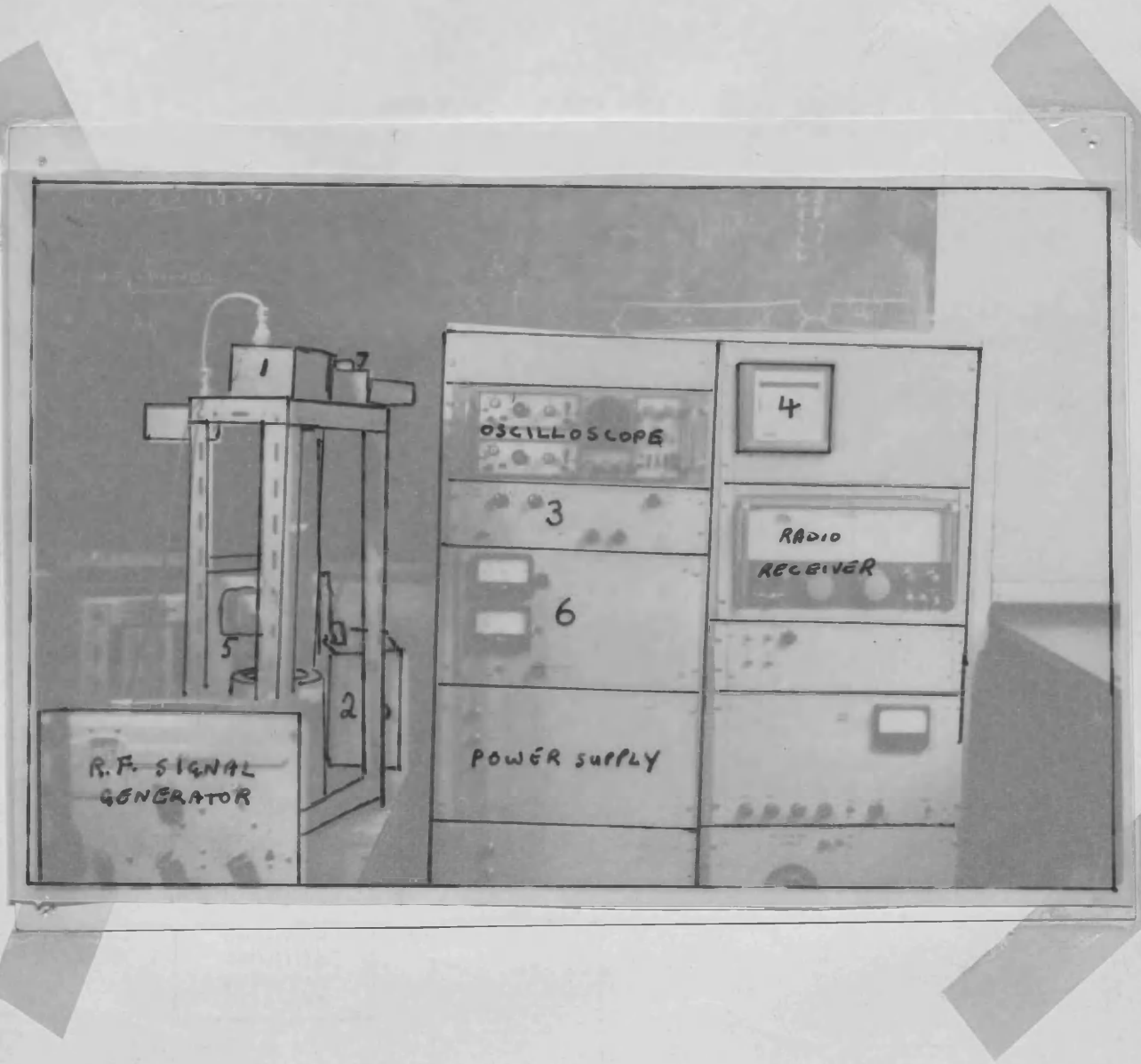
1
2
3
4
5
6
OSCILLOSCOPE
RADIO
RECEIVER
POWER SUPPLY
R.F. SIGNAL
GENERATOR

FIGURE 8.2.1

FIGURE 8.2.1

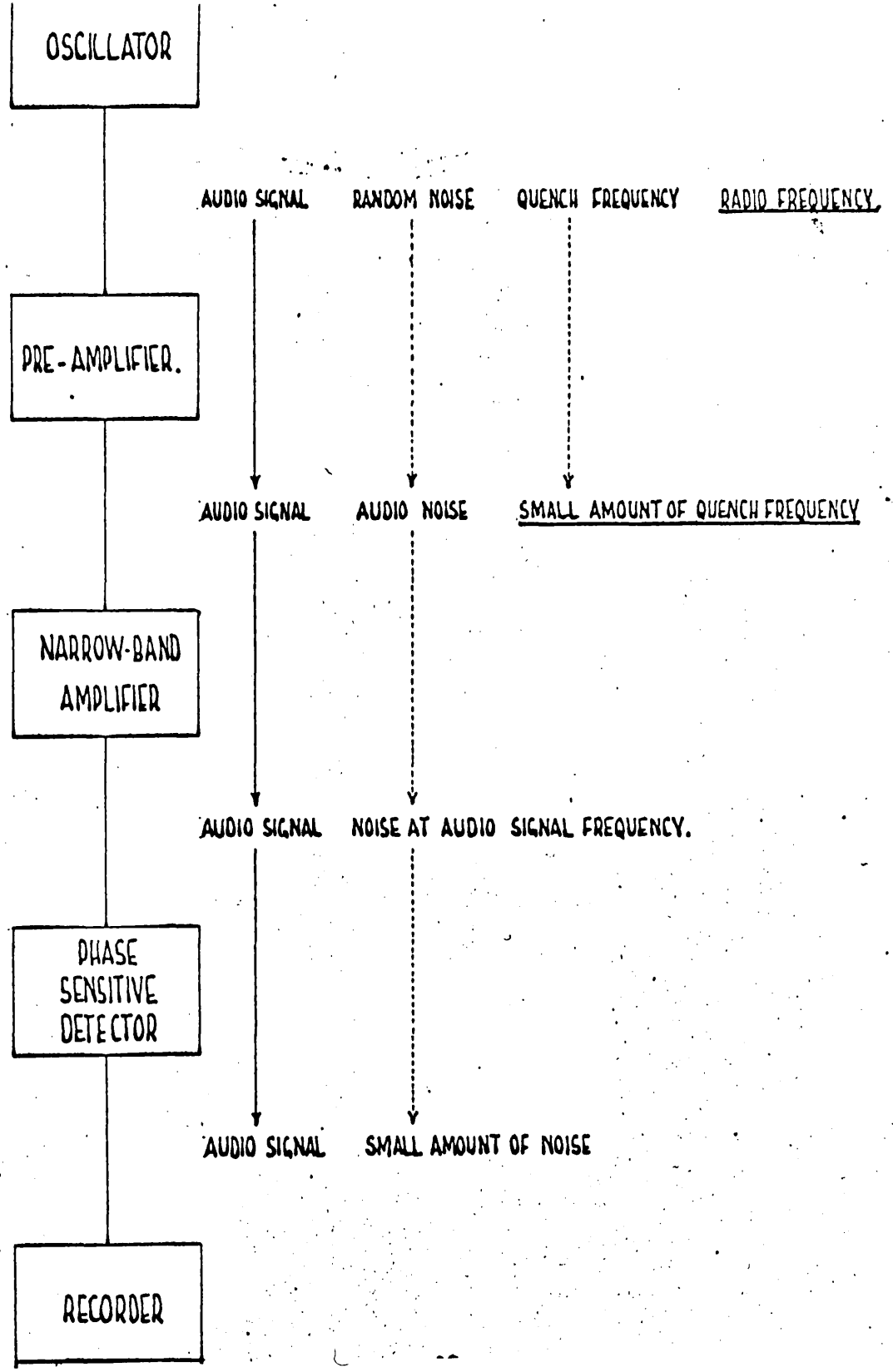
OSCILLATOR
AUDIO SIGNAL
RANDOM NOISE
QUENCH FREQUENCY
RADIO FREQUENCY
PRE-AMPLIFIER.
AUDIO SIGNAL
AUDIO NOISE
SMALL AMOUNT OF QUENCH FREQUENCY
NARROW-BAND AMPLIFIER
AUDIO SIGNAL
NOISE AT AUDIO SIGNAL FREQUENCY.
PHASE SENSITIVE DETECTOR
AUDIO SIGNAL
SMALL AMOUNT OF NOISE
RECORDER

Figure 8.2.2

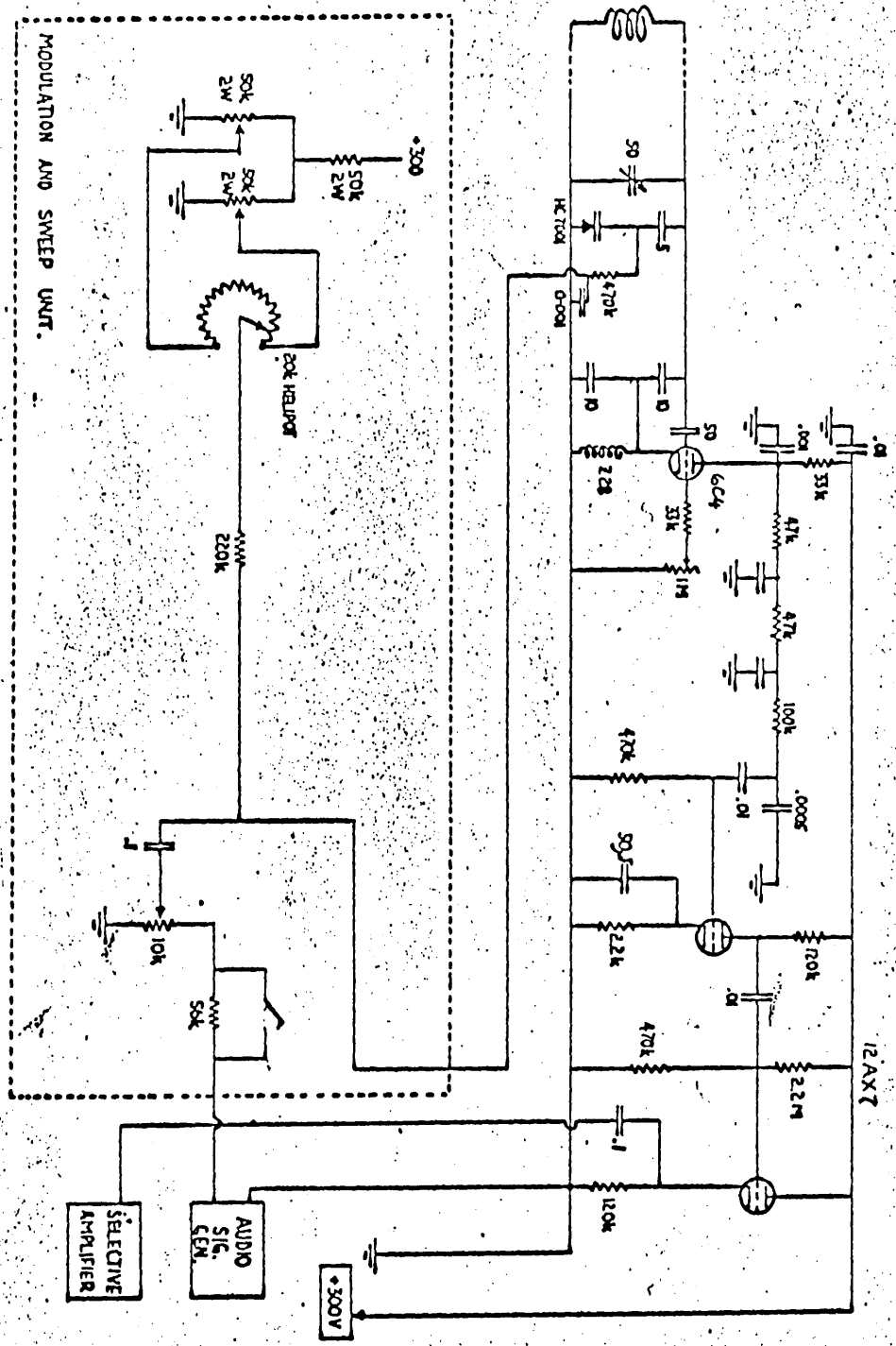

Circuit diagram of the Self-Quench Super-regenerative Oscillator Preamplifier and Modulation Unit of the N.Q.R. Spectrometer.

Figure 8.2.3

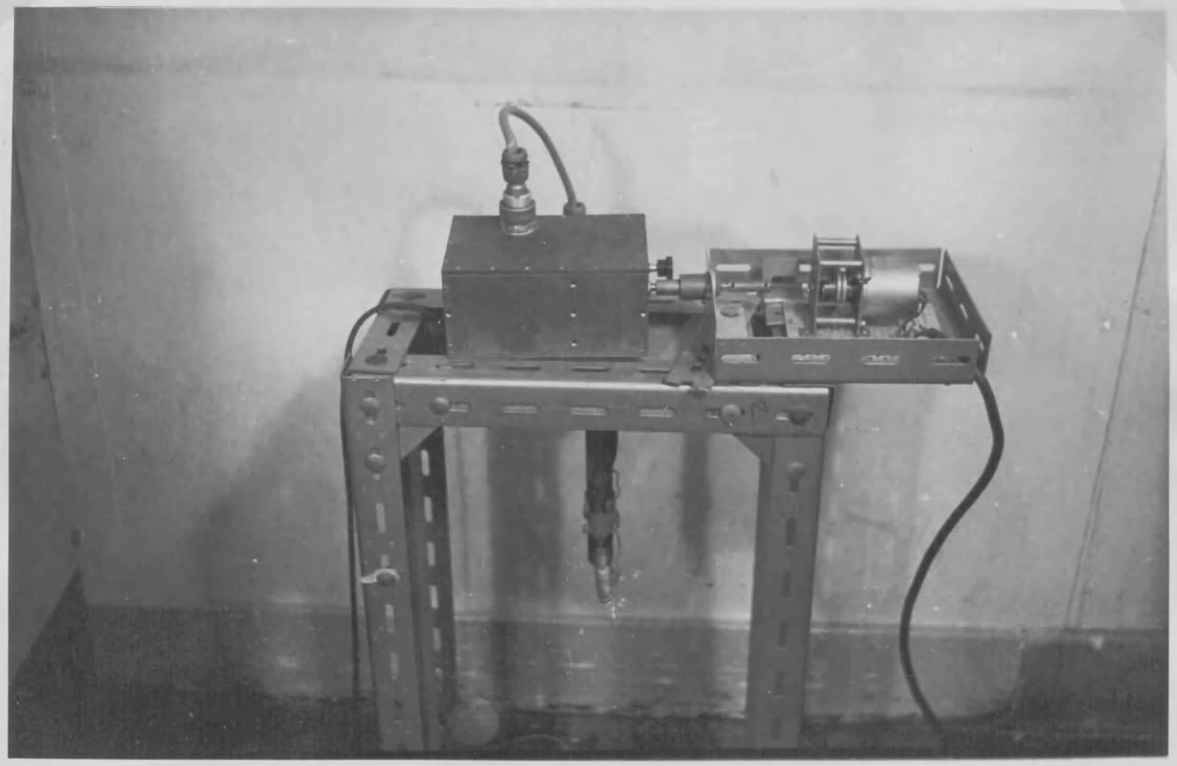

FIGURE 8.2.4

frequency of the oscillator is set by the 1 M potentiometer in the grid circuit. The frequency is swept by driving the variable 50pf tuning condenser of the oscillator. An electric motor (7) and a reduction gear turn the shaft of this condenser at a rate of 1rev/120hrs. Although the frequency sweep by this method is not linear with time, with the condenser operating over the middle of its range 6 to 7 Mc/s can be covered in as many hours.

Four coils, each one inch in length and ½" cross-sectional diameter, of from seven to eleven turns of 18 guage copper wire, enable the oscillator to cover the frequency range 20-40Mc/s. Figure 8.2.4 shows the oscillator-preamplifier assembly together with the frequency driving mechanism. With this arrangement it is a simple matter to immerse the sample in a bath of liquid nitrogen. Frequently resonances become detectable at low temperatures because motional broadening of lines is reduced and signal strength is enhanced as a result of the increase in the Boltzmann factor exp (E/kT) which determines the population excess of the lower of two quadrupole energy levels.

8.3. Operation of the Spectrometer at Maximum Sensitivity

Because of the inherent weakness of nuclear quadrupole resonances the sensitivity of the spectrometer must be maintained at a maximum throughout the whole frequency range of a resonance search. There are six parameters or controls to be set so that the spectrometer operates most satisfactorily. These are:

(1) The oscillator frequency scanning width, which is controlled by the slow variation of the tuning capacitor in the grid circuit of the oscillator, together with the value of the d.c. bias to the oscillator's diode.

(2) The quench frequency which is determined by the grid leak 1 M potentiometer in the oscillator circuit.

(3) The modulation amplitude which is controlled by a potentiometer and switch in the modulation unit.

(4) The input attenuation to the narrow-band amplifier.

(5) The input attenuation to the phase-sensitive detector.

(6) The time constant of the phase-sensitive detector.

Most of the difficulties in locating quadrupole resonances lie with the selection of the three parameters, oscillator frequency, quench

frequency and modulation amplitude.

An amplitude of modulation several times the resonance line width must be used so that a signal output from the oscillator of twice the modulation frequency is produced, the response being approximately equal to the second derivative of the absorption line shape. About 1.5 - 2.0 volts of 150c/s modulation signal superimposed on the 30 volts d.c. bias to the diode is satisfactory for most diamagnetic chlorine compounds.

The quench frequency required to produce maximum signal depends on the radiofrequency of the oscillator. The following technique was employed to maintain optimum conditions throughout a frequency sweep.

A single loop of 18 guage copper wire, soldered to the end of a coaxial lead, is clipped to the brass extension tube connecting the oscillator to the tank coil so that the loop is close to the sample coil, as in figure 8.2.4. This test coil can be fed with an r.f. voltage from an Advance Signal Generator. When the frequency of the oscillator is swept through the frequency in the test coil a signal is produced in the oscillator and can be recorded. A test voltage of less than 10 μV amplitude is found to produce responses on the recorder with a signal-to-noise ratio of about 20:1 if the spectrometer sensitivity is maximum. That setting of 1MΩ potentiometer which produces the strongest response from a 10μV test signal is taken as the best setting for the particular frequency at which the responses are detected. Such checks can easily be performed during a wide frequency scan at intervals of about 1Mc/s.

The validity of this approach was tested using mercuric chloride and sodium chlorate samples. The ^{35}Cl N.Q.R. frequencies in $HgCl_2$ at 303°K are known to be 22.2303 Mc/s and 22.0503 Mc/s [73]. The oscillator frequency was set to about 21.5 Mc/s using a suitable coil and the 50 pf tuning condenser, and the 1MΩ potentiometer was set so that a quench frequency of 30kc/s was generated. The frequency range 21.5-23Mc/s was swept in about one hour and two resonances were detected, the S/N ratio being better than 20:1. With 25kc/s and 35kc/s quench frequencies a poorer S/N ratio was obtained. When the sample was removed and the oscillator re-tuned to 21.5Mc/s, a test signal of amplitude 10 μV at frequency 22.2Mc/s produced a spectrum with S/N of about 20 whenthe quench frequency was 30kc/s but not with frequencies below 28kc/s or

above 33kc/s.

A resonance is expected for the ^{35}Cl in $NaClO_3$ at about 29.83Mc/s at room temperature [77]. A similar set of tests proved that, over the frequency range 29 - 31 Mc/s, optimum spectra are obtained when the quench frequency is about 35kc/s.

Investigations in the range 17 - 18 Mc/s using $HgCl_2$, whose ^{37}Cl nuclei are known to absorb in this range at room temperature, failed to produce resonances. It was also found that a response of S/N greater that 10:1 could only be detectedusing a test signal of amplitude 70-80μV. This loss of sensitivity was found to apply to the range 15-20Mc/s and is overcome by replacing the r.f. choke Z28 in the oscillator feedback circuit with one whose operating range was 12-45Mc/s; the operating range of the Z28 choke is 20-60Mc/s. With the 12-45Mc/s choke, ^{37}Cl resonances in $HgCl_2$were detected at 17.52Mc/s and 17.38Mc/s with S/N of about 15 when the ν_Q was about 25kc/s. Further, a 10μV test signal from the r.f. generator could be detected satisfactorily over the range 16-21Mc/s, using ν_Q's of between 25 and 30 kc/s.

By this procedure with the r.f. signal generator, the spectrometer, with the new r.f. choke, was shown to operate satisfactorily over the frequency range 15-32 Mc/s.

CHAPTER 9

NUCLEAR QUADRUPOLE RESONANCE INVESTIGATION OF SOME MERCURIC CHLORIDE COMPLEXES

The six compounds $HgCl_2$, $K_2HgCl_4H_2o$ and each of the members of the series $HgCl_2nSC(NH_2)_2$ with n = 1-4, were investigated by N.Q.R. spectroscopy. Of these solids the crystal structures of $HgCl_2$, $K_2HgCl_4H_2O$ and $HgCl_2 2SC(NH_2)_2$ are known[66,67,72].

Samples of analar $HgCl_2$ and $K_2HgCl_4H_2O$ were used in the investigation and the polycrystalline samples of the thiourea complexes were prepared according to the method of Aucken[78]. The compositions of all compounds were checked by standard sulphur and nitrogen analyses. X-ray powder photographs of the polycrystalline dithiourea complex were found to be identical to those of the single crystal specimen which was used for X-ray analysis[72].

The chlorine nuclear quadrupole resonances in mercuric chloride at 300°K and 77°K were found at frequencies given in table 9.1.1. Frequencies can be measured, using the radiofrequency signal generator and a Counter Frequency Meter, with an accuracy of better than ±1kc/s.

Signal-to-noise ratios of about 20:1 were recorded, the ^{35}Cl spectrum at 300°K and the ^{37}Cl spectrum at 77°K being shown in figures 9.1.1a and 9.1.1b respectively. The ^{35}Cl resonance in $NaClO_3$ was found at 29.830±0.001 Mc/s at 298°K. The above values are in good agreement with published values.

$K_2HgCl_4H_2O$ was investigated at room and liquid nitrogen temperatures over the frequency range 15-23Mc/s. It was felt that, because of the double negative charge associated with each $HgCl_4^{2-}$ group in the $HgCl_6$ chains, the two chlorine resonances would be found at frequencies lower than those in mercuric chloride itself. One resonance was detected at room temperature, at about 16.23 Mc/s, and attributed to a ^{35}Cl N.Q.R. absorption. At 77°K resonances were detected at 16.653±0.001Mc/s and 16.201±0.001Mc/s. Figure 9.1.2 shows the spectra obtained at 77°K.

Each of the members of the mercuric chloride-thiourea series was exhaustively examined over the frequency range 15-32Mc/s at both 298° and 77°K, but no resonances were detected. The spectrometer sensitivity was optimised at intervals of 500-700kc/s throughout these frequency

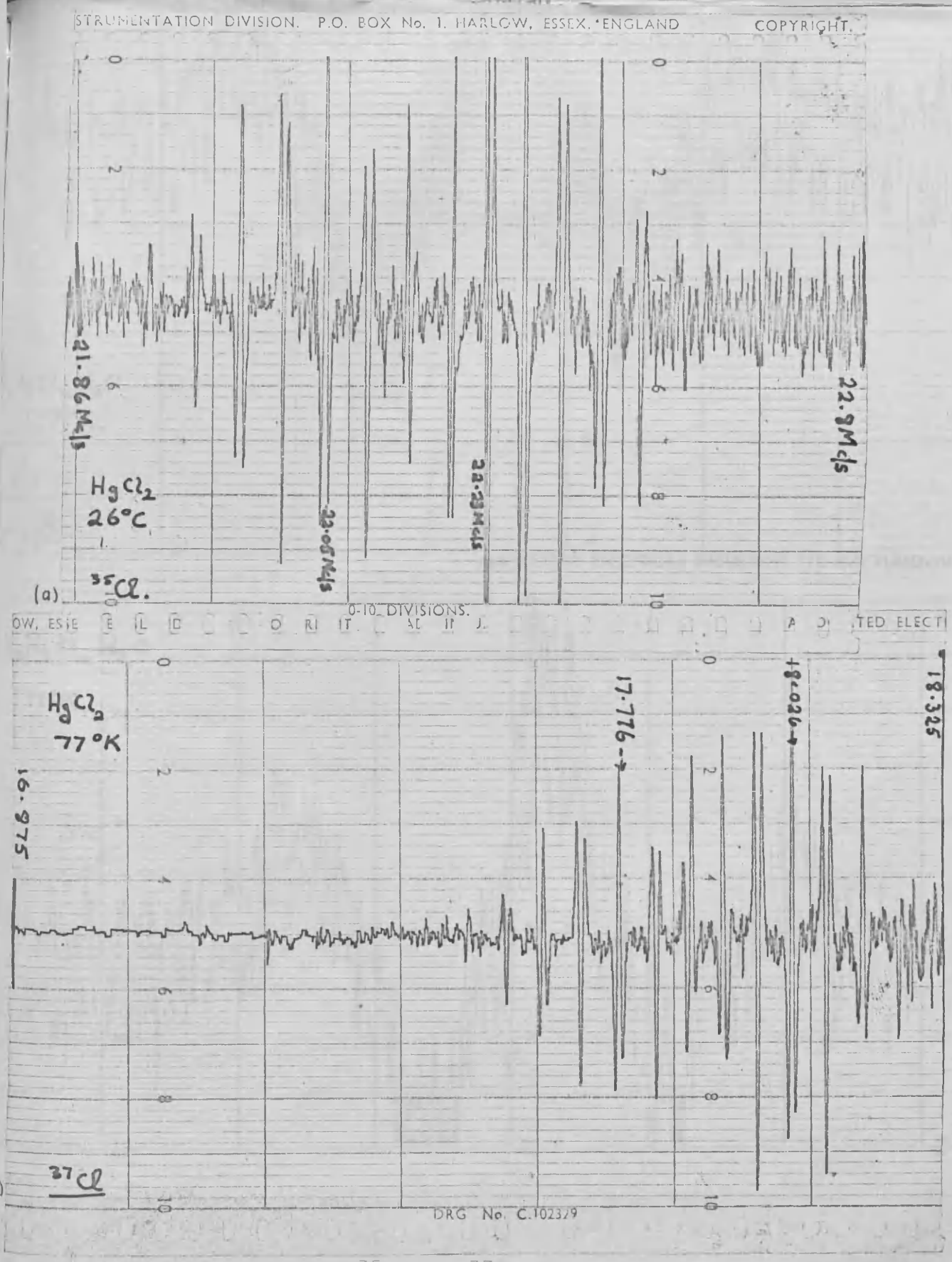

Spectra of the ^{35}Cl and ^{37}Cl N.Q.R. absorptions of $HgCl_2$ at, respectively 299°K and 77°K.

Figure 9.1.1

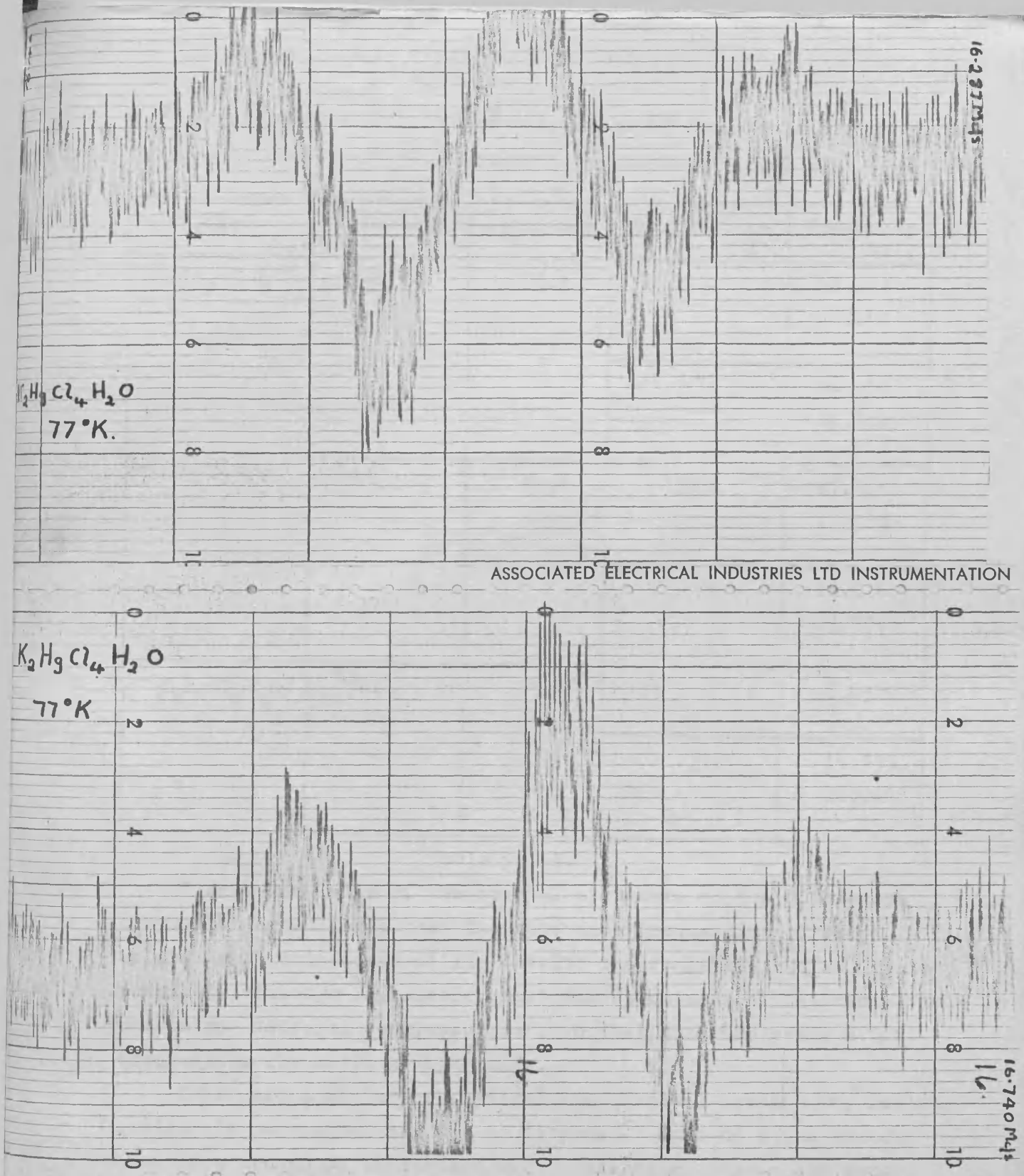

Spectra of the ^{35}Cl N.Q.R. absorption in $K_2HgCl_4H_2O$ at 77°K

Figure 9.1.2

sweeps. Neither the use of freshly prepared samples of the complexes nor slower cooling to 77°K produced a resonance signal over this range.

Compound	Nucleus	Abundance %	Temperature °K	Frequency Mc/s
$HgCl_2$	^{35}Cl	75.4	300	22.231 22.051
			77	22.857 22.514
	^{37}Cl	24.6	300	17.523 17.380
			77	18.026 17.776
$K_2HgCl_4H_2O$	^{35}Cl	75.4	300	16.23
			77	16.653 16.201

Table 9.1.1.

From a knowledge of the crystal structure of the dithiourea complex it is unlikely that the resonance frequencies of the chlorines in this compound lie outwith the range 15-32Mc/s. It is possible, although improbable, that the structures of the mono-, tri- and tetra- thiourea complexes are such that their chlorine N.Q.R. frequencies lie outwith this range.

There are a number of physical and chemical reasons why nuclear quadrupole resonances may not be detected. Some of these reasons have been mentioned in section 6.7. Molecular motions can cause broadening of resonance line widths to a point where detection becomes almost impossible. These effects should be removed by using low sample temperatures. Magnetic dipole-dipole interactions cause broadening of N.Q.R. spectra. The effect of these interactions in the thiourea complexes should be only slightly greater than in mercuric chloride

itself. Dislocations and strains and the presence of impurities in the powder grains can cause sufficient broadening of lines to prevent their detection. Preparation and careful purification of fresh samples of the complexes and different rates of cooling might have been expected to overcome the effects of these imperfections. Possibly some disorder in the crystal structure, causing the chlorine nuclei in each crystalline constituent to experience a slightly different field gradient from those in neighbouring crystallites, is leading to a spread of resonance frequencies for each "equivalent" nucleus. This effect would cause resonances to be broadened or undetected.

Whatever the reasons are, resonances of the ^{35}Cl and ^{37}Cl nuclei in the series $HgCl_2nSC(NH_2)_2$ with n = 1,2,3,4 were not detected in the frequency range 15-32 Mc/s.

Values of nuclear quadrupole coupling constants can frequently be obtained by studying the effects of quadrupolar interactions on N.M.R. spectra. The following chapter discusses the possibility of using ^{35}Cl N.M.R. spectroscopy to obtain the $^{35}Cl\,|eQq|$ values in the polycrystalline mercuric chloride-thiourea series.

CHAPTER 10

QUADRUPOLAR EFFECTS ON N.M.R. SPECTRA

10.1. The "High Field" Case

When a nucleus of spin greater than $\frac{1}{2}$ is subjected to both a magnetic field and an electric field its dipole moment interacts with the magnetic field and its electric quadrupole moment interacts with the electric field gradient. If the former interaction energy is large compared with the latter interaction energy, the nuclear spin energy is, to first-order,[79]

$$E = E_H + E_Q\,(3\cos^2\theta - 1) \qquad 10.1.1$$

Here E_H is the nuclear magnetic interaction energy

$$g_N\,\beta\,Hm_I \qquad 10.1.2$$

and the axis of nuclear orientation is the field direction. E_Q is the electric quadrupole interaction energy given for an axially symmetric field gradient, by

$$\frac{eQq}{4I(2I-1)}\left[3m_I^2 - I(I+1)\right] \qquad 10.1.3$$

with the symmetry axis of the field gradient, q, as the orientation axis. θ is the angle between H and q. For a nucleus with $I = \frac{3}{2}$ the energy level diagram is as shown in figure 10.1.1.

Transitions between these levels can be induced by means of an r.f. field perpendicular to H. The selection rule $\Delta m_I = \pm 1$ is still valid, so that the three transitions between the four levels no longer occur at exactly the same frequency ν_L, the Larmor frequency.

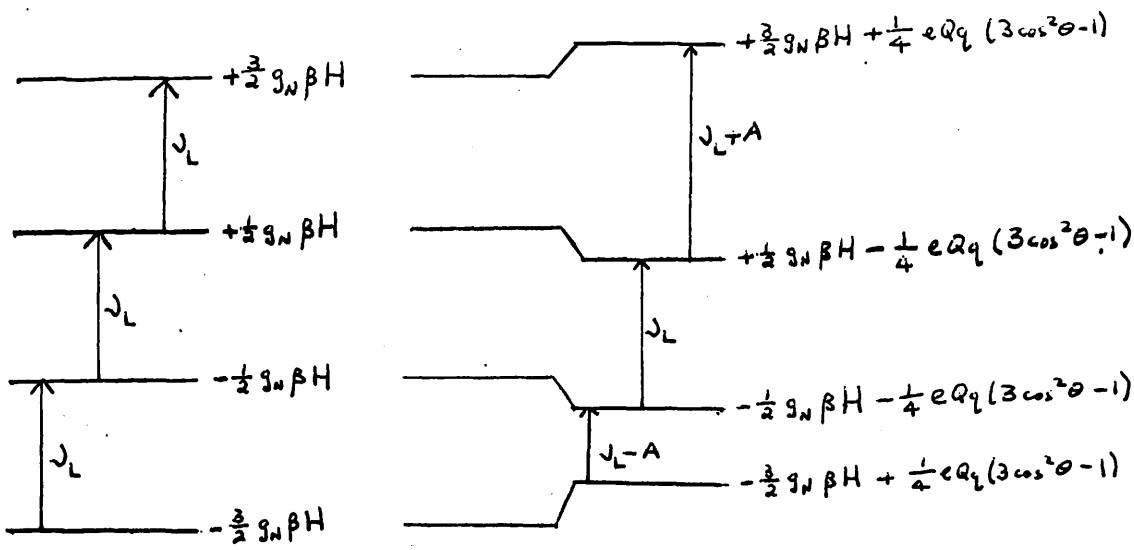

Figure 10.1.1

The frequencies of the the three transitions are $\nu_L - A$, ν_L and $\nu_L + A$ where $A = \frac{1}{2}eQq(3\cos^2\theta - 1) = \nu_Q(3\cos^2\theta - 1)$, in the intensity ratio 0.3, 0.4, 0.3 with respect to the unperturbed degenerate line. In this first-order treatment, the central component, due to the $\frac{1}{2} \rightarrow -\frac{1}{2}$ transition, is unshifted. When the calculation is taken to second order [80] a shift of frequency equal to

$$-(3\nu_Q^2/16\nu_L)(1-\cos^2\theta)(9\cos^2\theta - 1) \qquad 10.1.4$$

is expected for nuclei with $I = \frac{3}{2}$.

Thus measurements of the quadrupole splitting of N.M.R. lines can provide information on ν_Q, the pure N.Q.R. absorption frequency, and θ, the orientation of q with respect of H.

In a single crystal specimen each crystallite is identically orientated in the magnetic field so that unique values of θ exist. The angle θ can be altered systematically by rotating the crystal about an axis normal to the field direction and, by plotting the frequency separation between the two satellite lines, which are, to first-order, symmetrically placed about the central component, as a function of orientation of the crystal in the magnetic field, values of ν_Q and θ can be obtained.[79] Maximum separation, equal to ν_Q, occurs when $\theta = 0^\circ$ and no splitting should occur when $\theta = \cos^{-1}(1/\sqrt{3}) = 54^\circ 44'$

The random distribution of orientations in a polycrystalline or powdered material can be shown [81] to give rise to a powder spectrum of the form shown in figure 10.1.2.

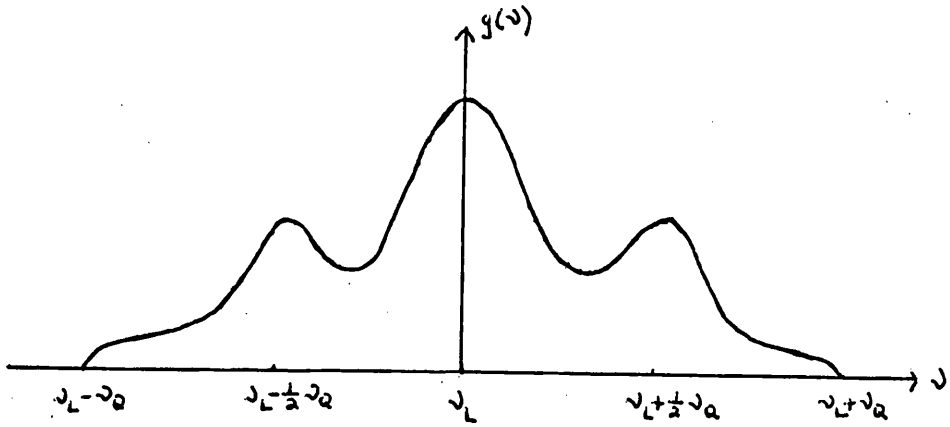

Figure 10.1.2

From such a powder pattern the separation of the satellite lines is a direct measure of ν_Q. However for this "high field" treatment to be valid ν_L must be very much greater than ν_Q. For the nucleus ^{35}Cl with $I = \frac{3}{2}$, $\nu_L = 4.172$ Mc/s with a magnetic field of 10^4 gauss, so that this approach can be applied only provided ν_Q is of the order of kilocycles per second or less. Quadrupole coupling constants of very ionic compounds in which the electron distribbutions are almost spherical, have been extracted using both single crystal and powder pattern N.M.R. studies[79].

Mercuric chloride has a ν_Q value for ^{35}Cl of 22.2 Mc/s so that a field of about 10^6 gauss would be required for "high field" condition of $\nu_L \gg \nu_Q$ to be obeyed. At present such high fields are not feasible.

10.2. The "Low Field" Case

The effect of a small magnetic field on a nuclear quadrupole resonance spectrum has been discussed, for $\eta = 0$, in section 6.6. For a nucleus of spin $\frac{3}{2}$, the α and β lines occur as small frequency shifts around the pure N.Q.R. frequency

$$\nu_Q = \tfrac{1}{2}eQq/h$$

and their detection requires the knowledge of ν_Q and the use of single crystals to prevent broadening due to distributions of θ values.

Detection of the $|+\rangle \longleftrightarrow |-\rangle$ transition, which reduces to zero frequency when the Zeeman field is reduced to zero, requires a frequency of

$$\begin{aligned} \nu &= f\gamma H\cos\theta / 2\pi \\ &= \frac{\gamma H}{2\pi}\left[\cos^2\theta + 4\sin^2\theta\right]^{\frac{1}{2}} \end{aligned} \qquad 102.1$$

The Zeeman splitting of this line can be described by an apparent magnetogyric ratio $\gamma'(\theta)$ so that the energy of this transition is described in terms of an N.M.R. transition

$$\nu = \frac{\gamma'(\theta)\,H}{2\pi}$$

in which $\gamma'(\theta)$, equal to

$$\gamma\left[\cos^2\theta + 4\sin^2\theta\right]^{\frac{1}{2}}$$

can vary between γ and 2γ as the orientation between the applied field and the symmetry axis of the field gradient changes.

For a polycrystalline specimen, the intensity distribution of resonance frequencies, averaged over all crystallite orientations, is

given by

$$I(\cos\theta) \propto \left[\frac{d\nu}{d(\cos\theta)}\right]^{-1} \qquad 10.2.2$$

Substitution of 10.2.1 into 10.2.2 gives

$$I(\cos\theta) \propto \frac{(4-3\cos^2\theta)^{\frac{1}{2}}}{3\cos\theta} \qquad 10.2.3$$

Clearly, at $\theta = 90^\circ$ there is a singularity in the intensity $I(\cos\theta)$. Therefore to first-order in the Zeeman field, H, strong resonant absorption should be observed in a polycrystalline specimen at frequency

$$\nu = 2(\gamma H/2\pi) = 2\nu_L \qquad 10.2.4$$

A more exact expression for the frequency ν in 10.2.4. can be shown for $I = \frac{3}{2}$ [82] to be

$$\nu_2 = \nu_L + \tfrac{1}{2}\left[(\nu_Q + 2\nu_L)^2 - 2\nu_Q\nu_L\right]^{\frac{1}{2}} - \tfrac{1}{2}\left[(\nu_Q - 2\nu_L)^2 + 2\nu_Q\nu_L\right]^{\frac{1}{2}} \qquad 10.2.5$$

where ν_Q is the pure quadrupole resonance frequency.

With the "low field" condition, that $\nu_L \ll \nu_Q$, 10.2.5 yields an expression for the transition, to third-order in Zeeman field,

$$\nu_2 = 2\nu_L\left[1 - \tfrac{3}{4}(\nu_L/\nu_Q)^2\right] \qquad 10.2.6$$

This equation shows that the effect of a large quadrupole interaction is to cause the N.M.R. condition in a polycrystalline specimen to occur at a frequency lower than twice the Larmor frequency; that is the effective magnetogyric ratio is less than 2γ.

Because the resonance of 10.25 is independent of quadrupolar effects to first-order, unlike the normal N.Q.R. Zeeman transitions, inhomogeneities in the electric field gradients, which cause pure and Zeeman N.Q.R. signals to be broadened, even beyond detection, are expected to have little broadening effect on this resonance. Since the quadrupole coupling effects the N.M.R. condition in third-order, a relatively narrow frequency range need be covered in search for resonances for which ν_Q is unknown.

Consider the case of mercuric chloride. ν_Q is about 22Mc/s for the ^{35}Cl nuclei. The Larmor frequency for ^{35}Cl in a field of 10,000 gauss is 4.172Mc/s. With this value of ν_L the condition $\nu_L \ll \nu_Q$ required for this type of "low field" experiment is fulfilled. Furthermore, simple calculation shows that these values should produce

resonances at 8.124Mc/s, a shift of 220kc/s from the $2\nu_L$ value. With a field of 6360 gauss, the value used in the proton magnetic resonance experiment described at the beginning of this thesis, a shift of 56.6kc/s away from 5.3068Mc/s is expected.

Investigation at the higher field value is preferable for reasons of greater spectrometer sensitivity at the higher frequency region and larger shifts are involved at the higher field value so that more accurate values of ν_Q are expected.

Powdered samples of Cu_2O, K_2ReCl_6, $NaClO_3$ and $NaBrO_3$ have been studied [83] using ^{63}Cu, ^{35}Cl, ^{37}Cl and ^{81}Br nuclear magnetic resonances at a number of magnetic field strengths. Plots of resonance frequency against Zeeman field strength were compared with the linear plot for $\nu = 2\nu_L$. From these studies, values of ν_Q were obtained for the quadrupolar nuclei in these compounds, in good agreement with values obtained by pure N.Q.R. spectroscopy.

A study of this sort could supply the values for the ^{35}Cl quadrupole coupling constants of the four mercuric chloride thiourea complexes which failed to produce pure N.Q.R. spectra over the frequency range 15-30Mc/s.

10.3. A Chlorine Nuclear Magnetic Resonance Spectrometer

Three alterations are necessary so that the N.M.R. spectrometer described in chapter three can be employed for this type of investigation.

1. An oscillator which operates with maximum sensitivity over the frequency range 6-9Mc/s is required.
2. A magnetic field of about 10,000 gauss is desired.
3. A method of sweeping the oscillator frequency is required since the field sweep procedure provides only about 50 gauss or 40kc/s sweep width. Frequency shifts of the order of 200kc/s from 8.344 Mc/s are expected.

Since accurate line shapes are not essential in this investigation the super-regenerative oscillator-detector would seem to be suitable for the purpose of this investigation. A number of super-regenerative oscillators which operate over the frequency range 2.5-10Mc/s have been designed [84, 85, 86]. The most recent of these [86] claims to be able to detect weak, broad nuclear resonances, that is line widths greater than 20kc/s. An oscillator, identical to circuit (B) in reference [86] was constructed with the addition of a filtering network on the output

circuit to prevent quench frequency from reaching the oscillator output.

Figure 10.3.1. shows the circuit diagram of this oscillator.

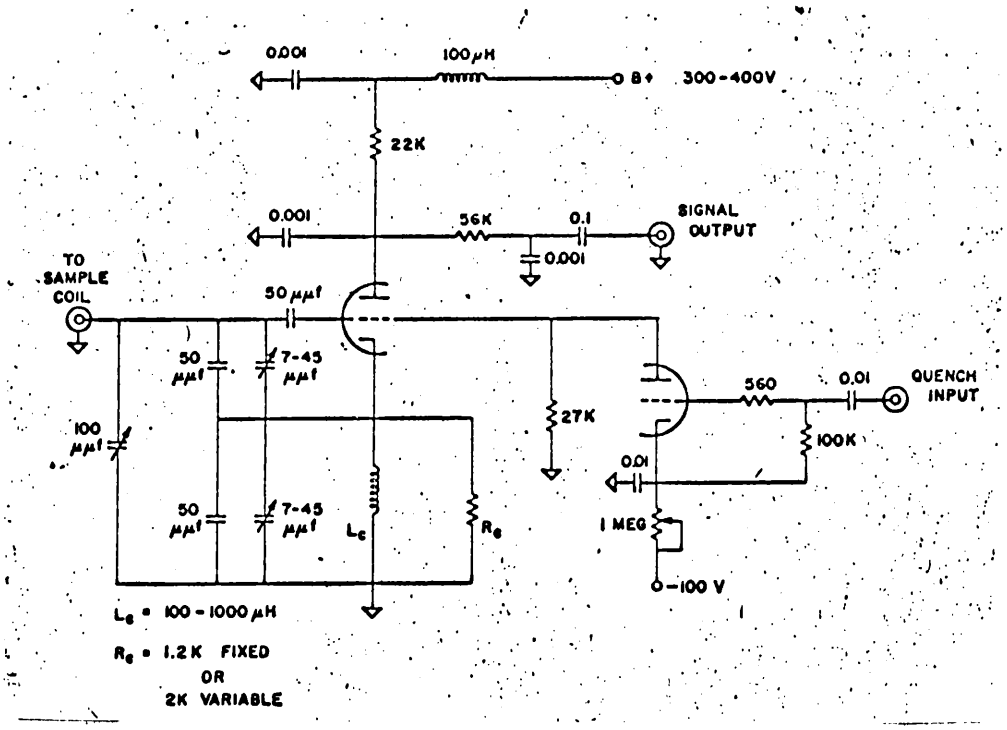

Figure 10.3.1

The magnet current supply to the A.E.I. magnet coils was set to a value of around 400mA so that the magnetic field in the magnet gap was about 10,000 gauss. The successful application of 10.2.6 to obtain accurate determinations of quadrupole coupling constants requires that the strength of the Zeeman field, which determines ν_L, be known exactly.

The field was measured using the ^{31}P resonance in 80% H_3PO_4. At 10,000 gauss, ν_L for ^{31}P (natural abundance 100%) is 17.235Mc/s. With the marginal oscillator and probe assembly used in the proton N.M.R. investigation tuned to 17.524±0.001Mc/s, the field was altered until the ^{31}P N.M.R. was detected. The resonance field is 10,168±1 gauss. The current control settings were fixed at the resonance field values.

With this field, $2\nu_L$ for ^{35}Cl is 8484±1kc/s.

The externally-quenched super-regenerative oscillator was tunable over the range 6-10 Mc/s with the probe assembly described in chapter three when a sample coil of about 20 turns of 26 S.W.G. enamelled copper wire was used. A low frequency signal generator supplied the quench frequency, 30kc/s. As before a modulation frequency of 64 c/s was superimposed on the magnetic field and the audio-signal output from the oscillator passed through Brookdeal Lock-in Amplifier and Meter Unit to the Servoscribe d.c. recorder. Frequency sweep at a rate of about 10 kc/s per minute was achieved by driving the spindle of the 7-45 pf. tuning condenser, using an electric motor and reduction gear, at 1.5 revs. per hour.

10.4. Investigation of the Mercuric Chloride Complexes

With a 1gm. sample of mercuric chloride, the frequency range 8.5 - 8.1 Mc/s was swept extensively, with a modulation amplitude of 1 gauss, but no resonance absorption was detected. Since ν_Q = 22.23 and 22.05 Mc/s for the ^{35}Cl nuclei in $HgCl_2$, resonances are expected at ν_2 = 8.252 and 8.248 Mc/s respectively. It is unlikely that these absorptions would be resolved. ^{35}Cl resonances in $K_2HgCl_4H_2O$, for which ν_Q = 16.23 Mc/s and about 15.9 Mc/s, were not observed in the range 8.5 - 7.8 Mc/s, although absorptions are expected at ν_2=8.049 and 8.030 Mc/s.

It is felt that the failure to detect these resonances is due to the small amount of sample which can be used and the small amplitude of modulation which is generated. A modulation level of 1 gauss corresponds to a modulation of less than 1 kc/s whereas the line widths of such Zeeman resonances are usually greater than 30kc/s. To expose more sample to the radiofrequency field a larger coil is necessary and to achieve this the coil assembly, probe insert and A.E.I. probe unit would need to be replaced and frequency modulation techniques used.

CHAPTER 11

SUMMARY OF THE WORK ON THE MERCURIC CHLORIDE COMPLEXES

The polycrystalline compounds $HgCl_2$, $K_2HgCl_4H_2O$ and $HgCl_2nC(NH_2)_2$ with n = 1,2,3 and 4 were investigated using N.Q.R. and N.M.R. techniques in search of the ^{35}Cl and ^{37}Cl nuclear quadrupole coupling constants for these materials. Only the ^{35}Cl and ^{37}Cl pure N.Q.R. absorption frequencies of $HgCl_2$ and the ^{35}Cl pure N.Q.R. absorption frequencies of $K_2HgCl_4H_2O$ were detected at room and liquid nitrogen temperatures. Table 11.1.1 lists the quadrupole coupling constants, in Mc/s, which were determined.

The arrangement of the mercury and chlorine nuclei is essentially the same in both the $HgCl_2$ and the $K_2HgCl_4H_2O$ polycrystalline materials so that the large reduction in the ^{35}Cl coupling constants of the hydrated complex relative to the values of mercuric chloride itself, about 32.9 Mc/s versus about 45.4 Mc/s, is due to the presence in $K_2HgCl_4H_2O$ of two additional electrons in each $HgCl_6$ octahedron. The representation

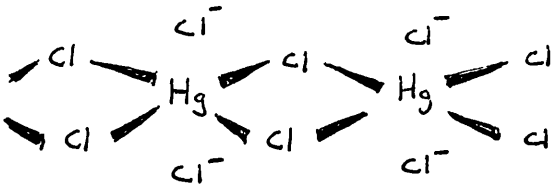

is ruled out as a possible description of the complex $(HgCl_4)_n^{2n-}$ in $K_2HgCl_4H_2O$ since the $|eQq|$ value of the chlorine nuclei in the $(HgCl_2)_n$ chains of this representation would be approximately equal to the values found for mercuric chloride itself and the chlorine ions would have an $|eQq|$ value very much less than the values found for the complex.

At 77°K the ^{35}Cl $|eQq|$ values of the two dissimilar chlorine nuclei in $K_2HgCl_4H_2O$ are 904 kc/s apart whereas in $HgCl_2$ itself the two chlorine nuclei have coupling constants differing by 686 kc/s. Therefore the electric field gradients associated with the two different chlorine environments in $K_2HgCl_4H_2O$ are less nearly identical than are the field gradients around the chlorines in $HgCl_2$.

Table 11.1.1

Nucleus	Temperature	Compound	eQq, Mc/s
^{35}Cl	$77^{o}K$	$HgCl_2$	45.714 45.028
		$K_2HgCl_4H_2O$	33.306 32.402
		$HgCl_2.nCS(NH_2)_2$ n = 1-4	——
	$300^{o}K$	$HgCl_2$	44.462 44.102
		$K_2HgCl_4H_2O$	32.46
		$HgCl_2.nSC(NH_2)_2$ n = 1-4	——
^{37}Cl	$77^{o}K$	$HgCl_2$	36.052 35.552
		$K_2HgCl_4H_2O$	——
		$HgCl_2.nSC(NH_2)_2$ n = 1-4	——
	$300^{o}K$	$HgCl_2$	35.046 34.760
		$K_2HgCl_4H_2O$	——
		$HgCl_2.nSC(NH_2)_2$ n = 1-4	——

This is reasonable on the basis of the repeating structure

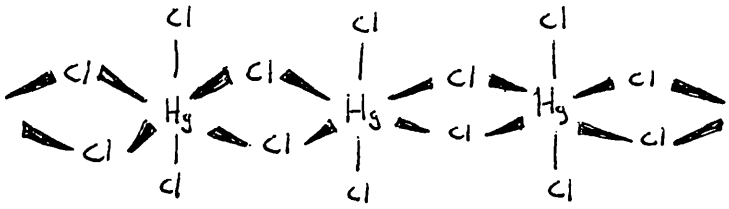

for $K_2HgCl_4H_2O$, where one type of chlorine nucleus is bonded to two mercury atoms and the other is bonded to only one mercury atom. In $HgCl_2$ all the chlorine atoms are bonded to two mercury atoms.

Nuclear quadrupole resonances of the ^{35}Cl and ^{37}Cl nuclei in the series $HgCl_2nCS(NH_2)_2$ with n = 1-4 were not detected in the frequency range 15-32 Mc/s at either room or liquid nitrogen temperatures, even after purification and cooling of the samples.

Attempts to detect shifts in the N.M.R. absorption frequencies of the ^{35}Cl nuclei arising from quadrupolar coupling, in the six compounds were unsuccessful, due to the inherent weakness of ^{35}Cl N.M.R. signals and to the smallness of sample size and modulation amplitude available in the experimental set-up used.

CHAPTER 12

OTHER METHODS OF OBTAINING QUADRUPOLE COUPLING CONSTANTS

A number of other methods of obtaining quadrupole coupling constants have been referred to earlier. Atomic beam experiments and the hyperfine splitting of optical spectra can yield values for eQq_{at}, the quadrupole coupling constant in atoms. Similarly molecular beam studies of simple diatomic molecules in the gas phase have supplied values for eQq_{mol}, the coupling constant in a molecule. Rotational spectra of gaseous or volatile dipolar molecules obtained by microwave spectroscopy can frequently be analysed to supply values of eQq_{mol}.

The magnitude of the quadrupole coupling constant in solids, $|eQq_{solid}|$, can be obtained by N.Q.R. studies, pure or Zeeman, and by N.M.R. studies, "high field" or "low field", as described in connection with Problem 2. Splitting of Mössbauer spectra [87,88] which can be obtained for a number of nuclei, can be shown to give values for $|eQq_{solid}|$. The sign of this coupling constant can also often be determined from Mössbauer spectra.

Another method which can often be used to obtain values of eQq_{solid} is that of Electron Paramagnetic Resonance Spectroscopy, E.P.R. In the proton N.M.R. investigation, only nuclear interactions needed to be considered, although electrons did play a part, in, for example, the relaxation mechanisms of the nuclear spin from upper to lower spin states. In the quadrupole resonance study the electrons were considered only as charges which contributed to the total electric field gradient at the quadrupolar nucleus. This was valid in both cases because the systems dealt with did not possess unpaired electrons. Each electronic orbital in the molecules considered was occupied by a pair of electrons whose spins must be antiparallel.

If, however, any of the orbitals had been only singly occupied, so that the atom, molecule or ion was paramagnetic, the spin of this unpaired electron would have had a great effect on the N.M.R. and N,Q.R. spectra obtained.

The magnetic moment of an electron is about 10^3 times that of most nuclei so that coupling between the resonant nucleus and this electron, and between other electrons and this unpaired electron, is equivalent to applying a very large internal magnetic field. This

large field causes shifts in nuclear magnetic resonance frequencies which supplies information about the unpaired electron distribution in the molecule. The presence of an unpaired electron spin alters the relaxation times of nuclear spins. The N.M.R. spectrum of a paramagnetic solid is broadened because the large internal field generated by the unpaired electrons causes T_2 for the nuclear spin to be small. As, in N.Q.R. spectroscopy the presence of paramagnetic species, even as impurities, causes broadening of lines and frequently prevents detection of the resonances.

In E.P.R. spectroscopy the application of a steady magnetic field to a paramagnetic species removes the spin degeneracy of the electronic orbital energy levels and transitions of the unpaired electron between the spin sub-levels of its orbital level are detected. In a crystalline paramagnetic compound, interactions involving the crystal field around the paramagnetic species, the orbital angular momentum of the electron and the nuclear spin of the paramagnetic species perturb the electronic spin sub-levels, so that the energy of transition between these levels depends on the paramagnetic species and its environment in the crystal.

The final topic in this thesis describes how the quadrupole coupling constant of the paramagnetic species, Cu(II), in $Na_2(Zn:Cu)(DCOO)_6 4D_2O$, where the ratio Zn:Cu is 1000:1, was obtained from analysis of E.P.R. spectra of a single crystal of the complex at 77°K. The nature of the bonding in this formate complex is discussed in the light of the information obtained from the E.P.R. analysis.

Before such a discussion can be given the effects of crystal field, spin-orbit and electron-nucleus interactions on E.P.R. spectra must be derived.

CHAPTER 13

INTERACTIONS AFFECTING THE E.P.R. SPECTRA OF TRANSITION METAL IONS

13.1. Basic Theory of Electron Paramagnetic Resonance

All electrons are charged and have a spin quantum number S of $\frac{1}{2}$ so that arguments analogous to those used in chapter one for the nucleus ($I = \frac{1}{2}$) are applicable.

The magnetic moment μ_e of an electron is given by the expression

$$\mu_e = -g_e \beta \underline{S} \qquad 13.1.1$$

where

$$\hbar \underline{S} = \hbar\sqrt{S(S+1)}$$

is the electron's spin angular momentum vector, g_e is the electronic g-factor and β is the electronic Bohr magneton, equal to $e\hbar/2Mc$ where $-e$ and M are respectively the charge and mass of the electron. μ_e as defined in 13.1.1 is negative.

As before this magnetic moment interacts with an applied magnetic field H, the Hamiltonian for the interaction being

$$\mathcal{H} = -\mu_e \cdot \underline{H} = g_e \beta H S_Z \qquad 13.1.2$$

if the field is applied in the Z-direction.

Since $S = \frac{1}{2}$ for the electron there are two allowed orientations of the spin, roughly parallel and antiparallel to the direction H_Z. The energies of these two spin states are given by

$$E = \pm \tfrac{1}{2} g_e \beta H$$

where, because μ_e is negative, the lower state corresponds to the $m_S = -\frac{1}{2}$ eigenvalue of S_Z

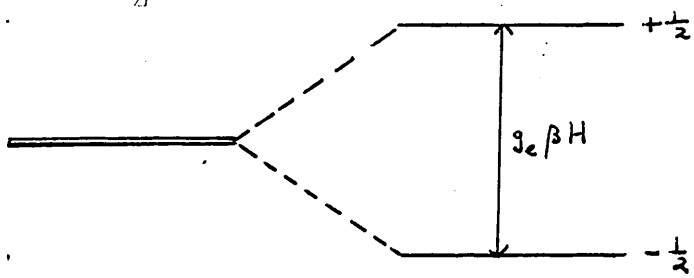

As with nuclear magnetic resonance, application of an oscillating field perpendicular to the applied field direction can induce transitions between these two levels provided the frequency ν is such that it satisfies the resonance condition

$$h\nu = g_e \beta H \qquad 13.1.3$$

For an applied field of 10^4 gauss it turns out that the

resonance frequency for an electron — the g-value of a free electron is 2.0023 — is 28.026 KMc/s, about a thousand times larger than that required for N.M.R. This frequency falls in the microwave region of the spectrum. Electron spin resonance experiments are usually carried out at fixed frequency and an X-band microwave spectrometer is commonly used. This generates a frequency of about 9500 Mc/s and so requires a field of about 3,400 gauss. A Q-band spectrometer provides a frequency of about 35 KMc/s so that a field of about 12000 gauss is needed to satisfy the resonance condition 13.1.3. Further information concerning instrumentation in electron spin resonance can be obtained from the textbook mentioned in reference 90.

It has already been mentioned in connection with N.M.R. that transitions between energy levels can only be detected if there is a population difference between the levels and if this difference is maintained during resonance. In a macroscopic specimen containing a large number of electron spins in equilibrium with their environment, Boltzmann's distribution law ensures that the lower level contains an excess of electrons in the presence of an applied magnetic field, so that net absorption of energy takes place. Spin-lattice and spin-spin relaxation processess similar to those encountered in chapter one in connection with nuclear spins, normally ensure that this excess is maintained throughout the resonance, unless the amplitude of the microwave power is so large that saturation occurs.

To chemists the interest in this type of spectroscopy lies in using unpaired electrons in molecules to transmit information about their environments. Besides possessing angular momentum associated with its spins an electron possesses an angular momentum associated with its motion within an orbital, which in the case of a hydrogen-like orbital is

$$\hbar \underline{l} = \hbar\sqrt{l(l+1)}$$

where l is the orbital angular momentum quantum number of the electron in a particular orbital, and can be 0,1,2 or 3. These l values correspond to the s,p,d and f atomic orbitals. In the case of an effectively isolated electron the spin and orbital angular momenta can couple to give a total angular momentum of value $\hbar \underline{j}$ where

$$\underline{j} = \sqrt{j(j+1)}$$

and $$j = l \pm s$$

If spin and orbital angular momenta couple, the appropriate form of 13.1.3 must be

$$h\nu = g_J \beta H \qquad 13.1.4$$

where

$$g_J = 1 + \frac{j(j+1) + s(s+1) - \ell(\ell+1)}{2j(j+1)}$$

If, in a crystal, the crystalline electric field is sufficiently strong to completely uncouple $\hbar \underline{\ell}$ and $\hbar \underline{s}$ then the g-factor is equal to the free electron value $g_e = 2.0023$.

g-values very close to 2.0023 are found for most free radicals.[91] In cases where there is incomplete uncoupling of the spin and orbital angular momenta the g-values may appreciably deviate from the value 2.0023. The extent of spin-orbit coupling, and hence the g-value, depends on the magnitude of the crystal field acting on the electron.

If the atom or ion possesses, in addition to an unpaired electron, a nucleus of spin I, then there is the possibility of hyperfine splitting of the E.P.R. spectrum due to the (2I+1) different orientations of the nuclear spin in the applied field, H.

The g-factors and hyperfine splittings of E.P.R. spectra are related, through spin-orbit coupling, to the molecular environment of the unpaired electron.

The following section discusses more quantitatively the interactions which affect the energy levels of transition metal ion complexes in the presence of a steady magnetic field, and which therefore affect the appearance of the E.P.R. spectra of such complexes.

13.2. Transition Metal Ion Complexes

Normally electrons in molecules are spin paired, but unpaired electrons in the d- or f-orbitals of transition metal ions may give rise to E.P.R. spectra.

In the rare earth transition series the 4f shell builds up to its maximum possible value of fourteen electrons. In the M^{3+} state each ion has the outer configuration of $5s^2 5p^6$. Measurements of static susceptibility, χ_0, yield, through the relationship

$$\chi_0 = N\mu^2\beta^2 (3kT)^{-1} = C/T,$$

a value for the magnetic moment μ of a paramagnetic species. In this equation, C is a constant characteristic of the substance and is known as its Curie constant, and for rare earth compounds, with only

a few exceptions, the value of μ obtained compare favourably with that calculated from the equation

$$\mu = g_J \beta \sqrt{J(J+1)}$$

where J is the total electronic quantum number for the ion obtained by coupling the angular momenta of the individual unpaired electrons.

For the first transition series, the iron group, the 3d shell is filled from $3d^0$ to $3d^{10}$. It is found that susceptibility measurements on complexes of the members of this series lead to μ values in approximate agreement with the spin-only relationship

$$\mu = g_e \beta \sqrt{S(S+1)}$$

where S is the total spin quantum number for the ion.

The palladium group, 4d, and the platinum group, 5d, of transition metal ions also have g-values close to the spin-only value.

In the rare earth series spin-orbit coupling is strong whereas in the d- groups of transition metal ions spin-orbit coupling is almost completely quenched. Quenching of spin-orbit coupling arises from electric fields generated in the environment of the ion. Since d- electrons are less shielded from the effects of the environmental fields than are the more deeply penetrating f- electrons, the former have less orbital contribution to the total angular momenta and hence g- factors close to 2.

There are many substances which obey a modification of the Curie relationship,

$$\chi_0 = \frac{C}{T-W}$$

where W is known as the Weiss constant. There are other forms of paramagnetism, in which the dependence of χ on both temperature and magnetic field strength is complicated. Two of the most important of these are ferromagnetism and antiferromagnetism. Figure 13.2.1 compares qualitatively the temperature dependence of the susceptibility for (a) simple paramagnetism, (b) ferromagnetism and (c) antiferromagnetism.

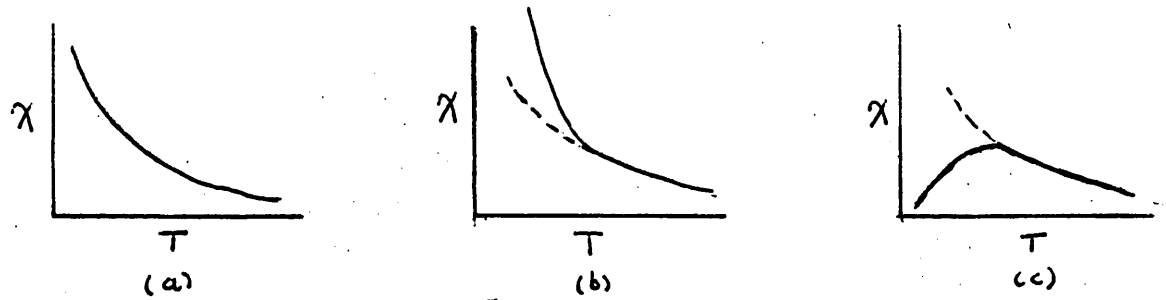

Figure 13.2.1

T_C and T_N are respectively the Curie and Néel temperatures, at which discontinuity is recorded.

Above T_C and T_N the substance has the behaviour of a simple paramagnet. The peculiarities in the behaviour of ferromagnetic and antiferromagnetic substances below their Curie or Néel points are due to interionic interactions which have magnitudes comparable to the thermal energies at T_C or T_N and this becomes progressively greater than thermal energies as temperature is further lowered.

In the case of antiferromagnetism the magnetic moments of the ions in the lattice tend to align themselves so as to cancel one another out. Above T_N thermal agitation prevents very effective alignment and the interactions are manifested only in the form of a Weiss constant which is of the same order of magnitude as T_N itself.

In ferromagnetic substances the moments of the separate ions tend to align themselves parallel and thus to reinforce one another. Above T_C thermal energies are more or less able to randomise the orientations. However below T_C the tendency to alignment becomes controlling and χ increases more rapidly with decreasing temperature.

The problem of studying the energy levels, and the effects on the E.P.R. spectra, of ionic complexes in a crystal in the presence of a steady magnetic field is best approached in stages. It is customary to consider the dominant term in the Hamiltonian for the system and treat the next most important term as a perturbation on that, and so on. It is useful in this connection to arrange the various effects according to the magnitude of their contribution to the total Hamiltonian. This, however, varies from compound to compound. In the rare-earth complexes, spin-orbit interaction is more powerful than most crystal field effects, whereas in complexes of the d- transition metal ions the converse is clearly more generally true.

Attention from now on is confined to the $3d^n$ transition metal ions. For these the Hamiltonian can be written as

$$= V_F + V_{XL} + V_{LS} + V_{SS} + V_H + V_N + V_h + V_Q \qquad 13.2.1$$

in which V_F = free ion energy $\approx 10^5 cm^{-1}$

V_{XL} = crystal field $\approx 10^4 cm^{-1}$

V_{LS} = spin-orbit coupling $\approx 10^2 cm^{-1}$

V_{SS} = electron spin-spin interaction $\approx 1 cm^{-1}$

V_H = electron-magnetic field interaction $\approx 1 cm^{-1}$

V_N = electron-nucleus interaction $\approx 10^{-1}-10^{-3} cm^{-1}$

V_h = nucleus-magnetic field interaction $\approx 10^{-3} cm^{-1}$

V_Q = nuclear quadrupole-electric field interaction $\approx 10^{-3} cm^{-1}$

V_F, the free ion contribution, is defined by the hamiltonian

$$\mathcal{H}_F = \sum_k \left(\frac{p_k^2}{2M} - \frac{Zc^2}{r_k} \right) + \sum_{j<k} \frac{c^2}{r_{jk}},$$

where p_k is the momentum of the kth electron, c and M are respectively the electronic charge and mass, -Zc is the nuclear charge and r_k is the distance from the k'th electron to the nucleus and r_{jk} is the distance between the j'th and k'th electrons.

The free ion is generally classified in terms of its spin and orbital degeneracy. For example a single electron in a 3-d orbital has $S = \frac{1}{2}$ and $\ell = 2$ and so its energy is $(2S+1)(2\ell+1)$-fold degenerate. In general a free ion is characterised by a group of $(2L+1)(2S+1)$-fold degenerate levels. The L values are determined using Hund's rule of maximum multiplicity. For the $3d^n$ series the following table lists the L and S values of the ions in their ground states.

N	0	1	2	3	4	5	6	7	8	9	10
L	0	2	3	3	2	0	2	3	3	2	0
S	0	$\frac{1}{2}$	1	$\frac{3}{2}$	2	$\frac{5}{2}$	2	$\frac{3}{2}$	1	$\frac{1}{2}$	0

The effect of the crystal field is to partly remove the degeneracy of the free ion.

In a large number of transition metal complexes the positive paramagnetic ion is surrounded by an octahedron of negatively charged ions or of polar molecules with their negative end towards the central ion. In most cases the octahedron is not regular. It is, however, convenient to consider first the effect of an octahedral crystal field and then treat distortions away from this cubic symmetry as small perturbations. Cu^{2+} has the configuration $3d^9$ which can be regarded as one "hole" in the completed shell $3d^{10}$. The effect of the crystal field, V_{XL}, on this is the same as it would be on a single particle of positive charge moving in a 3d-orbital. The ground state of V_F for Cu^{2+} is ^2D. In the true free ion spin-orbit interaction splits this level into two levels, with J = 5/2 and J = 3/2, the former being the lower. In the crystalline complex, however, this J-coupling classification is invalid since V_{XL} is sufficiently strong to break down

the free ion spin-orbit coupling.

There are five wave-functions for a D-orbital, characterized by ψ_{m_L}

where $m_L = 2,1,0,-1,-2$.

By selecting the linear combinations $\psi_m \pm \psi_{-m}$ the mutually orthogonal set of orbitals, Ψ_m

$d_{xy} = (15)^{\frac{1}{2}}xy$, $d_{xz} = (15)^{\frac{1}{2}}xz$, $d_{yz} = (15)^{\frac{1}{2}}yz$, $d_{x^2-y^2} = \frac{1}{2}(15)^{\frac{1}{2}}(x^2-y^2)$,

$d_{z^2} = \frac{1}{2}(5)^{\frac{1}{2}}(2z^2-x^2-y^2)$ is obtained.

The spatial arrangement of these orbitals is shown in figure 13.2.2.

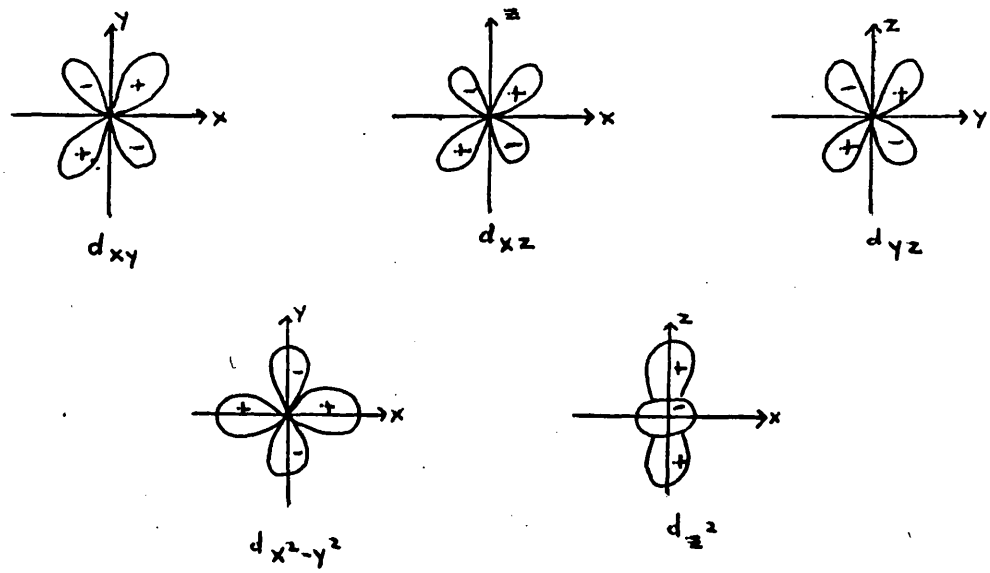

Figure 13.2.2

From symmetry considerations [92], the effect of V_{XL} on the first three orbitals (called d_ε) is the same, and the last two orbitals (d_γ) are affected equally by V_{XL}. The 5-fold orbital degeneracy of the D-state is split into a triplet plus a doublet by the action of an octahedral field.

Copper and many other ions do not form complexes which have exact octahedral symmetry. Even when the central ion is surrounded by six identical ligands the symmetry may not be exactly cubic.

This is to be expected according to the Jahn-Teller theorem which states that a non-linear molecule of a given symmetry having a degenerate ground state is unstable and distorts itself so as to lift the degeneracy. The usual distortions from octahedral symmetry are due to either a tetragonal field component, in which two ligands colinear with the central ion move either towards or away from each other, or a trigonal field component, in which the two three-fold systems of axes bend away from or towards each other.

In a tetragonal field the degeneracy of the D-orbitals is further removed since not all orbitals bear the same relationship to the axis of distortion.

In the case of Cu^{2+} the doublet $d\gamma$ has lower energy than the triplet $d\varepsilon$ because the "positive hole" prefers its orbital distribution to point towards the negative charges along the axes. In $[Cu(H_2O)_6]^{2+}$ the octahedron is always distorted by elongating along one axis, the Z-axis, and contracting along the other two. This causes the $d_{x^2-y^2}$ orbital to be favoured over the d_{z^2} orbital and the energy of the d_{xy} orbital to lie lower than that of the d_{xz} and d_{yz} orbitals. The energy level diagram for a Cu^{2+} in a tetragonal field of the type in $[Cu(H_2O)_6]^{2+}$ is shown in figure 13.2.3. The "positive hole" of Cu^{2+} is to be found in this case in the $d_{x^2-y^2}$ orbital.

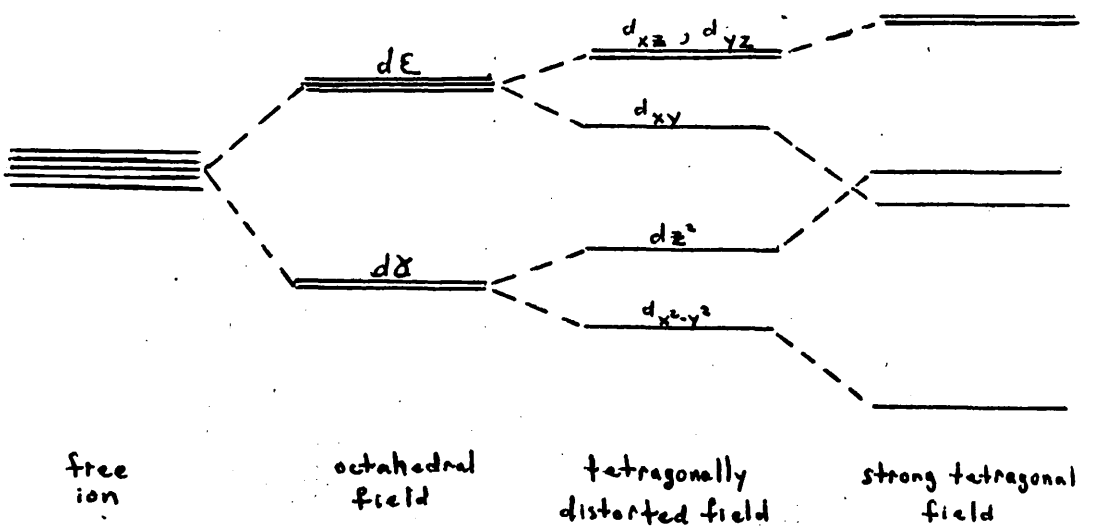

Figure 13.2.3

At this stage each level is still two-fold spin degenerate. By Kramers' theorem, which states that a purely electrostatic field acting upon a system of an odd number of electrons can never reduce its degeneracy below two, a magnetic field is necessary to lift the Kramers degeneracy and E.P.R. studies of transition metal complexes detect transitions between the two levels of such a doublet.

Before considering the effect of a magnetic field on the electronic energy levels, the spin-orbit coupling term, V_{LS}, must be considered.

In the case of Cu^{2+} the "positive hole" resides in the lowest energy level E_0 which is doubly degenerate. The ground states are $\psi_{0\alpha}$ and $\psi_{0\beta}$ where α and β are spin functions with $S_z = +\frac{1}{2}$ and $S_z = -\frac{1}{2}$ respectively. In a tetragonal field the "positive hole" of copper is in the $d_{x^2-y^2}$ or d_{z^2} state, depending on the type of tetragonal distortion.

$$\hat{V}_{LS} = \lambda\, \underline{L}.\underline{S} = \lambda\left[L_z S_z + \tfrac{1}{2}(L_+ S_- + L_- S_+)\right]$$

The constant λ is positive if the 3d shell is less than half-filled and negative if more than half-filled. For Cu^{2+} λ is negative. V_{LS} causes mixing of various other states, ψ_n, into the ground state

By first-order perturbation theory the new ground states are found to be

$$\psi_{0\alpha}' = \psi_{0\alpha} - \sum_n \psi_n \frac{\langle n|\lambda \underline{L}.\underline{S}|0,+\frac{1}{2}\rangle}{E_n - E_0}$$

$$\psi_{0\beta}' = \psi_{0\beta} - \sum_n \psi_n \frac{\langle n|\lambda \underline{L}.\underline{S}|0,-\frac{1}{2}\rangle}{E_n - E_0} \qquad 13.2.2$$

The $L_z S_z$ part of L.S mixes $\psi_{0\alpha}$ with $\psi_{n\alpha}$ and $\psi_{0\beta}$ with $\psi_{n\beta}$, leaving the electron spin unchanged, but the L_+S_- and L_-S_+ parts mix the α and β ground states with, respectively, β and α excited states, so that 13.2.2 becomes

$$\psi_{0\alpha}' = \psi_{0\alpha} - \tfrac{1}{2}\lambda \sum_n \frac{\langle \psi_n|L_z|\psi_0\rangle}{E_n - E_0}\cdot\psi_{n\alpha} - \tfrac{1}{2}\lambda \sum_n \frac{\langle \psi_n|L_+|\psi_0\rangle}{E_n - E_0}\psi_{n\beta}$$

and $$\psi_{0\beta}' = \psi_{0\beta} + \tfrac{1}{2}\lambda \sum_n \frac{\langle \psi_n|L_z|\psi_0\rangle}{E_n - E_0}\cdot\psi_{n\beta} - \tfrac{1}{2}\lambda \sum_n \frac{\langle \psi_n|L_-|\psi_0\rangle}{E_n - E_0}\psi_{n\alpha}$$

It is the extent of mixing which determines the amount of "unquenching" of orbital angular momentum. Spin-orbit coupling does not change the energies of the levels, to first-order, unless the levels are orbitally degenerate.

The interaction of the electron with the magnetic field is now considered,

$$V_H = \beta \underline{H} (\underline{L} + g_e \underline{S}) \qquad 13.2.3$$

First-order perturbation treatment gives

$$\langle \Psi_o | \mathcal{H}_H | \Psi_o \rangle = g_e \beta \langle \Psi_o | \underline{H} \cdot \underline{S} | \Psi_o \rangle$$

$$= g_e \beta S_i H_i$$

and second-order perturbation gives, as a result of spin-orbit coupling, the additional term

$$\sum_{n \neq o} \frac{\langle \Psi_o | \mathcal{H}_H | \Psi_n \rangle \langle \Psi_n | \mathcal{H}_H | \Psi_o \rangle}{E_n - E_o}$$

$$= -g_e \beta \lambda S_i H_j \sum_{n \neq o} \frac{\langle \Psi_o | L_i | \Psi_n \rangle \langle \Psi_n | L_j | \Psi_o \rangle}{E_n - E_o}$$

$$= -g_e \beta \lambda \Lambda_{ij} S_i H_j$$

Therefore, V_H becomes

$$V_H = g_e \beta (\delta_{ij} - \lambda \Lambda_{ij}) S_i H_j = \beta S_i g_{ij} H_j \qquad 13.2.4$$

giving an anisotropic g-value

$$g_{ij} = g_e (\delta_{ij} - \lambda \Lambda_{ij}) \qquad 13.2.5$$

g_{ij} is a symmetric tensor of second rank. The values g_{xx}, g_{yy}, and g_{zz} are the principal components. For any kind of axial symmetry,

$$g_{xx} = g_{yy} \equiv g_\perp \qquad \text{and} \qquad g_{zz} \equiv g_\parallel$$

For cubic symmetry $g_\parallel = g_\perp$

Λ_{ij} is a real and symmetric tensor and is a measure of the extent of mixing of states by spin-orbit coupling. For Cu^{++} in a tetragonal field.

$$\Lambda_{xx} = \Lambda_{yy} = \Lambda_\perp = \frac{1}{E(d_{xz}) - E(d_{x^2-y^2})} \quad \text{and} \quad \Lambda_{zz} = \Lambda_\parallel = \frac{4}{E(d_{xy}) - E(d_{x^2-y^2})}$$

if the "positive hole" is in the $d_{x^2-y^2}$ orbital, and

$$\Lambda_{xx} = \Lambda_{yy} = \Lambda_\perp = \frac{3}{E(d_{xz}) - E(d_{z^2})} \quad \text{and} \quad \Lambda_{zz} = \Lambda_\parallel = 0$$

if the d_{z^2} orbital is lowest lying. Since λ for Cu^{++} is negative, g-values greater than 2.0023 are expected.

By measuring g-values it is possible to determine whether the

"positive hole," is in a perturbed $d_{x^2-y^2}$ or a perturbed d_{z^2} orbital. Measurements on $K_2(Zn:Cu)(SO_4)_2 6H_2O$ at 20°K with the ratio Zn:Cu between 20:1 and 1000:1 gave[93] $g_{\parallel} = 2.44$ and $g_{\perp} = 2.13$ which suggests that the groundstate level of the positive hole in this complex of copper(II) is the perturbed $d_{x^2-y^2}$ orbital and hence that the tetragonal distortion is in the form of an extension of the ligands along the Z-axis. Complex fluorides with Cu(II) and alkali metals, of the form M_2CuF_4[94] and $MCuF_3$ are the only known example of a copper complex in which the ligands along the Z-axis are compresed so that the positive hole is in the perturbed d_{z^2} orbital.

This has been a purely crystal field approach, in which no bonding between the central metal ion and its ligands is assumed. In most chemical compounds this assumption is not true. The molecular orbital theory[95] starts with the premise that overlap of metal and ligand orbitals occurs, to some degree, whenever symmetry permits. The crystal field (electrostatic) situation is clearly one extreme. It is necessary to find out which orbitals can and cannot overlap because of energy and symmetry requirements.

The 3d, 4s and 4p orbitals have comparable energies so that these orbitals are available for bond formation in a first row transition metal ion complex. For metal-ligand bonding the symmetry of the orbitals on the metal and ligand must match. Whenever two orbitals combine to form molecular orbitals, two new orbitals are obtained, one of which is more stable and the other less stable than either of the original orbitals. More generally the number of new orbitals formed is equal to the number of combining orbitals, and one of the new orbitals is less and another more stable than any of combining orbitals.

Six of the metal orbitals, the d_{z^2} $d_{x^2-y^2}$, s, p_x, p_y and p_z, have lobes lying along three metal ligand bond directions and are therefore suitable for σ-bonding. The three p-orbitals and the remaining three d-orbitals, are available for π-bonding to ligand orbitals of appropriate symmetry.

Each of the six ligands is assumed to possess one σ-orbital; in H_2O this σ-orbital is a lone pair sp^3 hybrid orbital. These individual σ-orbitals are combined into six "symmetry" orbitals, each contructed so as to overlap effectively with a particular one of the six metal ion orbitals which are suitable for σ-bonding. Each of the metal ion orbitals is then combined with its matching symmetry orbital of the ligand group to give a bonding and an anti-bonding molecular orbital.

If the ligands also possess π-orbitals, such as pure p-orbitals, these too may be combined into "symmetry" orbitals constructed so as to overlap with the three metal ion π-type orbitals, and the bonding and antibonding orbitals then formed by overlap.

Figure 13.2.4 shows qualitatively the molecular orbital energy level diagram for an octahedral complex between Cu^{2+} and six ligands which do not possess π-orbitals. Figure 13.2.5 shows diagramatically the metal orbitals and their matching ligand group orbitals.

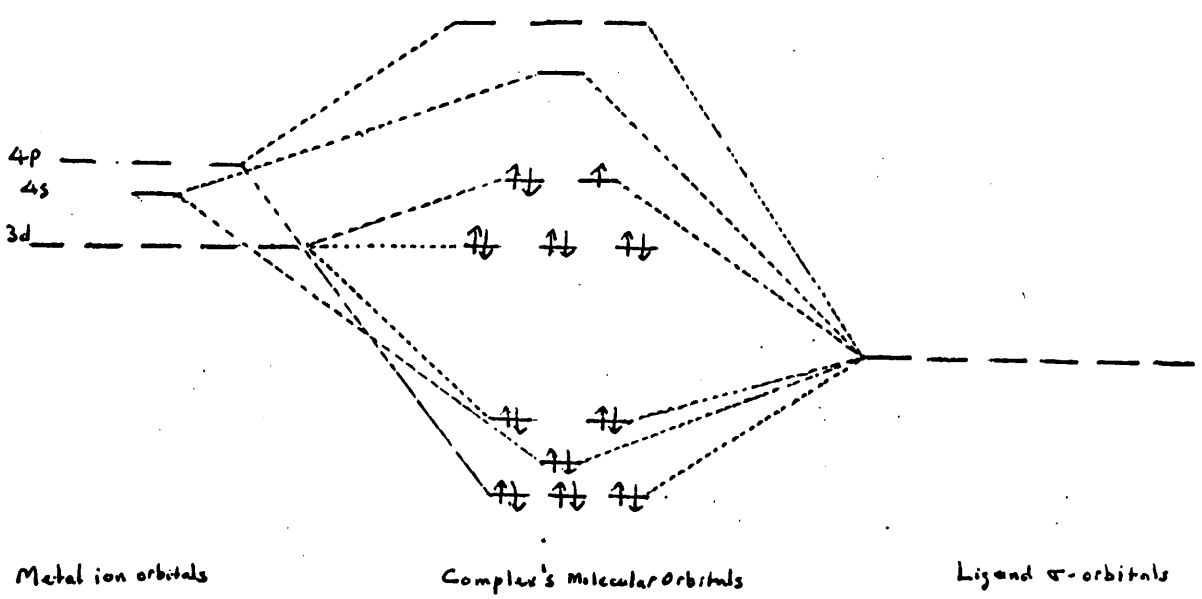

Figure 13.2.4

Six electron pairs occupy the six bonding molecular orbitals, which are mainly ligand orbitals in character. The three degenerate non-bonding orbitals are pure metal ion orbitals and the six anti-bonding orbitals are mainly metal orbitals in character. The nine

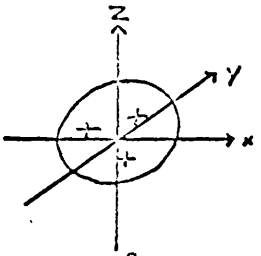

s

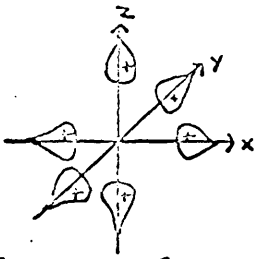

$\frac{1}{\sqrt{6}}\left(\sigma_x + \sigma_{-x} + \sigma_y + \sigma_{-y} + \sigma_z + \sigma_{-z}\right)$

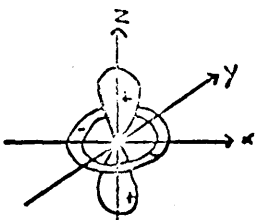

d_{z^2}

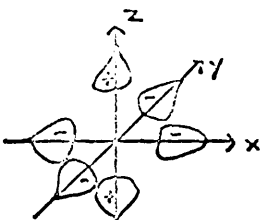

$\frac{1}{2\sqrt{3}}\left(2\sigma_z + 2\sigma_{-z} - \sigma_x - \sigma_{-x} - \sigma_y - \sigma_{-y}\right)$

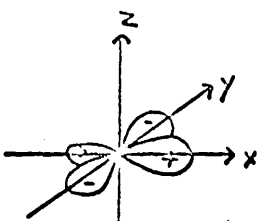

$d_{x^2-y^2}$

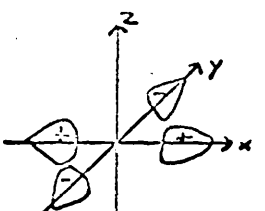

$\frac{1}{2}\left(\sigma_x + \sigma_{-x} - \sigma_y - \sigma_{-y}\right)$

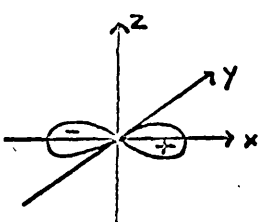

p_x

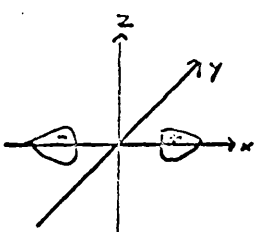

$\frac{1}{\sqrt{2}}\left(\sigma_x - \sigma_{-x}\right)$

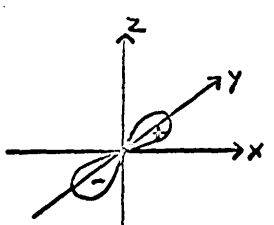

p_y

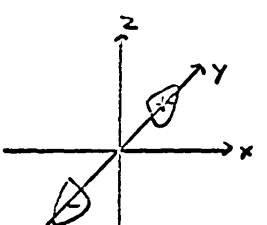

$\frac{1}{\sqrt{2}}\left(\sigma_y - \sigma_{-y}\right)$

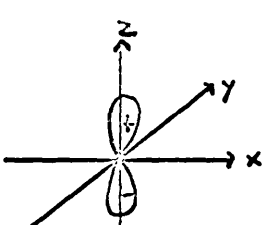

p_z

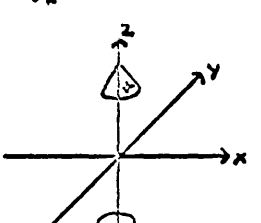

$\frac{1}{\sqrt{2}}\left(\sigma_z - \sigma_{-z}\right)$

METAL AND LIGAND GROUP ORBITALS OF SYMMETRY SUITABLE FOR σ- BONDING

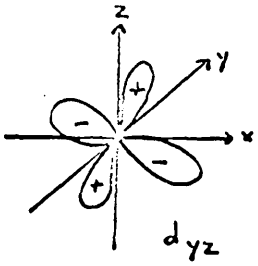

d_{yz}

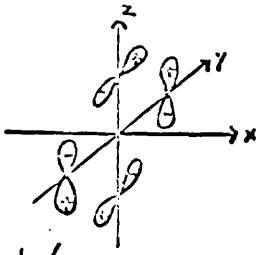

$\frac{1}{2}\left(p_z(y) - p_z(-y) + p_y(z) - p_y(-z)\right)$

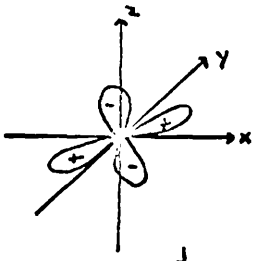

d_{xy}

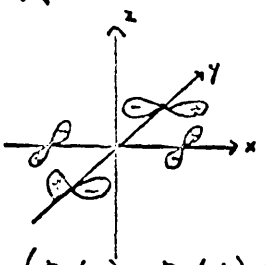

$\frac{1}{2}\left(p_x(y) - p_x(-y) + p_y(x) - p_y(-x)\right)$

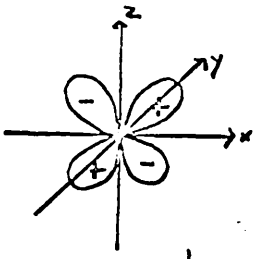

d_{xz}

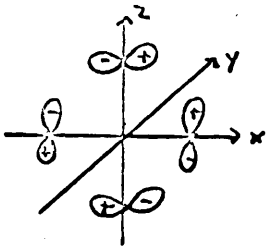

$\frac{1}{2}\left(p_x(z) - p_x(-z) + p_z(x) - p_z(-x)\right)$

METAL d-ORBITALS AND LIGAND GROUP ORBITALS OF SYMMETRY SUITABLE FOR π-BONDING.

Figure 13.2.5

remaining electrons occupy the non-bonding and the lowest lying antibonding molecular orbitals. The "positive hole" resides in one of the degenerate antibonding molecular orbitals compounded out of the $d_{x^2-y^2}$ or d_{z^2} metal orbitals and suitable ligand group orbitals.

The effect of tetragonal distortion arising from extension of the metal ion-ligand bonds along the Z-axis of the complex is to remove some of the degeneracy of the complex energy levels, causing the positive hole to be in the antibonding molecular orbital compounded out of the $d_{x^2-y^2}$ orbital and its appropriate ligand group orbitals.

Throughout the remainder of this section the crystal field approximation is used, for convenience. In chapter fifteen the specific problem of cupric formate complexes is treated using the molecular orbital approach.

The energy level diagram of Cu^{++} ion in a tetragonal crystal field and a steady magnetic field is shown in figure 13.2.6. The energy of separation between the two spin components of the perturbed $d_{x^2-y^2}$ orbital, assuming that the magnetic field is applied parallel to the Z-axis of the crystal field

$$E = g_Z \beta H$$

since $\langle S_Z \rangle = \pm\frac{1}{2}$.

This equation should be compared with the free electron spin energy level separation 13.1.3. or the free atom equation 13.1.4.

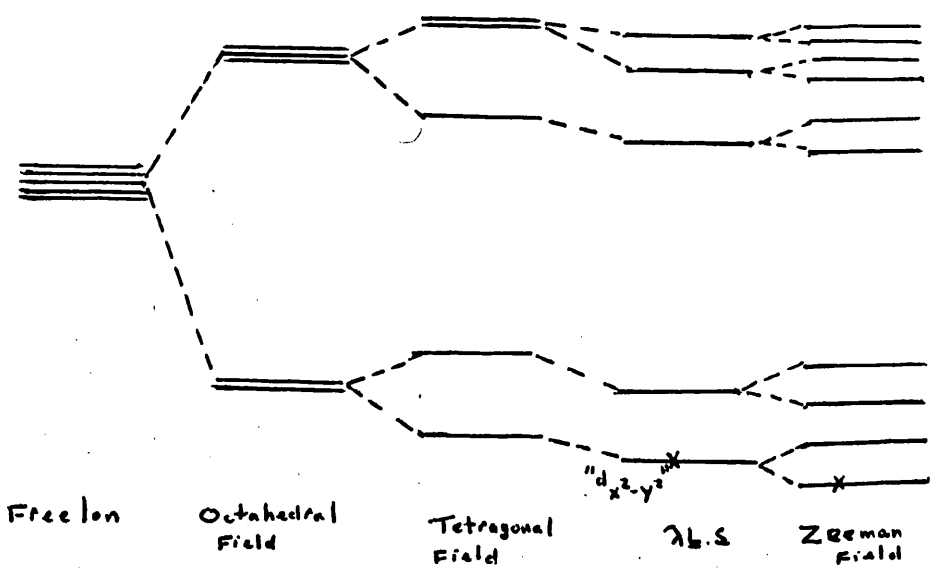

Figure 13.2.6

If the magnetic field is applied perpendicular to the Z-axis, the energy of separation is

$$E = g_{\perp} \beta H$$

Only in a perfectly cubic crystal field are these two energies the same. Therefore in an E.P.R. experiment on a single crystal of a Cu^{++} ion in a tetragonal crystal field the resonance frequency $\nu = E/h$ depends on the orientation of the crystal in the magnetic field. In normal practice ν is kept fixed and H is varied so that resonance takes place when

$$H = \frac{h\nu}{g\beta}$$

where $g^2 = g_{\parallel}^2 \cos^2\theta + g_{\perp}^2 \sin^2\theta$ 13.2.6

and θ is the angle between the crystal field tetragonal axis, Z, and the magnetic field direction.

The transition probability, and therefore the absorption intensity, is proportional to the square of the microwave power amplitude H_1, which is applied at right angles to the magnetic field direction, and to the square of μ, the magnetic moment component along the axis of the microwave field

$$\mu_{H_1} = - g_{H_1} \beta S$$

where $g_{H_1}^2 = g_{\parallel}^2 \cos^2(90-\theta) + g_{\perp}^2 \sin^2(90-\theta)$

Therefore intensity of absorption varies with orientation of the crystal in the magnetic field in a manner governed by

$$I \propto (g_{H_1})^2 = g_{\perp}^2 + g_{\parallel}^2 - g^2 \qquad 13.2.7$$

If the crystal field is only slightly anisotropic, so that $g_{\parallel}$ and $g_{\perp}$ are nearly equal little intensity variation is observed as the crystal is rotated about an axis normal to the applied magnetic field.

Ignoring interactions involving the nuclear spin of the transition metal ion the "spin Hamiltonian" for a transition metal ion complex of tetragonal symmetry in a steady magnetic field has been shown to be

$$\mathcal{H}_s = g_{\parallel} \beta H_Z S_Z + g_{\perp} \beta (H_x S_x + H_y S_y) \qquad 13.2.8$$

The interaction of the unpaired electron with the nuclear spin arises from two causes; magnetic interaction with the magnetic moment of the nucleus, which is linear in nuclear spin I, and electrostatic interaction with the electric quadrupole moment of the nucleus, which

is quadratic in $\underline{I}$. Higher electric and magnetic multipoles need not be considered since their effects are negligibly small. This interaction, $V_N + V_Q$ can be written

$$V_N + V_Q = 2\gamma\beta\beta_N \sum_k \left\{ \frac{(\underline{l}_k - \underline{S}_k)\,\underline{I}}{r_k^3} + \frac{3(\underline{r}_k \cdot \underline{S}_k)(\underline{r}_k \cdot \underline{I})}{r_k^5} + \frac{8\pi}{3}\delta(\underline{r}_k)(\underline{S}_k \cdot \underline{I}) \right\}$$

$$+ \frac{eQ}{2I(2I-1)} \sum_k \left\{ \frac{I(I+1)}{r_k^3} - \frac{3(\underline{r}_k \cdot \underline{I})^2}{r_k^5} \right\}$$

where $\underline{l}_k$ and $\underline{S}_k$ are the orbital and spin angular momenta of the k-th upaired electron, β is the Bohr magneton and β_N is the nuclear magneton. γ is the magnetogyric ratio and Q the quadrupole moment of the nucleus. r_k is the distance of the k-th electron from the nucleus. The delta function in the first summation takes account of the Fermi contact interaction term.[96]

By anology with V_H, $V_N + V_Q$ can be written in the form

$$S_i A_{ij} I_j + I_i Q_{ij} I_j$$

where A_{ij} and Q_{ij} are the hyperfine coupling and quadrupole moment tensors. In tetragonal symmetry, these tensors, like g_{ij}, are characterised by two principal values, each parallel and perpendicular to the symmetry axis. Taking the latter again as the Z-axis,

$$V_N + V_Q = AS_Z I_Z + B(S_x I_x + S_y I_y) + Q'\left[I_z^2 - \tfrac{1}{3}I(I+1)\right] \qquad 13.2.10$$

For any given nucleus A_{ij} and Q_{ij} are complicated functions of the electron distributions in its neighbourhood but these functions have been derived by Abragam and Pryce.[97] For Cu^{++} ion a tetragonal field, the following approximate values of A, B and Q' have been found

$$A = P\left[-\tfrac{4}{7} - K_o + g_{\parallel} - 2 + \tfrac{3}{7}(g_{\perp} - 2)\right]$$
$$B = P\left[+\tfrac{2}{7} - K_o + g_{\perp} - 2 - \tfrac{2}{14}(g_{\perp} - 2)\right] \qquad 13.2.11$$
$$Q' = 3eQq\left[4I(2I-1)\right]^{-1}$$

where $P = 2\gamma\beta\beta_N\langle r^{-3}\rangle$ and $\langle r\rangle$ is the effective radius of the $d_{x^2-y^2}$ orbital. K_o is a factor introduced to represent the admixture of configurations with unpaired s-electrons. For Cu^{++}, the $3s3d^{10}$ and $3d^8 4s$ configuration contribute and K_o has been shown[98] to be 3/7. eQq is the quadrupole coupling constant of the transition metal nucleus in the complex. The (2I+1) eigenvalues of I_z produce four component levels in each electronic state.

Finally the nuclear magnetic moment of the nucleus interacts with the Zeeman field to further shift the electronic energy levels, by an amount,

$$V_h = \gamma \beta_N H . I$$

When a cupric complex is subjected to an applied magnetic field the energy levels of the ground state are determined by the spin Hamiltonian.

$$\mathcal{H} = g_{\parallel} \beta H_z S_z + g_{\perp} \beta (H_x S_x + H_y S_y) + A S_z I_z + B(S_x I_x + S_y I_y) \qquad 13.2.12$$

$$+ Q' \left[I_z^2 - \tfrac{1}{3} I(I+1) \right] - \gamma \beta_N \underline{H} . \underline{I}$$

The energy level diagram for the system is shown in Figure 13.2.7

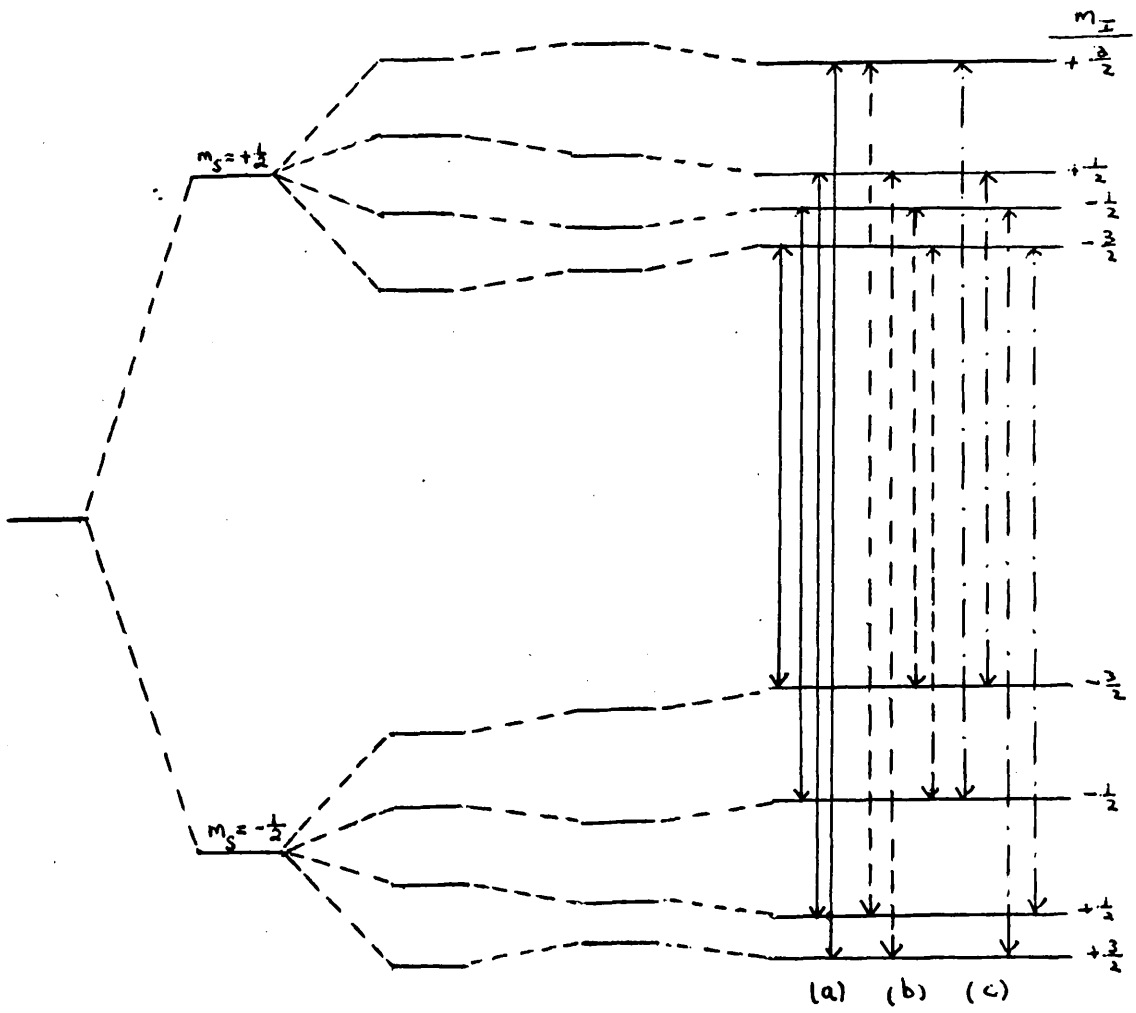

Figure 13.2.7.

The normal selection rule governing transitions between these levels is $\Delta m_s = \pm 1$, $\Delta m_I = 0$. Owing to the order of the (2I+1) components levels being inverted from the electronic spin states of opposite sign a splitting of the E.P.R. spectrum into (2I+1) hyperfine components is obtained. (a) of figure 13.2.7 shows the normal Δ transitions for $I = 3/2$. Transitions also occur which obey the selection rules $\Delta m_s = \pm 1$. $\Delta m_I = \pm 1$ [(b) of 13.2.7] and $\Delta m_s = \pm 1$, $\Delta m_I = \pm 2$ [(c) of 13.2.7]. These transitions become "allowed" because the quadrupolar interaction tries to align the nuclear spin along the symmetry axis while the magnetic field set up by the electrons tries to align the nucleus at right angles to the symmetry axis. This results in several nuclear spin states being admixed, producing a breakdown in the "normal" selection rule.

13.3. Quadrupolar Interaction in Paramagnetic Resonance Spectra

The Hamiltonian, 13.2.12, represents the different interaction energies which affect the ground state energy level of a paramagnetic ion. The numerical constants are related to the electron orbitals and the energy levels of the ion. Only parameters along and perpendicular to the crystal field symmetry axis enter into the expression 13.2.12 and it is useful to know how an E.P.R. spectrum is expected to behave with variation in crystal orientation. Bleaney[99] has dealt with this in detail. The external Zeeman field is applied at an angle θ to the crystal field symmetry axis. Frequency is held fixed and the Zeeman field is swept through the resonance condition. For the "normal" transitions, $\Delta m_s = \pm 1$, $\Delta m_I = 0$, the expression for the resonance field is, for $S = \frac{1}{2}$,

$$H = H_o - Km_I - \frac{B^2}{4H_o}\left[\frac{A^2+K^2}{K^2}\right]\left[I(I+1) - m_I^2\right] - \frac{1}{2H_o}\left[\frac{A^2-B^2}{K}\right]^2\left[\frac{g_{\parallel}\, g_{\perp}}{g^2}\right]^2 m_I^2 \sin^2\theta\cos^2\theta$$
$$+ \frac{2Q'^2}{K}\left(\frac{ABg_{\parallel}\, g_{\perp}}{K^2 g^2}\right)^2\left[4I(I+1) - 8m_I^2 - 1\right] m_I \sin^2\theta\cos^2\theta$$
$$- \frac{Q'^2}{2K}\left(\frac{Bg_{\perp}}{Kg}\right)^4\left[2I(I+1) - 2m_I^2 - 1\right] m_I \sin^4\theta \qquad 13.3.1$$

where H_o is the resonant field in the absence of hyperfine coupling, i.e. $H_o = \frac{h\nu}{g\beta}$, K is the hyperfine splitting factor given by

$$K^2 g^2 = A^2 g_{\parallel}^2 \cos^2\theta + B^2 g_{\perp}^2 \sin^2\theta$$

and varies from A at $\theta = 0^o$ to B at $\theta = 90^o$ and g is equal to

$g_{\parallel}^2\cos^2\theta + g_{\perp}^2\sin^2\theta$

H_o, g and K are obtained from the four lined E.P.R. spectrum at an orientation θ, for the case of $S = \frac{1}{2}$, $I = \frac{3}{2}$ in the following way.

$$H_\theta(m_{I=-\frac{1}{2}}) + H_\theta(m_{I=+\frac{1}{2}}) = 2H_o - \frac{28}{16}\frac{B^2}{H_o}\left[\frac{A^2+K^2}{K^2}\right] - \frac{1}{4H_o}\left[\frac{A^2-B^2}{K}\right]^2\left[\frac{g_{\parallel}g_{\perp}}{g^2}\right]^2 \sin^2\theta\cos^2\theta$$

$$H_\theta(m_{I=-\frac{3}{2}}) + H_\theta(m_{I=+\frac{3}{2}}) = 2H_o - \frac{12B^2}{16H_o}\left[\frac{A^2+K^2}{K^2}\right] - \frac{1}{4H_o}\left[\frac{A^2-B^2}{K}\right]^2\left[\frac{g_{\parallel}g_{\perp}}{g^2}\right]^2 \sin^2\theta\cos^2\theta$$

Therefore

$$H_o = \frac{1}{8}\left\{7(H_\theta(m_{I=-\frac{3}{2}}) + H_\theta(m_{I=+\frac{3}{2}})) - 3(H_\theta(m_{I=-\frac{1}{2}}) + H_\theta(m_{I=+\frac{1}{2}})\right\} + C_H \qquad 13.3.2$$

where C_H is a small correction factor equal to

$$\frac{15}{8H_o}\left[\frac{A^2-B^2}{K}\right]^2\left[\frac{g_{\parallel}g_{\perp}}{g^2}\right]^2 \sin^2\theta\cos^2\theta$$

From this value of H_o can be obtained the g-value, since

$$g = \frac{h\nu}{\beta_e H_o} = \frac{\text{constant}}{H_o}$$

Similarly,

$$H_\theta(m_{I=-\frac{1}{2}}) - H_\theta(m_{I=+\frac{1}{2}}) = K - \frac{24Q'^2}{K}\left[\frac{ABg_{\parallel}g_{\perp}}{K^2g^2}\right]^2 \sin^2\theta\cos^2\theta + \frac{3Q'^2}{K}\left[\frac{Bg_{\perp}}{Kg}\right]^4 \sin^4\theta$$

$$H_\theta(m_{I=-\frac{3}{2}}) - H_\theta(m_{I=+\frac{3}{2}}) = 3K + \frac{24Q'^2}{K}\left[\frac{ABg_{\parallel}g_{\perp}}{K^2g^2}\right]^2 \sin^2\theta\cos^2\theta + \frac{3Q'^2}{K}\left[\frac{Bg_{\perp}}{Kg}\right]^4 \sin^4\theta$$

so that

$$K = \frac{1}{4}\left\{H_\theta(m_{I=-\frac{3}{2}}) - H_\theta(m_{I=+\frac{3}{2}}) + H_\theta(m_{I=-\frac{1}{2}}) - H_\theta(m_{I=+\ }\ )\right\} + C_K \qquad 13.3.3.$$

where C_K is a small correction factor equal to

$$\frac{-6}{4}\frac{Q'^2}{K}\left(\frac{Bg_{\perp}}{Kg}\right)^4 \sin^4\theta$$

Thus by recording a large number of spectra at various orientations relative to well defined axes of the crystal in the magnetic field, θ, A, B, $g_{\parallel}$ and $g_{\perp}$ can be obtained.

From the equation for H_θ, 13.3.1, a value for $|Q'|$, the quadrupole coupling factor, should be obtainable knowing H_o, g, $g_{\parallel}$ $g_{\perp}$, A, B, K and θ. In most cases, the terms involving Q'^2 are so small that they are comparable with the limits of error associated with

the other parameters, especially K, so that Q' cannot usually be determined from the "normal" transition lines of an E.P.R. spectrum.

Bleaney has derived formulae for the "normally forbidden" transitions involving simultaneous changing of m_s and m_I for nuclei with $S = \frac{1}{2}$

For the $\Delta m_s = \pm 1$, $\Delta m_I = \pm 1$ transitions it is convenient to define a quantum number k, equal to

$$I-\tfrac{1}{2},\ I-\tfrac{3}{2},\ I-\tfrac{5}{2},\ \ldots\ldots,\ -I+\tfrac{1}{2}\ .$$

Using this parameter the magnetic fields at which these transitions occur are

$$H'_\theta = H_o - Kk \pm (Q''k - \gamma') \qquad 13.3.4$$

and their intensities are given by

$$I'_\theta = 4k^2\left[(I+\tfrac{1}{2})^2 - k^2\right]X \qquad 13.3.5$$

The $\Delta m_s = \pm 1$, $\Delta m_I = \pm 2$ transitions occur at fields

$$H''_\theta = H_o - Km_I \pm (2Q''m_I - 2\gamma') \qquad 13.3.6$$

with intensities

$$I''_\theta = \left[(I+1)^2 - m_I^2\right]\left[I^2 - m_I^2\right]Y \qquad 13.3.7$$

where

$$X = \frac{Z}{2I+1}\left(\frac{Q'}{-2K}\right)^2\left(\frac{ABg_{\parallel}g_{\perp}}{K^2g^2}\right)^2 \cos^2\theta\sin^2\theta$$

$$Y = \frac{Z}{(2I+1)}\left(\frac{Q'}{-2K}\right)^2\left(\frac{Bg_{\perp}}{Kg}\right)^4 \sin^4\theta$$

$$Q'' = Q'\left[3A^2g_{\parallel}^2\cos^2\theta\,(Kg)^{-2} - 1\right] \qquad 13.3.8$$

$$\gamma' = \gamma\beta_N H_o (Kg)^{-1}\left[Ag_{\parallel}\cos^2\theta + Bg_{\perp}\sin^2\theta\right]$$

Z involves the partition function and a line - shape factor.

Transitions for which $\Delta m_I = \pm 1$ clearly have zero intensity at $\theta = 0^\circ$ and $\theta = 90^\circ$. If $A = B$ they have maximum intensity at $\theta = 45^\circ$. The lines for which $\Delta m_I = \pm 2$ are strongest at $\theta = 90^\circ$. Figure 13.3.1. illustrates how these transitions vary with angle for the idealised isotropic cases, with $A = B = 5Q'$

For Cu(II), $I = \frac{3}{2}$ so that $k = 1, 0, -1$. The $\Delta m = \pm 1$, $\Delta m_I = \pm 1$ transitions occur at fields

$$\begin{aligned} &H_o - K + Q'' - \gamma' \\ &H_o - K - Q'' + \gamma' \\ &H_o + K - Q'' - \gamma' \\ &H_o + K + Q'' + \gamma' \end{aligned} \qquad 13.3.9$$

Therefore from these lines values of H_o, K, Q'' and γ' can be

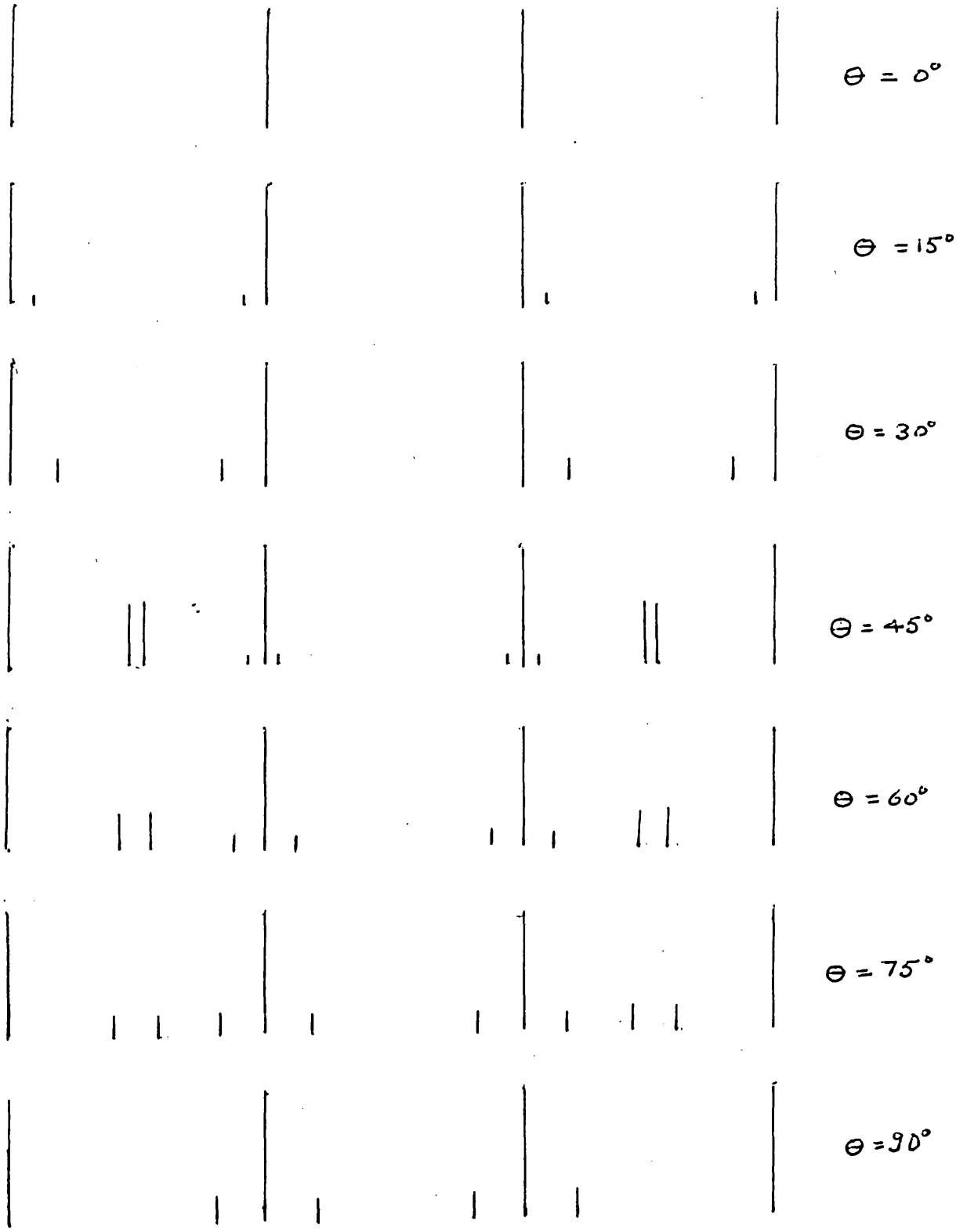

Figure 13.3.1

obtained. The intensities of these transitions for Cu^{++} are determined by

$$12\, Z\, (Q'AB g_{\parallel} g_{\perp})^2 \cos^2\theta \sin^2\theta K^{-6} g^{-4} ,$$

$\Delta m_s = \pm 1$, $\Delta m_I = \pm 2$ transitions have, for Cu^{++}, intensities given by

$$\tfrac{3}{4}\, Z\, (Q'B^2 g_{\perp}^2)^2 \sin^4\theta K^{-6} g^{-4}$$

for $m_I = \pm\frac{1}{2}$. When $m_I = \pm\frac{3}{2}$, $I''_{\theta} = 0$. The resonance fields are

$$H_o - \tfrac{1}{2}K + (-Q'' - 2\gamma')$$
$$H_o - \tfrac{1}{2}K + (Q'' - 2\gamma')$$
$$H_o + \tfrac{1}{2}K - (Q'' - 2\gamma')$$
$$H_o + \tfrac{1}{2}K - (-Q'' - 2\gamma')$$

These lines, also, should supply values for H_o, K, Q' and θ.

If "normally forbidden" transitions can be detected in an E.P.R. spectrum it would appear that it is possible to obtain values for the nuclear quadrupole coupling constant, eQq, of the paramagnetic ion, by way of the parameter Q''.

With copper, lines due to the two stable isotopes ^{63}Cu and ^{65}Cu may be detected. These isotopes occur naturally in nature in the ratio 70:30 respectively and both have $I = \frac{3}{2}$. Their hyperfine coupling constants are different.

In addition to hyperfine structure due to the metal nucleus, complexes may show extra splittings in E.P.R. spectra arising from ligand nuclei. This superhyperfine structure is due partly to covalent bonding between the electrons of the central ion and ligand orbitals and partly to direct dipole-dipole coupling.

In order to resolve the large number of resonance lines which may be present in an E.P.R. spectrum, effects which cause broadening of line-widths should be minimised.

Spin-lattice relaxation times are increased, with a resultant decrease in broadening, by working at low temperatures.

Spin-spin interactions produce broadening by the mutual effect of one paramagnetic ion on another. This effect is reduced by diluting the paramagnetic salt with an isomorphous diamagnetic equivalent and effectively moving the paramagnetic ions further apart. If the dilution factor is large, the interaction between the magnetic moments of neighbouring diamagnetic atoms and the isolated electronic moments determine the line width. In hydrogen-containing

complexes the line width can often be reduced further by replacing ^1H by deuterium since the magnetic moment of ^2D is considerably less than that of the proton.

If in a concentrated paramagnetic complex the paramagnetic ions are close enough the unpaired electron wave-functions on neighbouring complexes may overlap, causing the electron spins to couple by exchange forces, the exchange energy being of the form

$$\mathcal{H} = J\,\underline{S}_1 \cdot \underline{S}_2 \,.$$

This coupling allows electrons on neighbouring lattice sites to exchange spin states rapidly and it usually averages out the hyperfine structures so that only a single "exchange narrowed" resonance line remains. Copper acetate mono hydrate [100,101] is the best known example of a complex in which pairs of neighbouring copper ions couple strongly. The two electronic spins (both $S = \frac{1}{2}$) are exchange coupled into a single ground state with an excited triplet state $300 cm^{-1}$ above. At room temperature there is a large proportion of triplet states $S = 1$ and no hyperfine structure is resolved, but on cooling to $77^{\circ}K$ the triplet concentration decreases greatly and, because of the decrease in line broadening at low temperatures, hyperfine splitting from two equivalent copper atoms appears. At $20^{\circ}K$ all spins are paired, $S = 0$, and the E.P.R. spectrum disappears.

CHAPTER 14

DETERMINATION OF THE QUADRUPOLE COUPLING CONSTANT OF COPPER (II) IN DILUTED DIBARIUM CUPRIC FORMATE TETRAHYDRATE BY MEANS OF ELECTRON PARAMAGNETIC RESONANCE SPECTROSCOPY

14.1. Analysis of E.P.R. Spectra

Dibarium zinc formate tetrahydrate and dibarium cupric formate tetrahydrate are isomorphous [102], their structures are known [103], their space group is $P\bar{1}$ and the asymmetric unit in their cells contains one formula weight. In the copper salt, the paramagnetic complex consists of a copper ion surrounded by a distorted octahedron of oxygen atoms. The oxygen atoms along the x- and y-axes of the crystal field of the complex lie at distances ± 1.97Å and 2.02Å from the Cu^{++} ion, the two along the z-axis being at ± 2.18Å from the central metal ion.

The crystal field around the Cu atom is clearly anisotropic, the symmetry being approximately tetragonal.

In order to remove the effects of both electron exchange interactions and proton-electron direct magnetic interactions on the E.P.R. spectra of $Ba_2Cu(HCOO)_6 4H_2O$, single crystals of $Ba_2Zn(DCOO)_6 4D_2O$ in which 0.1% of the Zn^{2+} ions is replaced by Cu^{2+} ions, were prepared by mixing together appropriate quantities of Analar ZnO, CuO, $BaCO_3$, Merck 99% (minimum) DCOOD and a slight excess of Koch-Light 99.8% D_2O and allowing slow crystallisation to take place in the presence of excess DCOOD. The composition of the crystals was confirmed by standard analytical procedures and the crystal habits checked against literature descriptions.[102]

Electron paramagnetic resonance spectra were recorded, at 77°K, on a Decca X3 spectrometer system operating at a fixed frequency of 9270 Mc/s and using a standard H_{102} cavity. A Newport Instruments 11" electromagnet system was used and resonance fields were calibrated using standard proton magnetic resonance techniques.

Spectra were recorded at 10° intervals with respect to arbitrary crystal axes and g-tensor components and hyperfine tensor components were extracted, using the method outlined on pages 132 and 133. By this method the following parameters were found

$$g_{\parallel} = 2.391 \pm 0.003$$

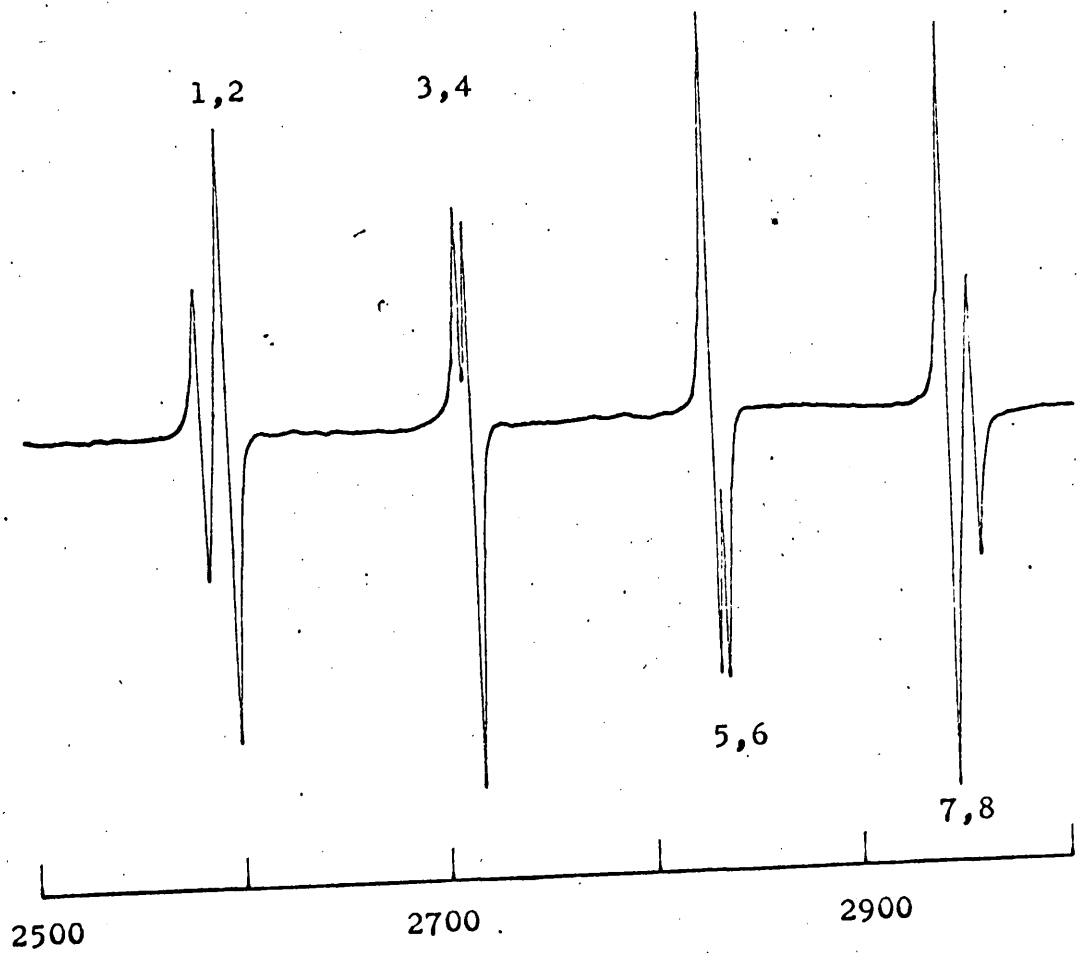

Figure 14.11a X-band first derivative paramagnetic resonance absorption spectrum of $Ba_2(Cu:Zn)(DCOO)_6 4D_2O$, Cu:Zn = 1:1000, at 77°K., $\theta = 0°$

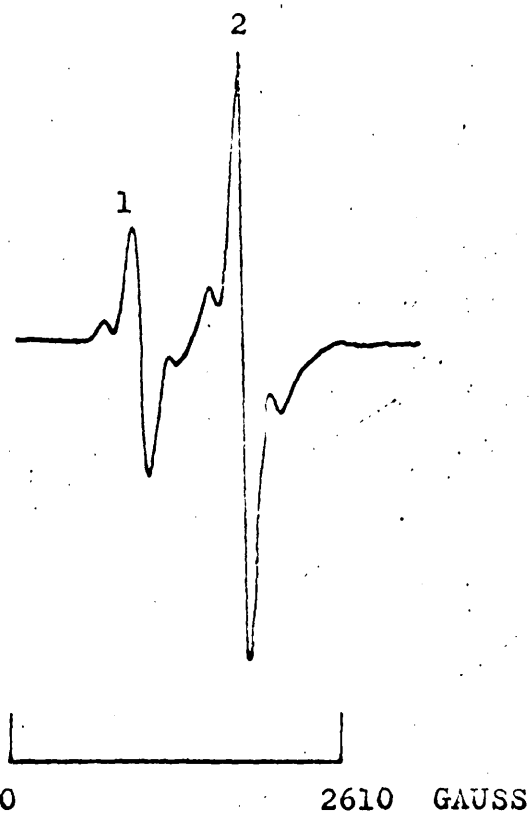

Figure 1411b Peaks 1 and 2 of figure 1a under higher resolution conditions.

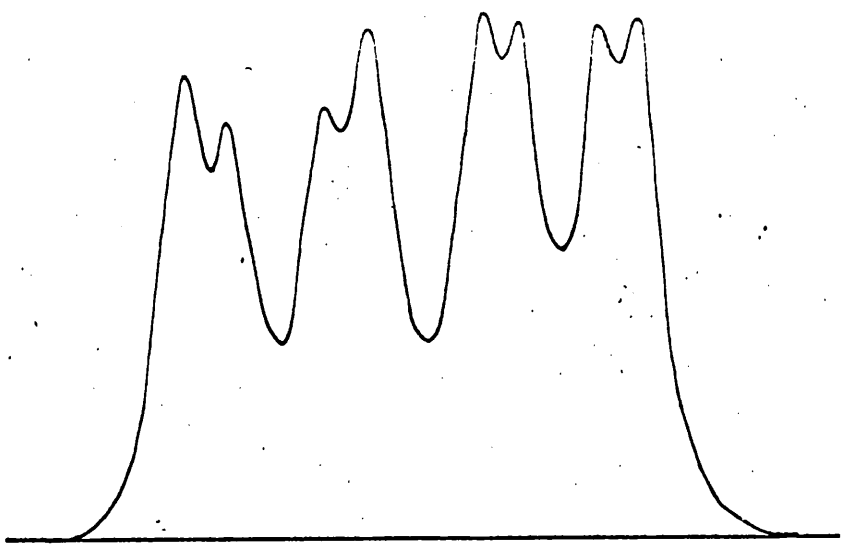

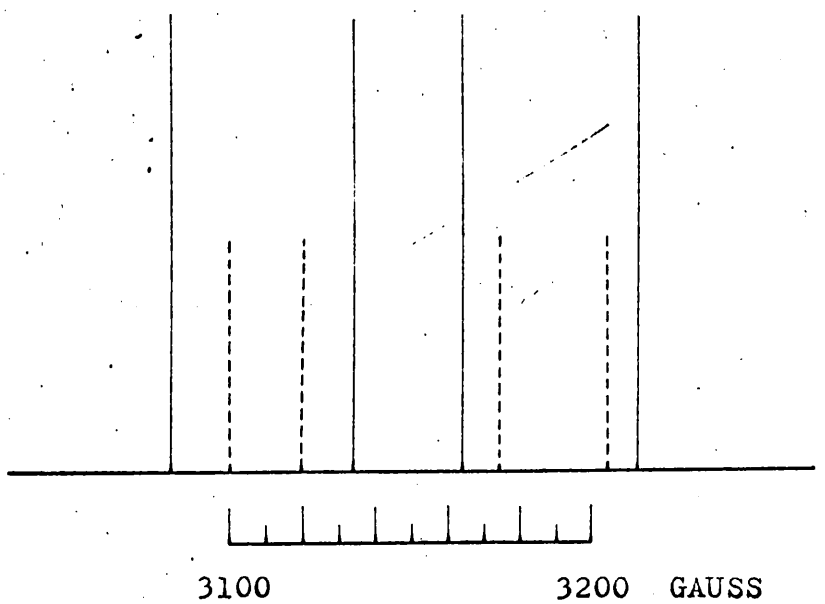

Figure 14.21 Observed and calculated X-band paramagnetic resonance absorption spectra of $Ba_2(Cu:Zn)(DCOO)_6 4D_2O$, Cu:Zn = 1:1000, at 77°K., θ = 75°. Transitions $\Delta M_S = \pm 1$, $\Delta m = 0$ are denoted by (_____). Transitions $\Delta M_S = \pm 1$, $\Delta m = \pm 1$ are denoted by (-----).

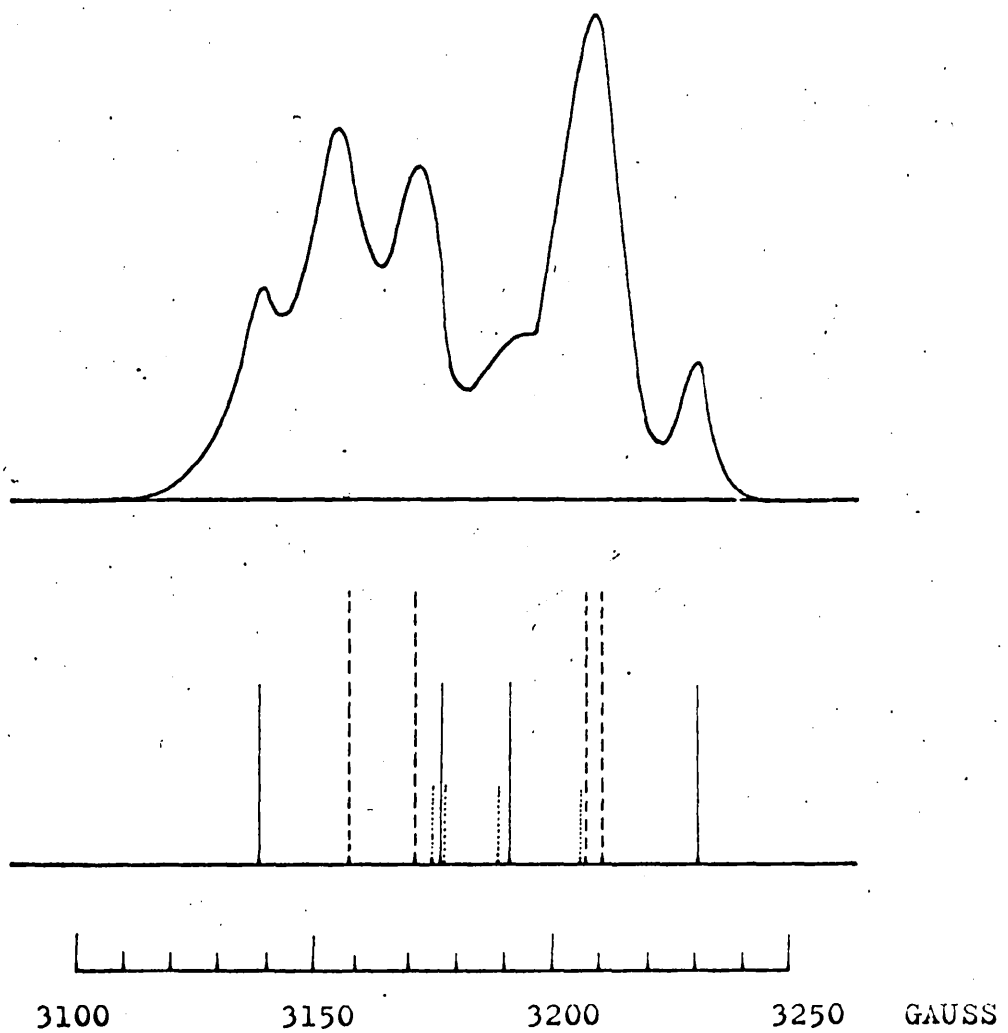

Figure 1422 Observed and calculated X-band paramagnetic resonance absorption spectra of $Ba_2(Cu:Zn)(DCOO)_6 4D_2O$, Cu:Zn = 1:1000, at 77°K, θ= 86°. Transitions $\Delta M_S = \pm 1$, $\Delta m = 0$ are denoted by (———). Transitions $\Delta M_S = \pm 1$, $\Delta m = \pm 1$ are denoted by (– – –). Transitions $\Delta M_S = \pm 1$, $\Delta m = \pm 2$, are denoted by (.....).

$g_\perp = 2.079 \pm 0.003$

$|A\ (^{63}Cu)| = 116.4 \pm 1$ gauss $= 0.0130 \pm 0.0001 cm^{-1}$

$|A\ (^{65}Cu)| = 123.9 \pm 1$ gauss $= 0.0139 \pm 0.0001 cm^{-1}$

$|B\ (^{63}Cu, ^{65}Cu)| = 22 \pm 3$ gauss $= 0.0024 \pm 0.0003 cm^{-1}$

Figure 14.1.1a shows the eight-line spectrum which corresponds to $\Theta = 0^\circ$. The ^{63}Cu and ^{65}Cu hyperfine splittings could only be resolved within the angular range $0^\circ \leq \Theta \leq 40^\circ$. $\Delta m_s = \pm 1, \Delta m_I = \pm 1$ transitions were observed within the angular range $60^\circ \leq \Theta \leq 88^\circ$ and $\Delta m_s = \pm 1, \Delta m_I = \pm 2$ transitions have significant intensities in the range $80^\circ \leq \Theta \leq 90^\circ$. Superhyperfine interaction with ^{13}C nuclei (of spin $\frac{1}{2}$) in the labelled formate ligands was detected and the isotropic contribution to this coupling has been found to be 6.1 ± 0.1 gauss, or $0.00068 \pm 0.00001 cm^{-1}$. Figure 14.1.1b shows this coupling at $\Theta = 0^\circ$.

14.2. Optimisation of Hyperfine Coupling Parameters

Complete analysis of the spectra, considering both the energies and intensities of all the transitions, yields the parameters listed in Table 14.2.1 as the best parameters. Figures 14.2.1 and 14.2.2 show the absorption spectra observed at angles of $\Theta = 75^\circ$ and $\Theta = 86^\circ$ respectively, along with line diagrams of the twelve transitions, four of type $\Delta m_I = 0$, four of type $\Delta m_I = \pm 1$ and four of type $\Delta m_I = \pm 2$, calculated using the parameters in table 14.2.1, superimposed on them. At these angles the isotopic differences can not be resolved.

Table 14.2.1

$g_\parallel = 2.391 \pm 0.003$ $\qquad$ $g_\perp = 2.079 \pm 0.003$

$A(^{63}Cu) = \pm 0.0130 \pm 0.0001 cm^{-1}$

$A(^{65}Cu) = \pm 0.0139 \pm 0.0001 cm^{-1}$

$B(^{63}Cu) = \mp 0.0020 \pm 0.0001 cm^{-1}$

$Q(^{63}Cu) = \mp 0.00093 \pm 0.00006 cm^{-1}$

The quadrupole coupling constant, eQq, for ^{63}Cu in this complex obtained by this analysis is

$$eQq = 4Q' = \mp 0.00372 \pm 0.00024 cm^{-1}$$
$$= \mp 111.6 \pm 7.2 \text{ Mc/s.}$$

It is important to consider both energies and intensities in the determination of eQq for ^{63}Cu because very large errors are

introduced if energies alone are used. These large errors arise because of the large variations in $\cos^2\theta$ at angles at which $\Delta m_I = \pm 1$ and $\Delta m_I = \pm 2$ transitions are present in the spectra.

CHAPTER 15

DISCUSSION OF BONDING IN $Ba_2Cu(DCO_2)_6 4D_2O$ FROM E.P.R. MEASUREMENTS

15.1. Introduction

The discovery of strongly exchange coupled pairs of Cu^{++} ions in $Cu(CH_3COO)_2H_2O$ [100,101] stimulated a widespread interest in the magnetic properties of the other members of the homologous series of copper (II) n-alkanoates and soon led to the discovery of similar paring of Cu^{++} ions in cupric propionate monohydrate [104,105] and in the higher members of this series [106]. At least six formates of Cu(II) have been isolated [107] and bulk magnetic properties of several of them have been studied by magnetic susceptibility measurements [107-110] by E.P.R. [104,111] and by proton N.M.R. studies [112] carried out either on powdered specimens or on single crystals of the normal magnetically concentrated compounds. These measurements and single crystal X-ray studies [113,114,115] all show that the crystal structures and the magnetic properties of the cupric formates differ considerably from those exhibited by the higher homologues. In particular, strongly coupled Cu^{++} pairs are not present in any of the copper formates, although in them the effective magnetic moment per cupric ion is rather less than should be expected for a magnetically isolated tetragonally coordinated cupric ion [107]. Between 80°K and 360°K several of the cupric formates can be fitted to Curie-Weiss laws with negative Weiss constants, that is, they are antiferromagnetic, and it is believed that the exchange demagnetisation is due to a superexchange mechanism in which the formate ion functions as a polyatomic counterpart of the monatomic ions customarily associated with other cases of antiferromagnetism [107].

Particularly intensive studies of the magnetic susceptibilities of $Cu(HCOO)_2 4H_2O$ have been made at very low temperatures [108-110,112]. This is the most magnetically concentrated of the copper formates and the lambda point in its χ versus T_A curve, often characteristic of antiferromagnetic ordering processes, has been detected at 16.8°K. The lambda point in this case arises from magnetic ordering processes, rather that from structural changes, since no differences in the extinction of polarized light or in the dielectric constant have been detected between 14°K and 20°K, nor has any specific heat anomaly been observed in this same temperature range. [110,116]

Careful quantitative analysis of the susceptibility changes which take place in the neighbourhood of this lambda point has shown [108] that the antiferromagnetic ordering in the tetrahydrate is accompanied by a superimposed, weaker, anisotrpic "parasitic" ferro-
panied by a superimposed, weaker, anisotrpic "parasitic" ferro-
magnetism whose saturation moment amounts to roughly 0.03 Bohr magnetons per Cu^{++} ion.

Exchange coupling of Cu^{++} spins in $Cu(HCOO)_2 2H_2O$ is much weaker than in the tetrahydrate. Low temperature susceptibility data on the dihydrate do not yet appear to be complete but measurements between 1.3°K and 20°K [109] and between 102°K and 360°K [107] can be represented by the Curie-Weiss law

$$\chi = 0.431/(T-2)$$

That is the sign of W implies a ferromagnetic cooperation although preliminary results from measurements in the gap between 20°K and 102°K appear to indicate the existence of a lambda point near 25°K [117].

There has been considerable discussion about the nature of the ordering processes which are responsible for these susceptibility changes and at present their details are still obscure. Since they must be defined by the electron distribution and electron spin polarizations within the solids, it might be possible to obtain information about them by detailed E.P.R. studies carried out on isomorphous, diamagnetic, single crystals which have been doped with appropriate amounts of Cu(II). In this way it is possible to obtain information about the properties of isolated paramagnetic species and then, by steadily increasing the doping level, to obtain information about the properties of pairs of interacting complexes, and so on.

Studies of this type were carried out with single crystals of fully deuterated zinc formate dihydrate, $Zn(DCOO)_2 2D_2O$ [118] and zinc formate dihydrate, $Zn(HCOO)_2 2H_2O$ [117] in which some of the Zn^{++} ions were substitutionally replaced by Cu^{++}. The findings of these two independent groups of investigators are essentially identical.

This chapter is concerned with the significance of the E.P.R. results on single crystals of $Ba_2(Zn:Cu)(DCO_2)_6 4D_2O$ in which Zn:Cu is 1000:1.

15.2. Bonding in The Formate Complexes of Copper (II)

$Ba_2Cu(HCOO)_6 4D_2O$ is a relatively rare type of compound which contains one kind of cupric complex; most cupric compounds contain at least two structurally different units.

Complex I of figure 15.2.1 is present in $Ba_2Cu(DCOO)_6 4D_2O$, and complex ions II and III are present in $(Zn:Cu)(DCOO)_2 2D_2O$. The isotopic species IV and V, present in $Cu(HCOO)_2 2D_2O$, are also shown in figure 15.2.1.

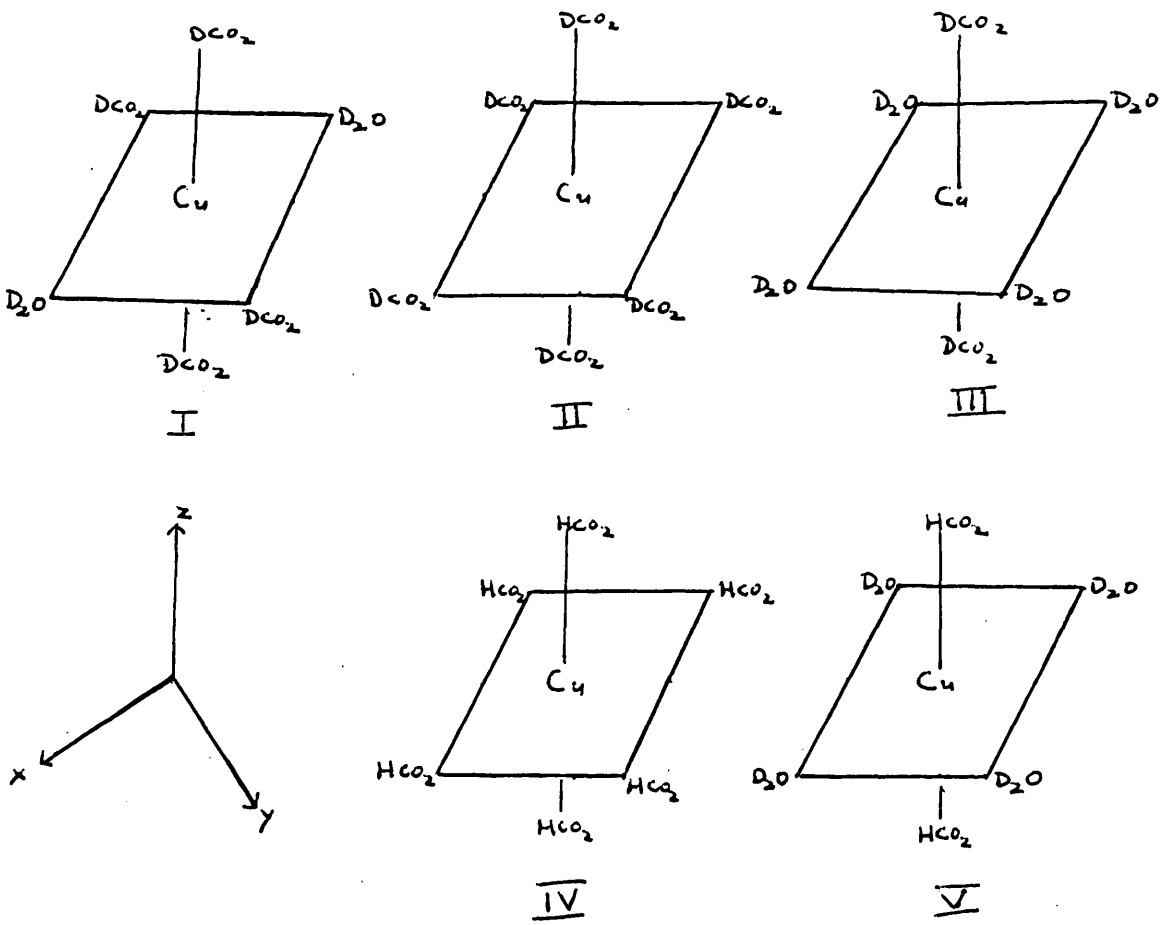

Figure 15.2.1.

According to the molecular orbital theory of bonding in a tetragonal cupric complex, the five-fold degenerate 3d orbitals, the 4s and three-fold degenerate 4p orbitals of the cupric ion combine with ligand group orbitals of appropriate symmetry to form molecular orbitals for the complex. Each combination produces a

bonding and an antibonding molecular orbital and the coefficients in the antibonding orbital are related to those in the bonding molecular orbital. In the "positive hole" formulation for a d^9 complex, the positive hole is, in the absence of spin-orbit coupling, Zeeman interactions and hyperfine interactions, in an antibonding orbital, $\psi(B_{1g})$, compounded out of the cupric ion $d_{x^2-y^2}$ orbital and suitable ligand σ-orbitals. In complex II, these σ-orbitals are all "lone pair" sp^2 hybridised σ-orbitals associated with the oxygen atoms of the formate groups and they can be written in the form

$$\sigma^{(i)} = (\tfrac{2}{3})^{\frac{1}{2}}\, p^{(i)} \pm (\tfrac{1}{3})^{\frac{1}{2}}\, s^{(i)} \qquad 15.2.1$$

where $s^{(i)}$ and $p^{(i)}$ are wave functions for 2s and 2p orbitals respectively, on oxygen atom i. In complex III they are "lone pair" sp^3 hybrid σ-orbitals associated with the oxygen atoms of the D_2O ligands.

$$\sigma^{(i)} = (\tfrac{3}{4})^{\frac{1}{2}}\, p^{(i)} \pm (\tfrac{1}{4})^{\frac{1}{2}}\, s^{(i)} \qquad 15.2.2$$

In complex I two of the ligand orbitals are of the type given by 15.2.1 and two are of the type described by 15.2.2.

Table 15.2.1. lists the Hamiltonian parameters extracted from E.P.R. spectra of complexes I, II and III. The bracketed figures refer to the isotopic species IV and V. There are no significant differencies in the magnetic parameters when the protonated species are compared with the corresponding deuterated species, so that in these complexes the molecular orbitals which define the magnetic properties are not sensibly perturbed by vibrational interactions at $77^{\circ}K$.

Although complex I is orthorhombic the spin Hamiltonian for the $Ba_2(Zn:Cu)(DCOO)_6 4D_2O$ crystal has tetragonal symmetry. This is in agreement with the observation that there are only small changes in $g_{\perp}$ for complexes II and III when the ligands $DCOO^-$ and D_2O are interchanged.

Therefore, as far as the copper atom is concerned, the oxygen atom in the formate is similar to the oxygen atom in the water molecule, so that the forms of the molecular orbitals involved in binding the central metal atom to the ligands in complexes I, II and III are very similar.

Table 15.2.1

Spin Hamiltonian parameters for formates of copper (II)

Complex	I	II	III
g_{11}	2·391 ±0·003	2·407 ±0·001 (2·416 ±0·005)	- (2·420 ±0·005)
$g_{\perp}$	2·079 ±0·003	2·081 ±0·004 (2·077 ±0·007)	- (2·066 ±0·007)
$A(^{63}Cu)(cm^{-1})$	±0·0130 ±0·0001	± 0·0129 ±0·0001 (0·0124 ±0·0002)	- (0·0134±0·0005)
$B(^{63}Cu)(cm^{-1})$	∓0·0020 ±0·0001	∓ 0·0021 ±0·0002 (0·0023 ±0·0002)	- (0·0026±0·0012)
$Q'(^{63}Cu)(cm^{-1})$	∓0·00093±0·00006	∓ 0·0009 ±0·0001 (0·00095±0·00002)	- -
$A(^{65}Cu)(cm^{-1})$	±0·0139 ±0·0001	± 0·0141 ±0·0001	-
$B(^{65}Cu)(cm^{-1})$	∓0·0020 ±0·0001	∓0·0021 ±0·0002	-

In complex II, for example, the forms of the $\psi(B_{1g})$ antibonding orbital and the higher antibonding orbitals, in the "positive hole" formalism, in order of increasing energy are

$$\psi(B_{1g}) = \alpha\, d_{x^2-y^2} - (\alpha'/2)(-\sigma_x^{(1)} + \sigma_y^{(2)} + \sigma_x^{(3)} - \sigma_y^{(4)})$$

$$\psi(B_{2g}) = \beta_1 d_{xy} - (\beta_1'/2)(p_y^{(1)} + p_x^{(2)} - p_y^{(3)} - p_x^{(4)})$$

$$\psi(A_{1g}) = \alpha_1 d_{z^2} - \left[\alpha_1'/2(1+2c_1^2)^{\frac{1}{2}}\right]\left[\sigma_x^{(1)} + \sigma_y^{(2)} - \sigma_x^{(3)} - \sigma_y^{(4)} - 2c_1(\sigma_z^{(5)} - \sigma_z^{(6)})\right]$$

$$\psi(E^1_g) = \beta\, d_{xz} - (\beta'/2)(p_z^{(1)} - p_z^{(3)} + p_x^{(5)} - p_x^{(6)})$$

$$\psi(E^2_g) = \beta\, d_{yz} - (\beta'/2)(p_z^{(2)} - p_z^{(4)} + p_y^{(5)} - p_y^{(6)}) \qquad 15.2.3$$

The coordinate system is a right-handed Cartesian system and ligands 1, 2 and 5 are placed on the positive x, y and z axes and ligands 3, 4 and 6 on the negative x, y and z axes, respectively. Allowance is made for the tetragonal distortion in the z-axis direction by introducing the constant c_1 as a factor, different from unity, to multiply the orbitals of the ligands on the z-axis. Overlap between the copper and ligand orbitals is considered. Normalisation of the $\psi(B_{1g})$ orbital gives

$$\alpha^2 + (\alpha')^2 - 2\alpha\alpha' S = 1 \qquad 15.2.4$$

where S is the overlap integral,

$$S = \tfrac{1}{2}\langle d_{x^2-y^2} | -\sigma_x^{(1)} + \sigma_y^{(2)} + \sigma_x^{(3)} - \sigma_y^{(4)} \rangle$$

$$= 2\langle d_{x^2-y^2} | -\sigma_x^{(1)} \rangle$$

and it has been shown [119] to have a value of 0.076. Similar relationships hold between the other coefficients but the overlap integrals are then much smaller and may be neglected.

Spin-orbit coupling, Zeeman and nuclear interactions all perturb the basis wave functions listed in 15.2.3 in a manner similar to that described in section 13.2 using pure $d_{x^2-y^2}$, d_{z^2} etc. orbitals.

In this molecular orbital treatment the parameters of the spin Hamiltonian 13.2.14 can be shown [119,120] to be

$$g_{\parallel} = 2.0023 - 8(\lambda/\Delta E_{xy})\left[\alpha^2 \beta_1^2 - f(\beta_1)\right] \qquad 15.2.5$$

$$g_{\perp} = 2.0023 - 2(\lambda/\Delta E_{xz})\left[\alpha^2 \beta^2 - g(\beta)\right] \qquad 15.2.6$$

$$A = P\left\{-\alpha^2(4/7 + K_o) - 2\lambda\alpha^2\left[(4\beta_1^2/\Delta E_{xy}) + (3\beta^2/7\Delta E_{xz})\right]\right\} \qquad 15.2.7$$

$$B = P\left\{\alpha^2(2/7 - K_o) - (22\lambda\alpha^2\beta^2)/(14\Delta E_{xz})\right\} \qquad 15.2.8$$

where

$$f(\beta_1) = \alpha\alpha'\beta_1^2 S + \tfrac{1}{2}\alpha\alpha'\beta_1(1-\beta_1^2)^{\frac{1}{2}}T(n)$$

$$g(\beta) = \alpha\alpha'\beta^2 S + 2^{-\frac{1}{2}}\alpha\alpha'\beta(1-\beta^2)^{\frac{1}{2}}T(n)$$

$$\Delta E_{xy} = E_{xy} - E_{x^2-y^2}, \quad \Delta E_{xz} = E_{xz} - E_{x^2-y^2}$$

and P, λ and K_o have the significances given in section 13.2. P can be estimated by theoretical calculations or experimentally from the optical hyperfine structure intervals of copper; it has been deduced[97] to be $0.036 cm^{-1}$ in cupric complexes. K_o has been shown[98] to be 3/7. The constant T(n) is an integral over ligand functions which arises in the calculation of the matrix elements of the Hamiltonian with the wave functions; its value has been shown[120] to be 0.22

To a good approximation, 15.2.7 can be recast to give

$$\alpha^2 = (-A/P) + (g_{\parallel} - 2) + (3/7)(g_{\perp} - 2) + 0.04 \qquad 15.2.9$$

in which the factor 0.04 approximates the various integrals in 15.2.5 and 15.2.6 by an average value.

α can be calculated from 15.2.9, α' from the normalisation relationship 15.2.4 and β and β_1 can then be evaluated from 15.2.6 and 15.2.5 respectively, provided the energy increments ΔE_{xz} and ΔE_{xy} are known. The values of these energy increments are not known for complex II but a value of $13,500 cm^{-1}$ is assumed for ΔE_{xy}, a figure slightly higher than that established from the single crystal spectra[121] and from the solution spectra[122] exhibited by $CuSO_4 5H_2O$. The value to be assigned to ΔE_{xz} is less certain but a simple crystal field calculation[123] shows that it can not be less than $17,000 cm^{-1}$. When this figure is inserted into 15.2.6, β is found to be unity. The values of α^2, $(\alpha')^2$, β_1^2 obtained by these

procedures for complexes I, II and III are listed in Table 15.2.2. As a check on the self-consistency of the procedures, the hyperfine tensor component B can be calculated from 15.2.6; the calculated and experimental B values are also included in Table 15.2.2.

Table 15.2.2

Molecular orbital coefficients and B values for formates of copper (II)

Complex	I	II	III
α^2	0.823	0.838	0.857
$(\alpha')^2$	0.246	0.229	0.207
β_1^2	0.97	0.99	0.99
β^2	1.0	1.0	-
B(calculated)(cm^{-1})	-0.0020	-0.0020	-0.0025
$\lvert B \rvert$(experimental) (cm^{-1})	0.0020±0.0001	0.0021±0.0002	0.0026±0.0012

15.3. Electron Spin Polarisation in Formates of Copper (II)

The molecular orbital coefficients listed in Table 15.2.2 show that while there is appreciable delocalisation of σ-electrons from the ligands to the metal ion $d_{x^2-y^2}$ orbital, there is no significant degree of bonding, either in the in-plane π-system involving the metal ion d_{xy} orbital (magnitude of β_1^2) or in the out-of-plane π-systems involving the metal ion d_{xz} or d_{yz} orbitals (magnitude of β^2). The most highly polarised electron spin interactions within the complexes I, II and III involve the electrons in the metal ion-ligand σ-orbitals in the xy plane, and if direct electron spin coupling through space can be ignored then the propagation of this polarisation through the σ-framework of the formate ion results in the electron-spin polarisation shown diagramatically in figure 15.3.1a. Extension of this polarisation route to a neighbouring cupric ion causes a net ferromagnetic coupling of the unpaired electron spins on neighbouring cupric ions. This kind of coupling is rapidly attenuated as the number of electrons involved in the interaction sequence is increased, and in the case of $Ba_2Cu(DCOO)_6 4D_2O$ it is possible to obtain some idea of the rate

of attenuation from the superhyperfine interaction with the ^{13}C nuclei in labelled formate ligands. It is this interaction that is responsible for the extra, weak splittings of the main peaks 1 and 2 in spectrum 14.1.1b, given by a sample in which the ^{13}C concentration had been enriched to a level of $3.5 \pm 0.1\%$. This spectrum shows that the hyperfine coupling constant for the ^{13}C nuclei amounts to 6.1 ± 0.1 gauss ($0.00068 \pm 0.00001 cm^{-1}$), a value that is far too large to be due to unpaired spin density in the π-orbitals of the formate ion; this hyperfine interaction arises from unpaired spin density in the σ-orbitals. No other components of this superhyperfine interaction were measured because the peaks shown in 14.1.1b collapse in towards each other when the magnetic field lies along the x or y axes of the complex, but the anisotropic contributions to the coupling of an electron in a sp^2 carbon orbital are very small compared to the isotropic contribution, so that only a small error results in assuming that the figure 6.1 ± 0.1 gauss represents this isotropic coupling. A simple calculation using self-consistent field wave functions [124] shows that one electron in a carbon atom sp^2 hybrid orbital results in ^{13}C hyperfine splitting of about 380 gauss, hence the observed ^{13}C hyperfine coupling in complex I is equivalent to that which would arise from 0.016 unpaired electron in the sp^2 hybrid orbital. 0.823 unpaired electron is associated with the cupric ion in the same complex, so that the degree of effective spin polarisation is attenuated by a factor of about seven for each pair of electrons in the sequence of interactions in figure 15.3.1(a)

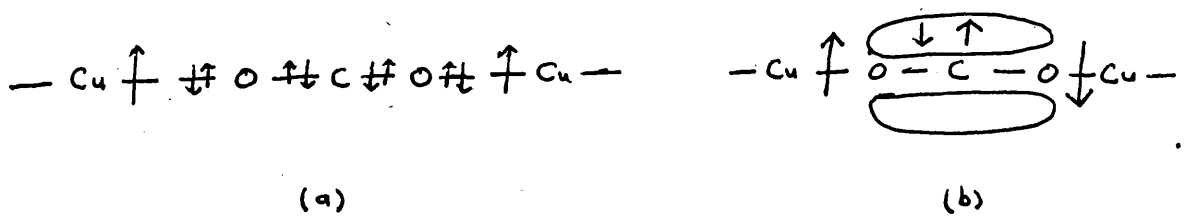

Figure 15.3.1

Although there is no direct overlap of the $d_{x^2-y^2}$ orbital with the π-orbitals of the formate ions, other interactions [125] can correlate the spins of electrons in these orbitals; the resultant

spin polarizations are shown schematically in figure 15.3.1(b). The first stage of this coupling is much weaker than the initial step involved in the coupling of the unpaired electron spin with the σ-framework shown in figure 15.3.1(a). Nevertheless the spins of the paired electrons in the π-molecular orbitals of the formate ion are strongly correlated so that any spin polarization induced into the π-system can be carried over quite large distances with very little attenuation compared with that involved in figure 15.3.1(a). The resultant coupling of the unpaired electron spins on neighbouring cupric ions should therefore be antiferromagnetic, but the dominant antiferromagnetic interaction, figure 15.3.1(b), is opposed by the weaker ferromagnetic interaction of figure 15.3.1(a). The lambda points and the superimposed anisotropic weaker ferromagnetism observed in the low temperature magnetic susceptibility experiments on $Cu(HCOO)_2 4H_2O$ [108,109,110,112] and on $Cu(HCOO)_2 2H_2O$ [109,117] involve the ordering of electron spins in the π-framework, figure 15.3.1(b), and in the σ-framework, figure 15.3.1(a), respectively.

REFERENCES

1 A.R. Edmonds, "Angular Momentum in Quantum Mechanics", Princeton University Press, 1957.

2 L.M. Jackman, "Applications of Nuclear Magnetic Resonance in Organic Chemistry", Pergamon Press, 1959.

3 J.A. Pople, H.J. Bernstein and W.G. Schneider, "High Resolution Nuclear Magnetic Resonance Spectroscopy", McGraw-Hill 1959.

4 G.E. Pake, J.Chem.Phys., 1948,16,327.

5 C.P. Slichter, "Principles of Magnetic Resonance, with Examples from Solid State Physics", Harper & Row, New York, 1963,46.

6 F. Reif and E.M. Purcell, Phys.Revs., 1953,91,631.

7 H.S. Gutowsky, G.E. Kistiakowsky and G.E. Pake, J.Chem.Phys., 1949,17,974.

8 E.R. Andrew and R. Bersohn, J.Chem.Phys., 1950,18,159.

9 R.E.Richards and J.A.S. Smith. Trans. Faraday Soc., 1951,47,1261.

10 A.L. Porte, H.S. Gutowsky and J.E. Boggs, J.Chem.Phys., 1962,36,1700.

11 Van Vleck, Phys.Revs., 1948,74,1118.

12 E.R. Andrew, Phys.Revs., 1953,91,425.

13 E.R. Andrew and R.G. Eades, Proc.Roy.Soc., 1953,A218,537.

14 H.S. Gutowsky and G.E. Pake, J.Chem.Phys., 1950,18,162.

15 N. Bloembergen, R.V. Pound and E.M. Purcell, Phys.Revs., 1948,73,679.

16 H. Morgenau and G.M. Murphy, "The Mathematics of Physics and Chemistry", New York 1943.

17 F.A. Rushworth, Proc.Roy.Soc., 1954,A222,526.

18 L.E. Sutton, editor, "Tables of Interatomic Distances and Configuration in Molecules and Ions", Spec. Publ. Noll, Chem.Soc.(Lond.) 1958,M67.

19 A.L. Porte, H.S. Gutowsky and J.E. Boggs, J.Chem.Phys., 1962,36,1695.

20 F. Bloch, Phys.Revs. 1946,70,460.

21 D.A. Tong, Ph.D. Thesis, Leeds Univ., 1965.

22 F.N.H. Robinson, J.Sci.Instrum. 1959,36,481.

23 D.B. Chalton and D.B. Mann, Cryogenic Data Book, Univ. of California Radiation Laboratory, Berkeley, California, U.C.R.L. Publication 342 Contract No. W-7405-eng-48-May, 1956.

24 Werner, Z. anorg. Chem., 1893,3,267.
25 A.F. Wells, "Structural Inorganic Chemistry", Oxford Univ. Press, London, 1962,572.
26 J.S. Griffith and L.E. Orgel, Quart.Revs.(Lond.) 1957,11,381.
27 International Tables for X-ray Crystallography, Kynock Press, 1962.
28 Z.G. Pinsker, "Electron Diffraction", Butterworth Scientific Publications, London, 1963.
29 G.E. Bacon, "Applications of Neutron Diffraction in Chemistry", 1963, Pergamon Press.
30 B.S. Garrett, Thesis, Oak Ridge National Lab. Report 1745,1954.
31 J.M. Robertson and I. Woodward, J.Chem.Soc., 1936,1817.
32 K. Nakamoto, "Infrared Spectra of Inorganic and Co-ordination Compounds", Wiley and Sons, 1963,155.
33 A.F. Wells, "Structural Inorganic Chemistry", Oxford University Press, London, 1962,561.
34 Y. Hariguchi, J.Sci. Research Inst.(Tokio), 48,27.
35 F.A. Miller and C.H. Wilkins, Anal.Chem., 1952,24,1253.
36 C.P. Slichter, "Principles of Magnetic Resonance, with Examples from Solid State Physics", Harper and Row, New York, 1963,161.
37 M.H. Cohen and F. Reif, "Solid State Physics", 1957,5,326.
38 C.P. Slichter, "Principles of Magnetic Resonance, with Examples from Solid State Physics", Harper and Row, New York, 1963,163-170.
39 T.P. Das and E.L. Hahn, "Nuclear Quadrupole Resonance Spectroscopy", Solid State Physics, Suppl.1, 1958,12.
40 R. Bersohn, J.Chem.Phys., 1952,20,1505.
41 E.I. Fedin and G.K. Semin, Zhurnal Struckt. Khim., 1960,1,252 and 464.
42 M.H. Cohen, Phys.Revs., 1954,96,1278.
43 G.D. Watkins and R.V. Pound, Phys.Revs., 1952,85,1062.
44 Y. Koi, A. Tsujimura and T. Fuke, J.Chem.Phys., 1955,23,1346.
45 R. Livingston and H. Zeldes, J.Chem.Phys., 1957,26,351.
46 S. Kozima and K. Tsukada, J.Phys.Soc. Japan, 1955,10,591.
47 T.S. Wang, Phys.Revs., 1955,99,566.
48 H. Bayer, Z.Physik, 1951,130,227.
49 H.W. Dodgen and J.L. Ragle, J.Chem.Phys., 1956,25,376.
50 T.P. Das and E.L. Hahn, "Nuclear Quadrupole Resonance Spectroscopy", Solid State Physics, Suppl.1, 1958.

51 R.M. Sternheimer, Phys.Revs., 1951,84,244; 1952,86,316; 1954,95, 736.

52 C.H. Townes and B.P. Dailey, J.Chem.Phys., 1949,17,782.

53 R.G. Barnes and W.V. Smith, Phys.Revs., 1954,93,95.

54 H.A. Bethe and R.F. Bacher, Rev.Mod.Phys., 1936,8,226.

55 L. Davis, B.T. Feld, C.W. Zabel and J.R. Zacharias, Phys.Revs., 1948,73,525.

56 L. Pauling, "The Nature of the Chemical Bond", Cornell Univ. Press, Third Edition, 1959,66

57 C.H. Townes and A.L. Schawlow, "Microwave Spectroscopy", McGraw-Hill New York, 1955.

58 N.F. Ramsay, "Molecular Beams", Oxford Univ. Press, New York 1956.

59 H.C. Heal, J.Chem.Phys., 1956,24,1011.

60 P.J. Bray and R.G. Barnes, J.Chem.Phys., 1955,23,1955.

61 C. Dean, Phys.Revs., 1954,96,1053.

62 C. Dean and R.V. Pound, J.Chem.Phys., 1952,20,195.

63 R.M. Cotts and W.D. Knight, Phys.Revs., 1954,96,1285.

64 A.G. Gregg, G.C. Hampson, G.I. Jenkins, P.L.F. Jones and L.E. Sutton, Trans. Faraday Soc., 1937,33,852.

65 R.J. Havighurst, J.Amer.Chem. Soc., 1926,48,2113.

66 H. Brackken and W. Scholten, Z.Krist, 1934,89,448.

67 C.H. MacGillavry, J.H. de Wilde and J.M. Bijvoet, Z.Krist., 1938,100,212.

68 H. Harmsen, Z.Krist., 1938,100,208.

69 K.K. Cheung and G.A. Sim, J.Chem.Soc., 1965,5988.

70 R.C. Evans, F.G. Mann, H.S. Peiser and D. Purdie, J.Chem.Soc., 1940,1209.

71 J.A.D. Jeffreys, G.A. Sim, R.H. Burnell, W.I. Taylor, R.E. Corbett, J. Murray and B.J. Sweetman, Proc.Chem.Soc., 1963,171.

72 K.K. Cheung, R.S. McEwan and G.A. Sim, Nature, 1965,205,383.

73 H. Dehmelt, H. Robinson and W. Gordy, Phys.Revs., 1954,93,480.

74 J.R. Whitehead, "Super regenerative Receivers", Cambridge Univ. Press, 1950.

75 R. Wallace, Ph.D. Thesis, Glasgow Univ. 1964.

76 C. Dean, Rev.Sci. Instrum., 1960,31,934.

77 R. Livingston, Science, 1953,118,61.

78 I. Aucken, Inorganic Synthesis, Volume VI, McGraw-Hill, 1960.

79 R.V. Pound, Phys.Revs., 1950,79,685.
80 G. Becker and H. Krüger, Naturwissen., 1951,38,121.
81 N. Bloembergen, Rept. Conf. on Defects in Crystalline Solids, Bristol 1954, Phys.Soc. London 1955.
82 S. Kojima, K. Tsukada, A. Shimauchii and Y. Hinaga, J.Phys.Soc. Japan, 1954,2,795.
83 S.L. Segel and R.G. Barnes, Phys.Revs.Letters, 1965,15,886.
84 R.G. Barnes and S.L. Segel, Phys.Revs.Letters, 1959,3,462.
85 K.E. Weber and J.E. Todd, Rev.Sci.Instrum. 1962,33,390.
86 A. Narath, W.J. O'Sullivan, W.A. Robinson and W.W. Simmons, Rev.Sci.Instrum, 1964,35,476.
87 V.I. Gol'danskii, "The Mossbauer Effect and its Applications in Chemistry", D.Van Nostrand Co., Princeton, New Jersey, 1966.
88 N.N. Greenwood, "Chemistry in Britain", 1967,3,56.
89 W.D. Knight, Phys.Revs., 1949,76,1259.
90 D.J.E. Ingram, "Spectroscopy at Radio and Microwave Frequencies", Butterworths, London, Second Ed., 1967.
91 D.J.E. Ingram, "Free Radicals as Studied by Electron Spin Resonance", Butterworths Scientific Publications, London 1958.
92 H.A. Bethe, Ann.Physik, 1929,3,133.
93 B. Bleaney, K.D. Bowers and D.J.E. Ingram, Proc.Roy.Soc. 1955,A228, 147.
94 Knox, J.Chem.Phys., 1959,30,991.
95 V. Vleck, J.Chem.Phys., 1935,3,803 and 807.
96 E. Fermi, Z.Phys., 1930,60,320.
97 A. Abragam and M.H.L. Pryce, Proc.Roy.Soc.(Lond.) 1951,A205,135.
98 A. Abragam, M.H.L. Pryce and J. Horowitz, Proc.Roy.Soc.(Lond.) 1955,A230,169.
99 B. Bleaney, Phil.Mag., 1951,42,441.
100 B. Bleaney and K.D. Bowers, Proc.Roy.Soc.(Lond.), 1952,A214,451.
101 H. Kumagi, H. Abe and J. Shimada, Phys.Revs., 1952,87,385.
102 P.V. Groth, Chemis.Kristallographie, 1910,3,24.
103 R.V.G. Sundara Rao, K. Sundaramma and G. Swasankara Rao, Zeit.Krist., 1958,110,231.
104 H. Abe, Phys.Revs., 1953,92,1572
105 H. Abe, J.Phys.Soc. Japan, 1958,13,987.

106 R.L. Martin and H. Waterman, J.Chem.Soc., 1957,2545.
107 R.L. Martin and H. Waterman, J.Chem.Soc., 1959,1359.
108 T. Haseda, A.R. Miedema, H. Kobayashi and E. Kanda, J.Phys.Soc. Japan, 1962,17, Suppl. B-1. 518.
109 R.B. Flippen and S.A. Friedberg, J.Chem.Phys., 1963,38,2652.
110 H. Kobayashi and T. Haseda, J. Phys.Soc. Japan, 1963,18,541.
111 J. Shimada, H. Abe and K. Ono, J.Phys.Soc., Japan, 1956,11,137.
112 J. Itoh and Y. Kamiya, J.Phys.Soc. Japan, 1962,17,512.
113 R. Kiriyama, H. Ibamoto and K. Matsuo, Acta.Cryst., 1954,7,482.
114 K. Osaki, Y. Nakai and T. Watanabe, J.Phys.Soc., Japan, 1963,18,919.
115 M. Bukowska - Strzyzewska, Acta.Cryst., 1965,19,357.
116 V.V. Li, Phys.Rev., 1951,84,721.
117 G.R. Wagner, R.T. Schumacher and S.A. Friedberg, Phys.Revs., 1966,150,226.
118 D.A. Morton-Blake and A.L. Porte, Unpublished results.
119 D. Kivelson and R. Neiman, J.Chem.Phys., 1961,35,149.
120 A.H. Maki and B.R. McGarvey, J.Chem.Phys., 1958,29,31.
121 O.G. Holmes and D.S. McClure, J.Chem.Phys., 1957,26,1686.
122 J. Bjerrum, C.J. Ballhausen and C.J. Jorgensen, Acta.Chem.Scand., 1954,8,1275.
123 D. Polder, Physica, 1942,9,709.
124 E. Clementi, "Tables of Atomic Functions", I.B.M. Corporation Development Lab.Reports, 1965, I.B.M., Journal of Research and Development, 1965,9,2.
125 S. Koide and T. Oguchi, "Advances in Chemical Physics" (I.Prigogine, Editor), Interscience Publishers, London, 1963,Vol.5,p.189.